The PHILOSOPHICAL MAGAZINE

FIRST PUBLISHED IN 1798

L. 44 SEVENTH SERIES No. 353 June 1953

A Journal of Theoretical Experimental and Applied Physics

PRICE 15s. 0d.
Annual Subscription £8 0s. 0d. payable in advance

D AND PUBLISHED BY TAYLOR & FRANCIS LTD., RED LION COURT, FLEET ST., LONDON, E.C.4

LXI. *The Penetrating Component of Cosmic Radiation in the Upper Atmosphere*

By J. D. Pullar and E. G. Dymond*
Department of Natural Philosophy, University of Edinburgh†

[Received October 15, 1952, revised March 11, 1953]

Summary

The vertical intensity of the hard component of cosmic radiation has been measured in geomagnetic latitude 56°, to a minimum atmospheric depth of 4 g/cm². The intensity, determined with a precision of 2·5%, shows no maximum. This agrees closely with the results of Pomerantz. The primary particle flux at this latitude, capable of penetrating 90 g/cm² of lead is found to be $0{\cdot}164 \pm 0{\cdot}003$ particles cm^{-2} sec^{-1} ster^{-1}.

The flux of μ-mesons in the upper atmosphere has been derived, and shows a maximum of 0·039 particles cm^{-2} sec^{-1} ster^{-1} at a depth of 150 g/cm².

Penetrating showers produced in lead have also been measured to a minimum atmospheric depth of 7 g/cm², the primaries being found to have an absorption length of 120 g/cm² of air.

§ 1. Introduction

The primary object of this research has been to establish with accuracy the variation of the vertical intensity of the penetrating component of cosmic radiation as a function of atmospheric depth. In spite of much previous work on this subject, there has been little agreement about the exact form of the depth–intensity curve ; in particular the evidence as to whether or not a maximum exists has been conflicting. Recent measurements by Vidale and Schein (1952) at geomagnetic latitude 55°, using 7·5 cm of lead absorber to exclude the soft component, show an intensity maximum in the neighbourhood of 60 g/cm². On the other hand, the results of Pomerantz (1949 a) at latitude 52°, with the same quantity of lead, show a monotonic increase in intensity with altitude, a maximum around 100 g/cm² appearing only with absorber thicknesses of 4 cm and less. Winckler and Stroud (1949) working at 56° found no maximum with 7·6 cm of lead.

A principal cause of this lack of agreement has been the low statistical accuracy of the results, which in all cases have been the product of single balloon flights, although Pomerantz and McClure (1952) have extended

* Mr. E. G. Dymond, the senior author of this paper, died suddenly in Edinburgh on 26th October 1952. The revision of the paper, which he did not himself see, is confined to § 6, and was made by Mr. Pullar acting on comments by a referee (N.F.).

† Communicated by Professor N. Feather, F.R.S.

the earlier observations by three additional ascents which confirm Pomerantz's original conclusion of no maximum. In the work to be described here, seven flights using 8 cm of lead with identical apparatus have been made at latitude 56°. The average height reached by the balloons corresponded to 17 g/cm^2 depth in the atmosphere, with one flight reaching 4 g/cm^2. These experiments cover the period from April 1949 to March 1950, and the individual results, which agree in showing no time variation within an accuracy of 5%, confirm the monotonic rise in intensity found by Pomerantz.

The penetrating component as measured in all these experiments does not consist of a single type of particle, but is a mixture of the primary nucleonic constituent with secondary nucleons and mesons. In order to obtain some information on the relative quantity of mesons at various altitudes, some measurements have also been carried out with a counter arrangement to record penetrating showers which are initiated only by nucleons.

§ 2. Experimental Arrangements

The vertical intensity was measured with a triple coincidence counter telescope, with 8 cm of lead absorber interposed in the counter train as shown in fig. 1. The counters, type G.M.4 made by Cinema Television Ltd., had glass walls 0·25 g/cm^2 thick, and copper cathodes 0·08 g/cm^2 thick. They were filled with an ethylene–argon mixture, in the pressure ratio 17 to 83, to a total of 8·6 cm Hg. A 400-volt plateau extending from 1100 to 1500 volts, with a slope of 0·02 to 0·04% per volt, was readily obtained. These counters are completely insensitive to ambient temperature variations in the range +60°C to −60°C, while their limited life of about 10^7 counts was not harmful in the particular conditions of this research.

The average effective counter dimensions were : length, 10·0±0·3 cm ; diameter, 1·95±0·10 cm ; separation of axes of extreme counters, 12·4 cm. The effective diameter was determined by the method of Street and Woodward (1934), while the effective length was measured in a somewhat similar way by progressively displacing the centre counter of the triple set in a direction along its axis. A displacement of half the effective length causes the coincidence rate to fall to one-half its maximum value. In order to make the appropriate corrections to the observed counting rates, the resolving time of the coincidence circuit (5 μsec), the efficiency of the counters (99·8%) and their dead time (75 μsec) were measured.

Radio-telemetering of the counts was employed, with superimposed pressure and temperature signals derived from a modified form of the British Meteorological Office radio sonde (Dymond 1947). In this type of work the precision of standard radio sonde measurements is not adequate, owing to the great altitudes reached. The sensitivity of the pressure device was therefore increased by adding to the standard aneroid capsule a special high altitude capsule of about three times the sensitivity, which only came into operation below about 150 mb pressure. The use

of a radio sonde thermometer element, within the gondola housing all the apparatus, enabled the temperature of the pressure element to be measured and its temperature correction to be accurately evaluated. In addition, the usual technique of enclosing the gondola in double cellophane walls kept the whole apparatus within 20°c of ground temperature throughout the flight, so that the temperature corrections were small. The result of these measures was that pressures of 5 to 10 mb could be determined with an accuracy of ± 1 mb, a precision at least five times greater than can be expected in normal radio sonde practice.

Fig. 1

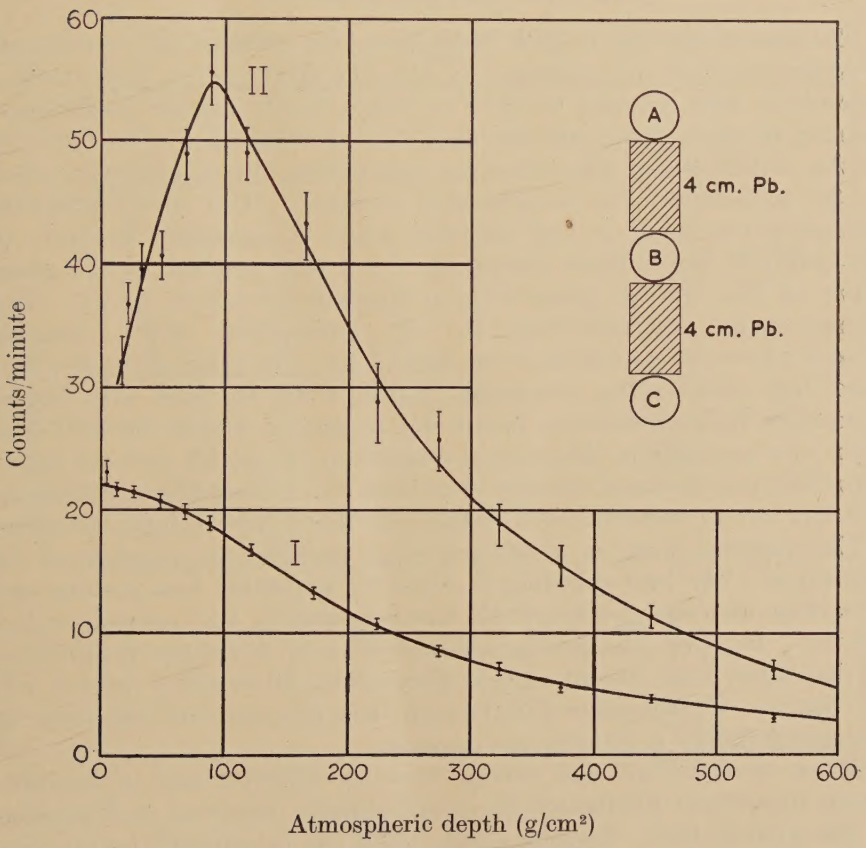

Vertical Intensities

Curve I : Coincidence rate of ABC with 8 cm lead absorber.
Curve II : Coincidence rate of ABC without absorber.

All flights were made from Edinburgh. Assuming an eccentric geomagnetic dipole with axis cutting the surface at 80·1° N, 82·7° W, the magnetic latitude is 56°. It is to be noted that the usual approximation

of a centred dipole, with axis pole at 78·5° N, 69° W, gives a magnetic latitude of 59°. According to Alpher (1950) the corresponding cut-off energies for vertically incident protons are 730 and 460 MEV. The difference is considerable so that some care is required in interpretation.

All counter telescopes were carefully checked on the ground to ensure that they gave comparable results. The observed counting rate at 100 metres altitude was $0{\cdot}957 \pm 0{\cdot}013$ counts/min, which corresponds to a vertical flux of 0·0077 particles $cm^{-2}\,sec^{-1}\,ster^{-1}$, in reasonable agreement with the measurement of the hard component by Greisen (1942) who found a flux of $0{\cdot}00738 \pm 0{\cdot}00007$ particles $cm^{-2}\,sec^{-1}\,ster^{-1}$.

§ 3. The Vertical Intensity

The counts recorded in each flight have been grouped into convenient pressure intervals and combined to give the final result. Instrumental corrections were required to allow for losses due to counter inefficiency, counter recovery time, and the dead time introduced by the circuitry of the balloon-borne transmitter in lengthening the coincidence pulses to 30 milliseconds for transmission purposes. The total correction reached a maximum at high altitude, where it amounted to 3·4% of the observed rate. These corrections have been applied to the mean curve of the vertical penetrating component shown in fig. 1. The highest point, corresponding to the atmospheric depth interval 10 to 3·4 g/cm^2 is derived from one flight only ; the range 40 to 10 g/cm^2 from four flights, the remaining points from at least six flights. Agreement between different flights was in general within the statistical error ; for example, in the interval centred on 122 g/cm^2, only one result departed from the mean value by more than 5%. There was no indication of a day to day variation such as has been found for the total radiation.

The question must be considered what particles are represented by this curve. The lead shielding excludes by ionization loss protons and α-particles with energies below 275 MEV per nucleon, and μ-mesons below 130 MEV. However, the geomagnetic cut-off at 56° is 730 MEV for protons, so that apart from loss in nuclear interactions all primary protons will be counted. On the other hand a slight loss of α-particles will occur as the cut-off energy is 250 MEV per nucleon.

A few electrons will also emerge from the absorber and be recorded owing to cascade production by very energetic electrons and photons in the 8 cm of lead. Bhabha (1944, 1950) has considered the question of how much electronic component will be found beneath given thicknesses of lead, and suggests that only some 0·5% will appear after traversing 90 g/cm^2.

In order to apply a suitable correction one flight was made with no lead shielding. The curve for the total radiation, capable of penetrating 1·65 g/cm^2 of glass and copper, is shown in fig. 1. The difference between the two curves in this figure gives the soft component ; this includes

mesons with energies below 130 MEV, and is therefore an upper limit only for the electronic component. It is found that the maximum correction is under 1%, which is less than the statistical errors and can therefore be neglected.

A much more difficult correction to deal with is that representing the simultaneous discharge of all three counters by showers of particles travelling nearly horizontally. Other workers in the field have allowed for this by displacing a central counter out of line, and have found by this means that lateral showers do not account for more than a few per cent of the coincidences at high levels. Such an arrangement is open to objection, as, besides recording soft side showers it will also respond to interaction products of the vertical primaries from the absorber above the displaced counter.

Fig. 2

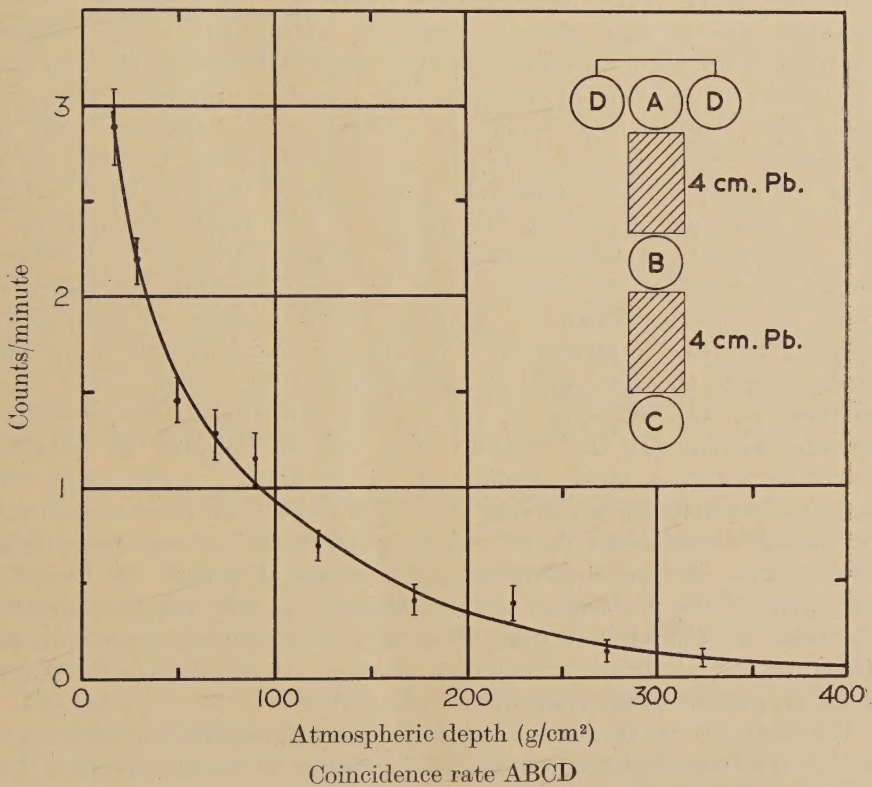

We accordingly made five flights with the counter arrangement shown in fig. 2, in which the geometry of the telescope ABC is identical with that used in the main series. The results of these flights, shown in the figure, are surprising in that the coincidence rate ABCD increases rapidly with decreasing air thickness to the highest point reached, corresponding

to 12 g/cm^2, where the rate is 15% of that due to verticals alone. In a preliminary communication (Pullar and Dymond 1951) we attributed this to cascade showers which can only reach development at great altitudes when travelling nearly horizontally. Further consideration, however, leads us to believe that this is unlikely to be the correct explanation.

The mass of air traversed by a ray at zenith angle θ in reaching a given atmospheric depth is closely proportional to $\sec\theta$ up to $\theta=85°$. At larger angles the curvature of the earth must be taken into account. Assuming the thickness for maximum development of air showers to be about 100 g/cm^2, and neglecting lateral spread, it is found that fully-developed radiation incident on the telescope ABCD at an atmospheric depth of 12 g/cm^2, the greatest elevation reached in these flights, must be moving close to zenith angle 85°. The coincidence rate observed at 12 g/cm^2 is approximately twice that at 50 g/cm^2, where soft radiation from 60° should reach its maximum intensity. This increase in the counting rate at high altitude might be attributed to the reduced screening of the lower counters from large angle radiation by the adjacent lead blocks. The effect of this screening, however, appears to be small, and various other factors which are probably more important must be considered. Since the linear dimensions of most showers are likely to be large compared with the recording system, the probability of detecting a given event will depend on the density as well as the multiplicity of the constituent particles. Since the particle density is inversely proportional to the air density there is less probability of recording events at extreme altitude. Another factor tending to reduce the counting rate due to showers arriving close to the horizontal is the fact that, owing to the very rapid change in $\sec\theta$ at large angles, even when modified by the influence of the earth's curvature, fully developed cascades arriving at the 12 g/cm^2 level will be initiated by particles travelling within a much smaller solid angle around zenith angle 85°, than, for example, those arriving at a depth of 50 g/cm^2 from around 60°. On balance therefore we do not expect a significant increase in counting rate due to electron showers between 50 and 12 g/cm^2. A complete treatment of the problem of inclined cascades is very complex and has not been attempted, but from these and other considerations we are driven to the conclusion that lateral showers are responsible for only a small proportion of the coincidence rate ABCD.

We shall assume therefore that the vertical intensities shown in fig. 1 do not need significant correction for the effect of lateral cascades. The interpretation of the events contributing to the ABCD rate will be discussed later.

Our curve is found to agree well with that of Pomerantz (1949 a) for 52° latitude and 7·5 cm of lead, when the difference in solid angle of the telescopes has been taken into account by reducing both sets of results to absolute flux in particles cm^{-2} sec^{-1} ster^{-1}, using the expressions given

by Pomerantz (1949 b). In table 1 we make a comparison of the absolute vertical particle intensity at a depth of 15 g/cm^2 as determined by recent workers.

Table 1

	Lead thicknesses (cm)	Latitude (° N)	Flux (particles cm^{-2} sec^{-1} ster^{-1})
Pomerantz (1949 a)	7·5	52	0·171 ±0·004
Winckler (1949)	7·6	56	0·170 ±0·020
Vidale and Schein (1952)	7·5	55	0·174 ±0·003
Pullar and Dymond	8·0	56	0·161 ±0·003

These figures agree more closely than is to be expected from the errors which arise from the uncertainty in the effective dimensions of the counters used by different workers.

We are also in agreement with Pomerantz in finding no maximum in the depth–intensity curve, a point of some controversy in the past. Vidale and Schein have recently reported such a maximum but their curve shows that the existence of this depends on a single point of low statistical weight. They were plainly influenced in interpretation by their results at lower latitudes where a maximum is in no doubt.

Extrapolation of our curve to zero depth can be made with little uncertainty and yields a primary flux of particles capable of penetrating 8 cm of lead of 0·164±0·003 particles cm^{-2} sec^{-1} ster^{-1}. It is satisfactory that the curves in fig. 1 for the total radiation and for the hard component extrapolate nearly to a common point at zero pressure, which is to be expected if the low energy cut-off of the incident spectrum is due to the magnetic latitude effect rather than to absorption in the lead.

§4. Penetrating Showers Produced in Lead

The particles making up the vertical flux measured by the telescope ABC consist largely of protons and μ-mesons. In order to assess the relative contributions of these two types a series of three flights was made with a counter array designed to record events initiated by protons and not by μ-mesons.

The arrangement of counters and absorbers is shown in fig. 3, five-fold coincidences PQRST being recorded.

The significant event for this array is one in which a single ionizing particle discharges a counter P and produces in the top lead block a shower of penetrating secondaries. At least two particles capable of penetrating 5 cm of lead are required to discharge counters Q, R, S and T.

Energetic electron–photon showers occurring in the air above may also be recorded, but the work of Bhabha, quoted previously, suggests that these will be very few in number. Likewise coincidences arising

from μ-mesons producing knock-on electrons in the lead can be neglected as these electrons will be stopped by the lower lead blocks.

The consolidated results are shown in fig. 3. The statistical errors of the data from each flight were large, but substantially the same result was obtained on each occasion. Few coincidences were obtained at depths greater than 200 g/cm², but the rate rose sharply to 2·3 counts/minute at 7 g/cm², the greatest elevation reached.

Fig. 3

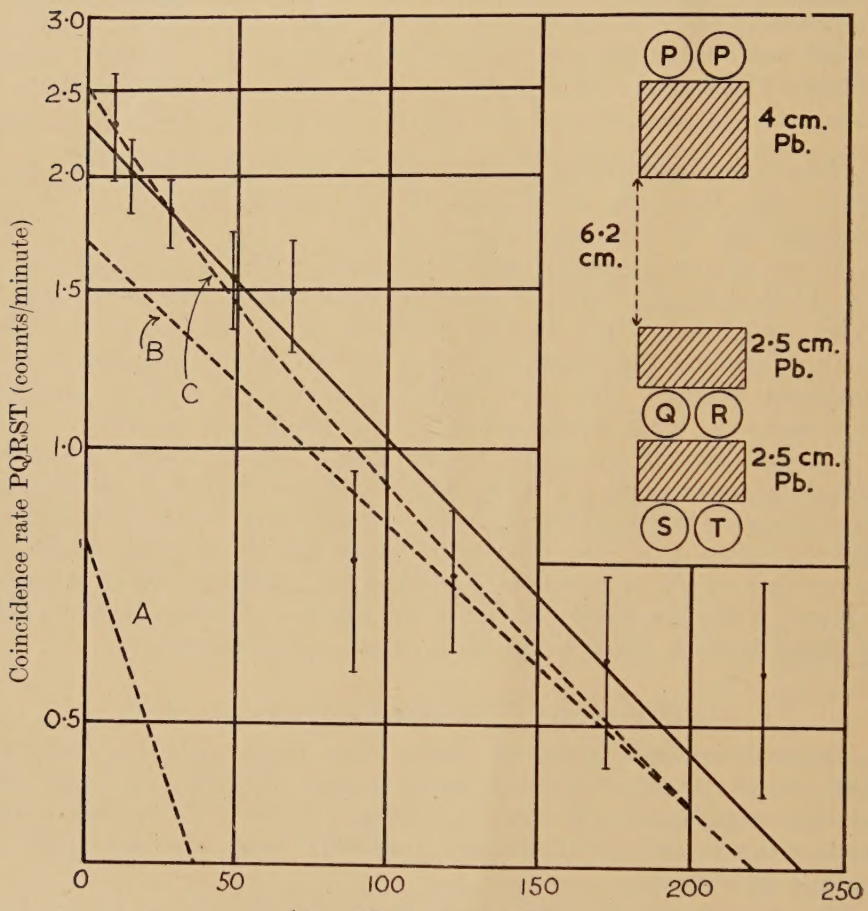

Penetrating Showers in Lead

Full line : $y=2{\cdot}3 \exp(-x/120)$
Broken lines : A α-particles $\lambda_A = 45$ g/cm²
B protons $\lambda_A = 140$ g/cm²
C sum of A and B

When plotted logarithmically, as in fig. 3, it is found that the data can be fitted by the curve $\exp(-x/\lambda_A)$, where $\lambda_A = 120$ g/cm². This value

for the absorption mean free path of the primaries causing the showers is in agreement with that derived, also from penetrating showers, by Tinlot (1949) at aircraft altitudes and by Teucher (1952) in the lower atmosphere. At the lower levels explored by these workers there can be very few primary α-particles, so the lack of variation of λ_A with height suggests that even in our case protons alone may be responsible for the observed coincidences. However, as shown in the diagram, our results would fit equally well a curve compounded from two exponentials such as $\exp(-x/140)$ for protons and $\exp(-x/45)$ for α-particles. Segrè (1952) suggests a considerably higher value (80 g/cm^2) for the absorption length for α-particles, which would further reduce the possibility of distinguishing between the two types of parent particle.

The absolute magnitude of the coincidence rate PQRST is in rough agreement with existing data on interaction cross sections. Taking the value $\lambda_I = 160$ g/cm^2 for protons in lead (Rochester and Rosser 1951) the expected interaction rate of primaries moving within the solid angle subtended by the counter array is 7·1/min compared with the observed shower rate of 2·3/min. The efficiency with which these interactions will be recorded depends partly on the angular aperture of the counter array relative to the average divergence of the shower particles, and partly on the proportion of charged to uncharged particles in the shower. The angular spread of nucleonic cascades can be estimated from the results of Green and Messel (1952). The root mean square angle of a cascade in 4 cm of lead is thus found to be 0·27 radians for primaries of 10^3 Mev, and 0·085 radians for 10^4 Mev particles. As the minimum angle subtended by the bottom counters at the centre of the upper block is about 0·25 radians, we see that nearly all cascade particles originating in the top lead from primaries travelling within the solid angle defined by the whole counter system will traverse the lower counters. About one-third of these particles will be uncharged, so the expected coincidence rate is 4·7/min, about twice the observed rate. No better agreement can be looked for from these rough methods of estimation.

§ 5. Discussion

The results of penetrating showers which we have obtained justify us in assuming that the primaries responsible are absorbed with an attenuation length of about 120 g/cm^2. We might then arrive at an estimate for the meson flux, predominantly that of μ-mesons, by subtracting from the hard component curve of fig. 1 the quantity $I_0 \exp(-x/120)$, where I_0 is the extrapolated value of the intensity at zero depth. This, however, would yield an inaccurate result, as it neglects the slower protons, which may penetrate the lead to operate the vertical telescope ABC, but which are insufficiently energetic to produce the showers. The lower limit of energy required to cause the PQRST coincidences is not known, but it is likely to be a few thousand Mev

while protons above 275 Mev will discharge ABC. These slow protons will consist partly of primaries and partly of secondaries from interactions in the air above. As there are no direct experiments to find their numbers, we may have recourse to the theoretical work of Messel (1951) on nucleonic cascades, to estimate the intensity of the total protonic component as a function of atmospheric depth. Messel gives curves, applicable to middle latitudes, showing the flux of particles with lower energy limits 2000 and 260 Mev. The latter corresponds closely with the conditions of our experiment. The higher limit gives a curve very close to exp $(-x/120)$ as found experimentally for the faster particles causing penetrating showers. We can therefore with some confidence take the

Fig. 4

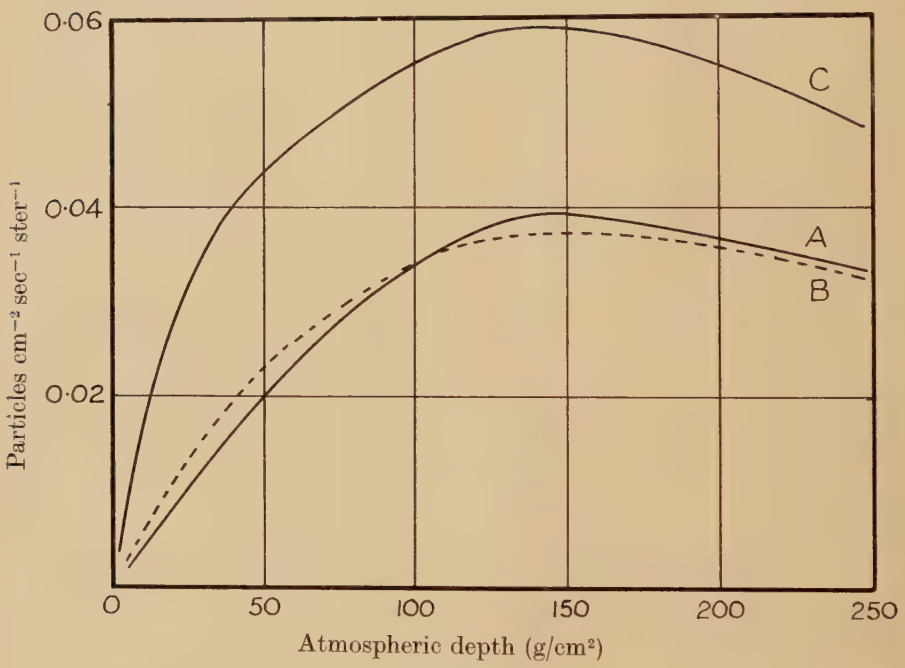

Meson Flux

Curve A : Authors (experimental)
B : Clark (experimental)
C : Caldirola (theoretical)

curve with the lower energy limit as describing the protons present in the hard component, through 8 cm of lead, and by subtraction arrive at the meson flux. This is done in fig. 4. The meson intensity so obtained rises to a maximum at about 150 g/cm² of air, and represents roughly one-third of the total hard component at this point.

The meson flux has also been derived by Clark (1952). Although of considerably different arrangement, his counter array was also designed

to separate particles which do and do not interact in lead. He finds a maximum value of meson intensity of 0·0365 particles cm^{-2} sec^{-1} $ster^{-1}$, at a depth of 140 g/cm^2, in good agreement with our figure of 0·039 at 150 g/cm^2. His curve is also shown in fig. 4, and is seen to lie close to ours throughout the range of 0 to 250 g/cm^2. It must, however, be emphasized that the accuracy of these determinations, arrived at by manipulating experimental curves which themselves are liable to statistical and other errors, is not high and the agreement is better than one would expect.

A theoretical comparison is provided by the work of Caldirola *et al.* (1952), who have made a phenomenological study of collision processes in the upper atmosphere. Unfortunately their computations need correction, as in allowing for μ-meson decay they have assumed a constant atmospheric temperature equal to that at the surface. The lower temperature in the upper 200 g/cm^2 of air gives a sensibly smaller decay constant than that which they have used. We have recomputed their curve for the μ-meson flux, using the revised decay constant, and find that the results reproduce reasonably the intensities deduced from our experiments. This theoretical curve is shown in fig. 4. The maximum is correctly placed though the absolute magnitude is high. The latter, however, depends critically on the form of the incident energy spectrum of the primaries. This is now thought to differ somewhat (Winckler *et al.* 1950, Kaplon *et al.* 1952) from the pure power law assumed by Caldirola.

§ 6. Penetrating Showers in Air

Some difficulty arises in interpreting the results obtained with the ABCD counter array described in § 1. It was there shown that it is unlikely that the major part of the coincidences can arise from electron–photon cascades travelling nearly horizontally. The other possibilities are :

(*a*) A nuclear explosion in the upper lead, initiated by a charged particle passing through A or D, giving a backward moving particle through D or A, and at least one forward particle to discharge B and C.

(*b*) Vertical showers containing two or more charged particles, one of which must be penetrating, arising in the air above.

(*c*) Local showers, with at least one penetrating particle, originating in the material above the counters.

(*d*) At high altitudes there is known to exist an appreciable flux of upward moving radiation (albedo). The possibility exists of coincidences ABCD being due to showers created in the lead by particles entering at the lower end of the telescope.

Of these possibilities, (*c*) and (*d*) are expected to make only small contributions.

The material immediately above the counters averages only 0·02 g/cm^2 excluding the top counter walls. The balloons, though

massive, are so distended and at such a distance that their effective thickness is about 0·03 g/cm². There is therefore quite negligible material above the counters and possibility (*c*) is excluded.

The albedo effect is due to low energy particles and few can penetrate 8 cm of lead. We may note the observations of Lord and Schein (1950), who show that at 95 000 ft. the proportion of penetrating showers in which the parent particle is travelling at zenith angles greater than 120° is extremely small.

It is possible that coincidences ABCD are due to vertical showers originating in the air, but we are faced with a real difficulty in accounting for a shower rate, at 12 g/cm², which is 15% of the total vertical flux. It is unfortunate that this set of flights failed to reach the altitudes gained in the previous work, but it is clear from the agreement between individual flights that there is no maximum in counting rate at depths greater than 12 g/cm². The interaction length of the hypothetical primaries giving rise to these events would have to be very short indeed, as in any transition effect the maximum is always at a depth greater than the interaction length of the primary particle. On the other hand, the known flux of heavy nuclei, which might have sufficiently short interaction lengths, is much too small to account for the observed results. Peters (1952) gives the flux of nuclei with $Z \geqslant 10$ as $4{\cdot}5 \times 10^{-4}$ particles cm^{-2} sec^{-1} ster^{-1}, i.e. about 0·2% of the total particle intensity.

We are left with the possibility (*a*) above. The view that the observed rate ABCD can be explained in terms of disintegrations occurring in the absorber has been supported by Fowler (1952). His calculations are based on the data obtained in photographic emulsions exposed at great heights by Camerini *et al.* (1951), it being assumed that these data can be applied to events in lead. He finds that when a primary proton of average energy passes through counter A and interacts within the upper lead block, there is a probability of about 0·3 that a counter D will be discharged by a secondary particle. The corresponding probability of discharging B and C is about 0·4. Up to 40% of the rate ABC at high altitude may be due to disintegrations in the upper lead block caused by primaries through counter A. Thus a contribution to the rate ABCD equivalent to 13% of the corresponding rate ABC may arise from this source alone. When we also consider the other contributions due mainly to primaries passing through a counter D, the total effect becomes of sufficient magnitude to explain the experimental data.

While this is the most feasible explanation of the observed results, it is rather surprising that in previous flights, including those by Pomerantz (1949 a), and by Winckler and Stroud (1949), the number of local events detected by out-of-line counters was very much smaller than in the present measurements. It is obviously desirable to obtain more experimental evidence on this matter and further work to this end is now being undertaken.

References

Alpher, R. A., 1950, *J. Geophys. Res.*, **55,** 437.
Bhabha, H. J., 1944, *Proc. Ind. Acad. Sci.*, **19,** 23.
Bhabha, H. J., and Ramakrishnan, A., 1950, *Proc. Ind. Acad. Sci.*, **32,** 141.
Caldirola, P., Fieschi, R., and Gulmanelli, P., 1952, *Nuovo Cimento*, **9,** 5.
Camerini, U., Davies, J. H., Fowler, P. H., Franzinetti, C., Muirhead, H., Lock, W. O., Perkins, D. H., and Yekutieli, G., 1951, *Phil. Mag.*, **42,** 1241.
Clark, M. A., 1952, *Phys. Rev.*, **87,** 87.
Dymond, E. G., 1947, *Proc. Phys. Soc.*, **59,** 645.
Fowler, P. H., 1952, private communication.
Green, H. S., and Messel, H., 1952, *Phys. Rev.*, **85,** 679.
Greisen, K., 1942, *Phys. Rev.*, **61,** 212.
Kaplon, M. F., Peters, B., Reynolds, H. L., and Ritson, D. M., 1952, *Phys. Rev.*, **85,** 295.
Lord, J. J., and Schein, M., 1950, *Phys. Rev.*, **77,** 19.
Messel, H., 1951, *Phys. Rev.*, **83,** 26.
Peters, B., 1952, *Progress in Cosmic Ray Physics* (Amsterdam : North Holland Publishing Co.), Chap. IV.
Pomerantz, M. A., 1949 a, *Phys. Rev.*, **75,** 69 ; 1949 b, *Ibid.*, **75,** 1721.
Pomerantz, M. A., and McClure, G. W., 1952, *Phys. Rev.*, **86,** 536.
Pullar, J. D., and Dymond, E. G., 1951, *Phil. Mag.*, **42,** 663.
Rochester, G. D., and Rosser, W. G. V., 1951, *Reports on Progress in Physics*, **14,** 227.
Segrè, G., 1952, *Nuovo Cimento*, **9,** 116.
Street, J. C., and Woodward, R. H., 1934, *Phys. Rev.*, **46,** 1029.
Teucher, M., 1952, *Zeits. f. Naturforsch.*, **7a,** 61.
Tinlot, J., 1948, *Phys. Rev.*, **74,** 1197.
Vidale, M. L., and Schein, M., 1951, *Nuovo Cimento*, **8,** 774.
Winckler, J. R., and Stroud, W. G., 1949, *Phys. Rev.*, **76,** 1012.
Winckler, J. R., Stix, T., Dwight, K., and Sabin, R., 1950, *Phys. Rev.*, **79,** 656.

LXII. *Comparison of Equations of State for Amorphous Long-Chain Polymers*

By A. Charlesby
Atomic Energy Research Establishment, Harwell*

[Received February 26, 1953]

§ 1. Introduction

It has been shown (Charlesby 1952) that, when exposed to high-energy radiation such as is present in an atomic pile, polyethylene, in common with a number of other polymers, can be crosslinked. Provided that the degree of radiation is not too great (e.g. about 10% crosslinking or less) some degree of crystallinity of the polymer persists at room temperature. It has since been observed that when irradiation takes place at a higher temperature, close to the melting point of polyethylene, the same degree of radiation and crosslinking (about 5–10 %) produces a polymer which is substantially amorphous even at room temperature. This difference is ascribed to the fact that during irradiation at these higher temperatures, the molecules are disorientated. The crosslinking produced then prevents the molecules realigning themselves at lower temperatures to produce crystalline regions.

This new material is very different from the usual crosslinked polythene. Apart from a yellow tint, which occurs in all long-chain polymers on irradiation, it is transparent, and very flexible. In ordinary polyethylene, or in polyethylene irradiated at a lower temperature, there is a sudden change in slope in the specific volume/temperature curve in the neighbourhood of the melting point (about 115°). This change arises from the transformation of the amorphous solid or liquid into a partially crystalline material, as the temperature is lowered. No such change is observed in the new type of crosslinked material, indicating that no appreciable amount of crystallinity is present, even at room temperature. This enables us to study the specific volume/temperature curve of the amorphous material over a much wider range.

In a previous paper (Charlesby and Ross 1953) it was shown that in the completely amorphous region (above 115°) an equation of state can be set up, relating specific volume V (reciprocal of density), external pressure P, degree of crosslinking c, and absolute temperature T.

$$(P+P_0(c))(V-V_0)=\frac{RT}{M}, \quad . \quad . \quad . \quad . \quad . \quad . \quad . \quad (1)$$

In this equation the internal pressure $P_0(c)$ is independent of volume V and temperature T, and increases with the degree of crosslinking c.

* Communicated by the Author.

The 'residual' volume V_0 obtained by extrapolation of the specific volume of amorphous polyethylene down to 0°K, varies slightly, if at all, with c. M is the molar weight of the C_2H_4 unit (28). Previous results give $P_0(0) \sim 3 \times 10^9$ dynes/cm², $V_0 \sim 0{\cdot}88$ cm³/g. This equation is somewhat analogous to the Van der Waals equation:

$$\left(P + \frac{a}{V2}\right)(V-b) = \frac{RT}{M}, \quad \ldots\ldots \quad (2)$$

which has been used to describe the relationship between volume, pressure and temperature for gases and liquids but a/V^2 is replaced by $P_0(C)$ which does not vary with V. With the polyethylene previously studied it was not possible to distinguish clearly between these two equations over the limited range of temperatures available in the amorphous region above 115°C. Using the new form of crosslinked polythene which is amorphous down to room temperature a more satisfactory comparison between the two equations can be made.

§ 2. Density Measurements

Rods of polyethylene, after annealing at 90°C to remove internal stress and orientation, were irradiated in the centre of the BEPO, at temperature of about 90–100°C. The radiation dose was monitored by cobalt specimens, where radioactivity gave a measure of the slow neutron flux. The fast neutron and gamma flux could not be measured separately, but were proportional to slow neutron flux. All radiations were carried out at constant pile power, and in a fixed position in the pile, so that the radiation dose was proportional to exposure time. Unit radiation dose is taken as a slow neutron flux of 10^{17} slow neutrons/cm², plus the associated fast neutron and gamma flux.

Small specimens weighing some three grams were cut from the irradiated rods, and the surface removed to avoid any surface oxidation effects. These specimens were weighed in silicone fluid (previously calibrated against a copper specimen of known density) over a range of temperatures, sufficient time being allowed for thermal equilibrium to be attained. Two typical curves for the specific volume are shown in fig. 1.

§ 3. Comparison with Equations of State

At negligible external pressure eqn. (1) predicts a linear variation in specific volume V with temperature. Equation (2) gives a relationship which is only approximately linear. To show more clearly the relationship between volume and temperature in the latter case the Van der Waals equation may be expressed in terms of the critical volume V_c, pressure P_c and temperature T_c:

$$\left(\alpha + \frac{3}{\beta^2}\right)\left(\beta - \frac{1}{3}\right) = \frac{8}{3}\gamma$$

where $\alpha = P/P_c$, $\beta = V/V_c$, $\gamma = T/T_c$. In our cases $\alpha = 0$, since $P = 0$. A plot of β against γ (proportional to a plot of V against T) is shown in fig. 2 in the relevant region.

To obtain the values of V_c and T_c for a given specimen the ratio $(V-V_0)/V$ at a given temperature is calculated by extrapolating the linear portion of the observed specific volume/temperature curve to 0°K to give V_0. If β_0 is the corresponding volume ratio V_0/V_c, then

$$\frac{V-V_0}{V}=\frac{\beta-\beta_0}{\beta}=\frac{\gamma d\beta}{d\gamma}\frac{1}{\beta}=\frac{9\beta-3}{6-9\beta}.$$

Fig. 1

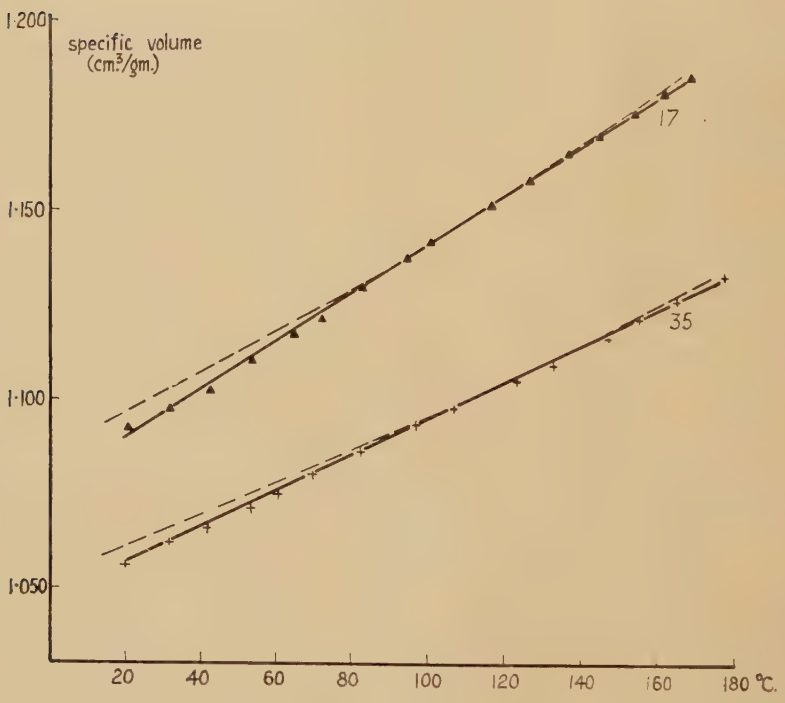

Specific volume of amorphous crosslinked polyethythene.
(17 and 35 units of radiation.)

▲ + observed specific volume.
———— calculated from eqn. (1).
— — — calculated from V. d. Waals eqn. (2).

By solving this equation for β in terms of $(V-V_0)/V$ a value for V_c may be deduced. The corresponding values for T_c and P_c can then be obtained. The following table shows the value for the critical constants for specimens subjected to varying degrees of irradiation. The approximate degree of crosslinking is also shown, taking a value of 0·5% of carbons being cross-linked per unit radiation, as deduced from the variation in the C/H ratio.

Figure 1 shows the observed specific volume/temperature curve, and that calculated from the Van der Waals equation using the above values, which were in fact calculated to give the correct slope at 127°C. It is

Critical Constants in Van der Waals Equation

Radiation Dose Units	3·86	7·12	9·36	17	35	54·5
Crosslinked Carbons (%)	1·9	3·6	4·7	8·5	17·5	27·3
V_c (cm³/g)	3·04	2·99	3·00	2·95	2·90	2·86
T_c (°K)	800	810	833	934	1070	1170
P_c (10^8 dynes/cm²)	2·94	3·03	3·09	3·53	4·11	4·56
$b = V_c/3$	1·01	1·00	1·00	0·98	0·97	0·95

Fig. 2

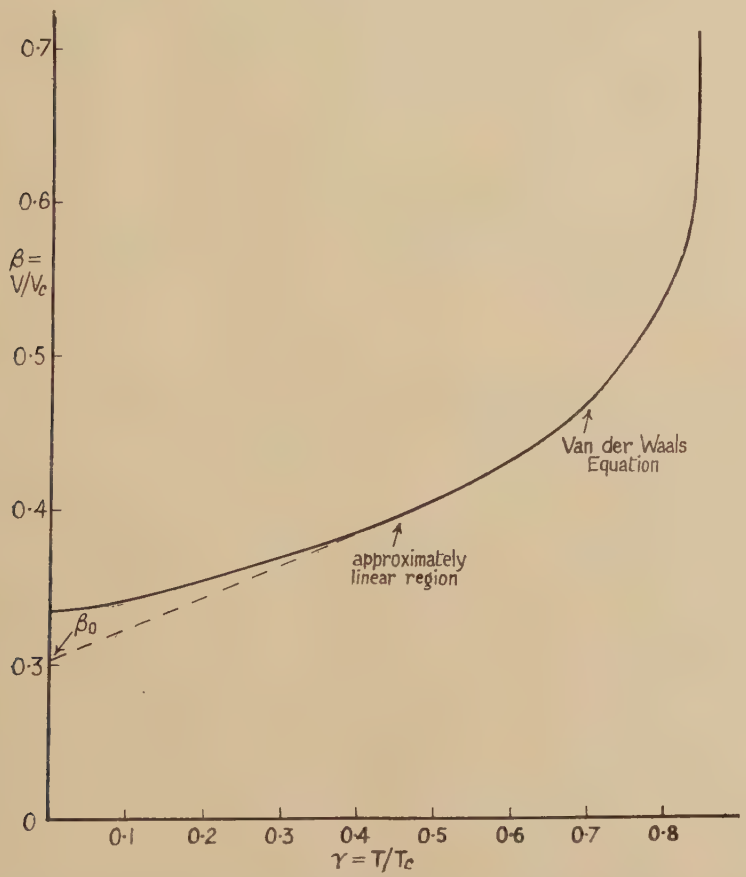

Volume/Temperature curve calculated from Van der Waals equation (assuming external pressure is zero).
Approximate linear region extrapolated to give β_0 at 0° K.

seen that there is a distinct curve in the plot of the Van der Waals equation. The experimental data gives a linear plot, in agreement with eqn. (1).

It is concluded that the Van der Waals equation offers a less satisfactory representation of the volume/temperature for amorphous polyethylene than does eqn. (1) which assumes a constant internal pressure $P(c)$ for a given degree of crosslinking. For rubber vulcanized to varying extents the specific volume/temperature curves likewise given linear plots over a considerable range of temperatures (Scott 1935). A relationship similar to (1) has also been shown to hold for other amorphous long-chain polymers, at least when uncrosslinked (Spencer and Gilmore 1950), so that this conclusion would appear to be true for all such amorphous materials. Richards (1924) has used an equation similar to (1) except for the temperature coefficient, to represent the equation of state of a number of metals. In his results the internal pressure $P(0)$ varies from 4×10^9 dynes/cm^2 for Cesium to 632×10^9 for Tungsten. For uncrosslinked polyethylene we find 3×10^9 dynes/cm^2. The Dicterici equation of state cannot be applied to these polymers, since it gives an infinite volume when the external pressure is zero.

Acknowledgments

The author wishes to thank the Director, A.E.R.E. for permission to publish this note, and Dr. H. M. Finniston for his interest in the general programme of research on the effects of radiation on polymers.

References

Charlesby, A., 1952, *Proc. Roy. Soc.* A, **215,** 187.
Charlesby, A., and Ross, M., 1953, *Proc. Roy. Soc.* A, **217,** 122.
Richards, T. W., 1924, *J. A. C. S.*, **46,** 1419.
Scott, A. H., 1935, *J. Res. N. B. S.*, **14,** 99.
Spencer, R. S., and Gilmore, G. D., 1950, *J. Appl. Phys.*, **21,** 523.

LXIII. *The Angular Distribution of Alpha Particles from the Proton Bombardment of* ^{18}O

By A. V. Cohen
Cavendish Laboratory, Cambridge*

[Received March 25, 1953]

Summary

Interference effects in the angular distribution of alpha particles from the reaction $^{18}O(p, \alpha)$ have been investigated over the range 430 to 890 kev proton energy. The experimental results have been fitted in terms of a series of overlapping levels. It is found that the levels in ^{19}F formed by resonant capture of protons of energy 640 kev and 850 kev have spins 3/2 and 1/2 respectively, and are of opposite parity to the level which gives the main contribution to the yield away from these energies, and which has a spin of 1/2. It is a feature of this reaction that absolute parities cannot be found from the study of the angular distributions.

§ 1. Introduction

The reaction $^{18}O(p, \alpha)$ was first observed by Burcham and Smith (1939). Freeman (1950) made a magnetic analysis of the alpha particles emitted at 90° and found a single Q-value of $3{\cdot}97 \pm 0{\cdot}05$ mev.

Mileikowsky and Pauli in a short note (1950) and a fuller paper (1951) described a study of the excitation curve of the alpha particles emitted at 90° with protons of variable energy between 420 and 740 kev. They found a small but definite resonance at 680 kev and a much less pronounced but repeatable irregularity at 600 kev superposed on a rising background.

Seed (1951) measured the excitation curve up to 960 kev proton energy by using magnetic analysis of the particles emitted at 120°. He found a resonance at 640 kev ; above this the yield passes through a pronounced maximum at 850 kev, and the yield at 950 kev is lower than that at 500 kev. No irregularity in the curve was observed below 640 kev proton energy, but not enough points were taken in the region where this small irregularity might be expected.

It will be noted that there is a discrepancy of 40 kev between the resonance energies quoted by Seed and by the Swedish workers. During the present work the excitation curve at various angles has been determined. Changes in angular distribution near 640 kev are such that

* Communicated by A. P. French.

the peak yield at 90° occurs about 5 kev higher than that at 120°; apart from this the present results agree with Seed's within 5 kev. An irregularity in the excitation curve was found at 560 kev which presumably corresponds to that found by Mileikowsky and Pauli at 600 kev, though we cannot account for the discrepancy in energy.

It is hard to explain the high yield between the comparatively narrow levels at 640 kev and 850 kev except by assuming that one or more excited states in the compound nucleus exist in this region, and if this hypothesis is true the states of the compound nucleus must overlap appreciably. One might then expect to observe interference effects varying with proton energy, which are most easily discovered by a study of the angular distribution of the emitted alpha particles. The present paper describes such measurements.

§ 2. Experimental Technique

2.1. *Apparatus*

It was decided to detect the alpha particles with proportional counters placed inside the vacuum chamber containing the target. Two counters were used throughout, one being used as a monitor at a fixed angle, while the position of the other could be varied. Scattered protons were removed by absorbers placed before the counters ; the absorber thickness was adjusted for a given angle and bombarding energy to secure the optimum pulse size. This technique was found practicable up to 890 kev proton energy, if proportional counters of short collection time (~1 microsecond) and amplifiers of even shorter time constant (~0·2 microsecond) were used so as to avoid ' pile-up ' of the small pulses due to the residual protons which enter the counters. Angular distributions were followed as far forward as 30° up to the 850 kev resonance, but only to 90° at 890 kev bombarding energy : a limit was reached when the difference between alpha range and proton range fell to 3 mm. The targets were prepared by forming an ^{18}O-enriched layer of oxide on a copper sheet by Seed's technique (Seed, *loc. cit.*).

The two counters were mounted in a cylindrical tank 12 in. in diameter and 5·2 in. deep (see fig. 1). In it were set two portholes P for viewing the target T. Protons from the 1 Mv High Tension Set entered the apparatus after being collimated by a series of aluminium stops and an $\frac{1}{8}$ in. molybdenum stop placed at the entrance to the tank.

The proportional counter C was mounted inside the tank on an arm L fixed to a cylindrical block M. It could thus be rotated about the axis of the tank by means of a lever outside. The vacuum was maintained by means of Gaco rings. The lead (not shown) from the counter anode was connected to the Cathodeon metal-glass seal F and thence to a standard high-frequency pre-amplifier. The monitor counter N was fixed so as to receive particles emitted at 90° to the proton beam. Collodion foils K of various stopping powers could be placed in front of the counter N by turning the cylindrical block R (similar to M). Through M and R passed

two smaller cylindrical blocks, H and U respectively, each of which could be turned from outside the vacuum. U carried the target T, and H carried a crown wheel G by means of which a wheel J mounted on L could be turned. J carried six collodion absorbers which could thus be placed successively in front of C.

The scale by which the angular position of L could be measured was checked optically ; the error in the scale was less than a degree and has been allowed for.

Fig. 1

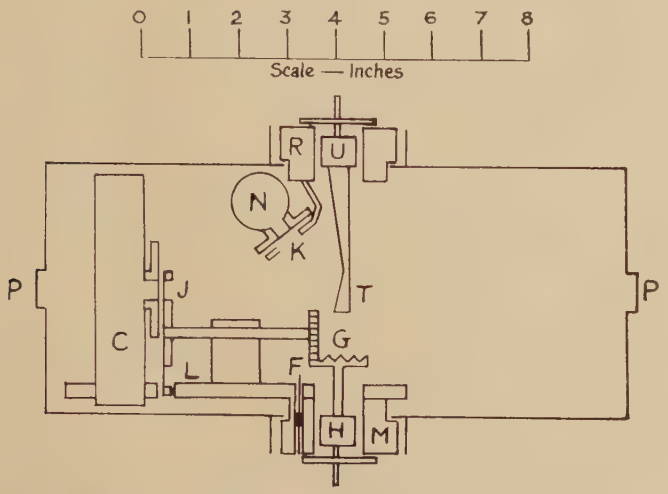

Diagrammatic view of apparatus : section at right angles to incoming proton beam.

The apparatus just described was found suitable for work down to about 580 kev proton energy ; below this the observed yield was too small. In order to examine the angular distributions at lower energies the apparatus was modified somewhat. At low energies no absorbing foils of any sort were needed, since the counter windows were thick enough to exclude any scattered protons. The counters could thus be moved much nearer the target. To reduce beam wandering, the molybdenum stop was supported about $1\frac{1}{2}$ in. from the target.

The apparatus in both forms was checked for inherent asymmetry after experimental runs by placing small thorium $C+C'$ alpha sources where the beam had struck the target. No departure from isotropy greater than $\frac{1}{2}\%$ with the earlier modification, and 3% with the later modification, was found.

2.2. *The Counters and Absorbers*

The proportional counters were designed to have collection times of about 1 microsecond and a gas amplification of about 40 for 700 volts on the anode. The windows, let into the sides of the counters, were of mica, 15 mm air equivalent stopping power.

The absorbers were made of collodion, and their air equivalents were measured to within 0·2 mm in an auxiliary apparatus. The wheel J carried absorbers of 0, 1, 2, 3, 4 and 5 mm stopping power, while the absorbers K in front of the monitor counter were 0, 1, 3 and 5 mm. No absorber was used if it caused undue straggling, or if it was less than 99% transparent.

The voltage to the anode was supplied by two standard stabilized power packs, through 5 MΩ resistors. The anodes were connected through 80 pf coupling condensers to the inputs of standard high-frequency pre-amplifiers. These led to commercial amplifiers, type 1008, with both integration and differentiation time constants set at 0·2 microseconds, and the outputs of these were connected through discriminators to scales of 1000.

2.3. *Beam Energy Definition*

The voltage of the High Tension Set is subject to a 30 kv ripple. To improve the energy definition of the beam an adjustable slit was placed at its focus just outside the deflecting magnet. Tests showed that the 'ripple' in the beam with a $\frac{3}{4}$-mm slit (the working width) was about ± 3 kev at ~ 700 kev. This was considered satisfactory for our purpose.

2.4. *Experimental Procedure*

(a) Angular Distributions

The counter C was set to various positions with the target at a fixed angle to the incident proton beam, and the number of alpha counts in each counter was observed for a given quantity of incident proton beam, as recorded by a current integrator. For the lower proton energies (<750 kev) bias curves at the extreme angles were taken, and the discriminators set at the appropriate biases; no absorbers were needed. Above this energy, bias curves were taken at each setting of C, and the appropriate absorber was selected for each counter.

With the earlier modification of the apparatus, the target was set at 45° to the incident proton beam and the ratio of counts in the two counters was determined at 10° intervals from 160° (the maximum attainable in practice) to 60°, the angles being taken at random. This process was repeated and then the target was set at 15° to the beam, and the measurements extended as far forward as 30° as well as at several backward angles. (With the later modification of apparatus only the angles between 145° and 40° could be explored.) Measurements were taken four times in random order, and then the target was reset to the 45° position, and another set of readings taken.

Readings for two different target settings were fitted so as to produce a single angular distribution curve. This seemed to be justified, for if the best curve of a given sort were fitted both to the backward points only, and to all the points, the two curves were never found to be significantly different from each other at the 5% level of significance.

With this procedure the only effect of a random beam wandering would be to make the points scatter about the best curve rather more than would be expected from the statistical error in each point. No serious effect of this nature was ever observed.

Angular distributions were taken at about 50 kev intervals from 850 kev down to 430 kev ; the yield was too small to be readily measurable below this point.

(*b*) *The* $I(150°)/I(90°)$ *Curve*

It is of doubtful value to take complete angular distributions at more than a few energies. From the practical point of view, it would take far too much time, and the deposit of carbon upon the target surface would render the energy scale uncertain in a lengthy run. Moreover, one would not expect very rapid changes of angular distribution with energy, except near narrow resonances where there may be quite drastic changes. To have some measure of such changes it was decided to observe the variation with energy of the ratio of the emitted intensities at two fixed angles. The monitor counter was fixed at 90° and the other counter (with the earlier modification of the apparatus) at 150° ; the excitation curves were determined simultaneously using a current integrator to monitor the target current. Complete angular distributions were then taken at those energies which a study of this curve suggested were of interest.

In the range 580 kev to 750 kev, bias curves were taken at extreme voltages and a suitable bias chosen. The excitation curves were then directly determined, and the absolute value of $I(150°)/I(90°)$ deduced by frequent measurements with the counter C at 90°. Above 750 kev it was considered wiser to normalize at 90° between each pair of determinations at 150°, taking the bias curves each time. Scattered protons made it impossible to observe above 890 kev. A suitable mean was taken of six runs, using two different targets.

At the lower energies, with the later modification of the apparatus, observations were taken at 140° and the results extrapolated to 150° assuming angular distributions of the type $1+a\cos\theta$, to which the observed angular distributions conformed closely over this energy region. A mean of eight runs with two targets was taken between 510 and 600 kev, and of twelve runs with three targets between 430 and 510 kev.

The voltage scale was established in the following manner. Seed had found that the higher resonance occurred at 850 kev by comparing it with the $^{19}F(p, \alpha\gamma)$ resonance at 874 kev. Taking this value as well-established, the true position of the lower resonance was found to be 635 kev at 150° and 640 kev at 90° to within 2–3 kev. This value of the resonant energy could then be used to establish the voltage scale in the lowest energy regions. Observations were taken at 10 kev intervals, except near the resonance at 640 kev and the suspected resonance at 560 kev where 5 kev intervals were taken.

The value of $I(150°)/I(90°)$ thus obtained is only a true measure of departure from isotropy if the apparatus is truly isotropic. Measurements

were always repeatable, within the expected limits of error, and always agreed closely with values obtained from angular distribution measurements. The apparatus was tested for isotropy with a natural source as described earlier—the observed departures from isotropy are not considered significant and have not been corrected for. The two parts of the $I(150°)/I(90°)$ curve, determined with the two modifications of the apparatus, joined together to within about 4%—just about the sum of the two expected *statistical* errors in each quantity: this may be taken as a measure of the limit of cumulative effects due to systematic errors of this sort.

All angular distributions, and the $I(150°)/I(90°)$ curve, are corrected for centre-of-mass motion.

§ 3. Results

3.1. *Excitation Curve*

The excitation curve observed at 90°, a synthesis of many runs, is shown in fig. 2. Following Mileikowsky and Pauli, we have divided the yield by the proton and alpha penetrabilities for s-waves as calculated from the tables of Bethe (1937) and multiplied the result by the proton energy (inversely proportional to $\pi\lambda^2$). This reduces the yield to a specifically nuclear function, which should presumably be of the form of a Breit–Wigner dispersion curve for each level.

The curve follows the main features of the excitation curves found both by Seed and by Mileikowsky and Pauli, except for the apparent displacement of the voltage-scale for the latter workers. We have fitted the best Breit–Wigner curve to the reduced yields for the resonances at 640 kev and at 850 kev. When these two curves are subtracted from the observed yield curve, the ' residual resonance curve ', also shown in fig. 2, is obtained. This contains the slight but repeatable discontinuity at 560 kev already mentioned, though it cannot be shown very clearly. It is evident from the shape of the residual curve that there are probably at least two rather broad states between the resonances at 640 kev and 850 kev. The 640 kev resonance appears to have a width of about 15 kev and the 850 kev resonance a width of about 45 kev. Mileikowsky and Pauli quote a width of about 100 kev for the level at 560 kev, but it would seem difficult to confirm this.

From the apparent width of the 640 kev level one may infer an upper limit to the target thickness, and so deduce that the integrated cross-section for the reaction is greater than 0·035 barns at 660 kev proton energy and greater than 0·25 barns at 850 kev.

3.2. *The* $I(150°)/I(90°)$ *Curve*

This curve is shown in fig. 3, together with the observed excitation curve at 150°. The most prominent feature is the sharp peak at 630 kev, representing the violent change in angular distribution as we pass through the 640 kev resonance. The peak occurs some 10 kev lower than the resonance proper.

Near the higher resonance $I(150°)/I(90°)$ drops to 0·75 ; this change is presumably connected in some way with the higher resonance. There is also a broad bump in the curve, with a maximum at about 540 kev ; this may possibly be correlated with the weakly-excited level which is suspected at 560 kev.

Fig. 2

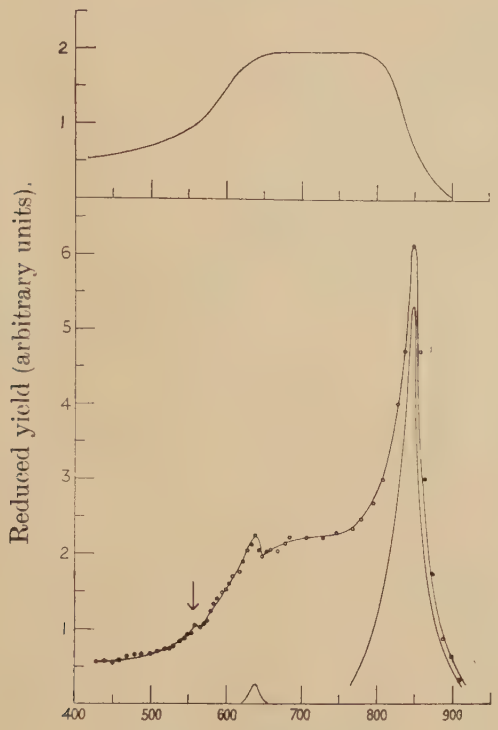

' Reduced excitation curve.' Yields have been divided by proton and alpha penetrabilities, and multiplied by proton energy. The upper curve shows the residual reduced yield after subtracting the yields due to the 850 kev and the 640 kev resonances. The arrow points to the discontinuity at 560 kev.

As will be described later, an interpretation of this curve is possible at the lower energies ; such a fit is shown in fig. 3 by the full curve.

3.3. *Angular Distributions*

Angular distributions were determined at many energies and each of them was fitted twice assuming it to be alternatively linear or parabolic in $\cos\theta$. The variance ratio test was then applied to find if the improvement in fit by taking the parabolic term was at all significant. If it was significant to better than the 5% level, it was assumed that there was a genuine $\cos^2\theta$ term in the angular distribution. A description of the variance ratio test is given by Quenouille (1950).

Angular distributions are found to be always of the form $1+a\cos\theta$ except near the 640 kev resonance, where four separate angular distributions (two with the earlier and two with the later modifications of the apparatus) showed significant terms in $\cos^2\theta$. The cumulative significance

Fig. 3

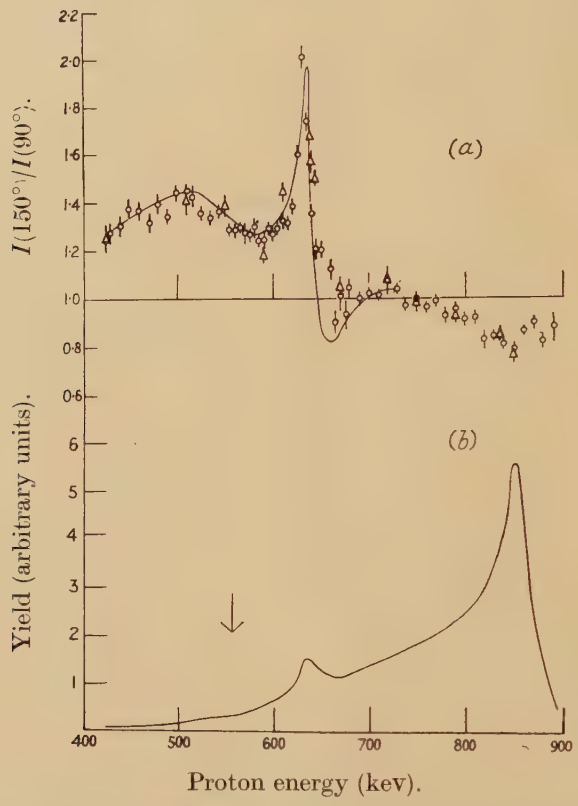

(*a*) Variation of $I(150°)/I(90°)$ with proton energy. Triangles represent points obtained from angular distributions. The full curve is obtained by the method described in the text. (*b*) Excitation curve at 150° (same energy scale as (*a*)). The arrow points to the position of the discontinuity at 560 kev.

of the parabolic term is about 10^6 : 1. This rather delicate variance ratio test is invaluable in detecting a weak parabolic term in the presence of a strong linear term.

In fig. 4 we show some typical angular distributions.

§ 4. Theory

4.1. *General Discussion*

Miller, Javan and Townes (1951) have found that the spin of the ^{18}O nucleus is 0, while Krüger (1938) and Wood and Dieche (1938) have shown that the spin of ^{15}N is 1/2. These conclusions were reached from

a study of band spectra. Any reasonable model of nuclear structure will predict even parity for the ^{18}O nucleus, and the shell model predicts odd parity for the ^{15}N nucleus (Hornyak *et al.* 1950). We shall work out the expected angular distribution patterns assuming these parities, and later examine the effects of the opposite assumptions. The proton

Fig. 4

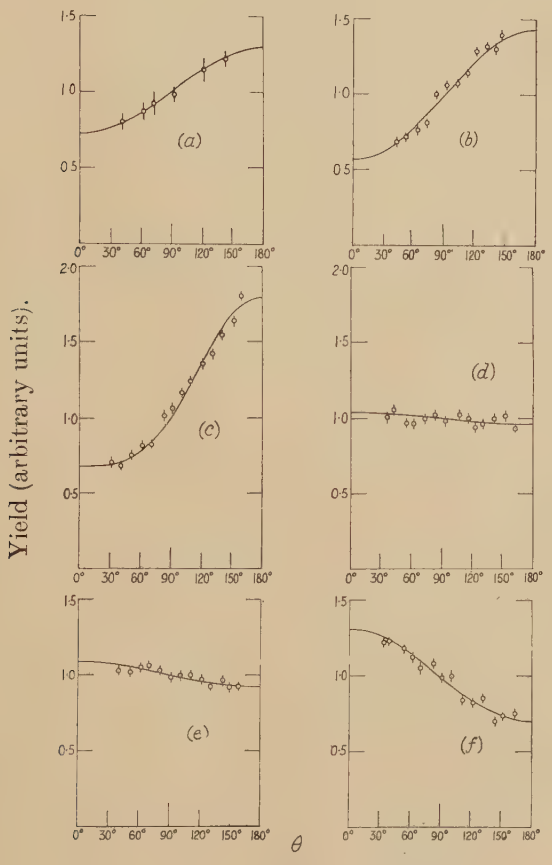

Some observed angular distributions.

(*a*) 430 kev : $(1 \pm 0{\cdot}02) - (0{\cdot}28 \pm 0{\cdot}05) \cos\theta$
(*b*) 550 kev : $(1 \pm 0{\cdot}01) - (0{\cdot}44 \pm 0{\cdot}02) \cos\theta$
(*c*) 635 kev : $(1 \pm 0{\cdot}02) - (0{\cdot}57 \pm 0{\cdot}03) \cos\theta + (0{\cdot}22 \pm 0{\cdot}05) \cos^2\theta$
(*d*) 720 kev : $(1 \pm 0{\cdot}01) + (0{\cdot}025 \pm 0{\cdot}015) \cos\theta$
(*e*) 790 kev : $(1 \pm 0{\cdot}01) + (0{\cdot}075 \pm 0{\cdot}04) \cos\theta$
(*f*) 850 kev : $(1 \pm 0{\cdot}015) + (0{\cdot}03 \pm 0{\cdot}02) \cos\theta$

is known to be (1/2, +) and the alpha particle to be (0, +). The initial and final spin states are then (1/2, +) and (1/2, −) respectively. It immediately follows that a given state of the compound nucleus ^{19}F, of definite spin and parity, can be formed only by protons of one definite orbital angular momentum l and can break up only by the emission of alpha particles of one definite orbital angular momentum l'.

This means that the angular distribution expected from a state of definite spin and parity does not contain any unknown parameters at all, and the interference effects between two or more nuclear levels are very simple in form. Moreover, the angular distribution of alpha particles from the reaction ^{18}O(p, α) through the level (J, +) (formation *without* parity change, break-up *with* parity change), must by the principle of microscopic reversibility be the same as the angular distribution at the corresponding energy of the reverse reaction ^{15}N(α, p) (formation *with* parity change, break-up *without*), through the level (J, +). As we have seen that the angular distributions in this reaction depend only on spatial terms such as spin and parity change, and do not depend on specifically nuclear terms, it follows that this angular distribution must also be that of the ^{18}O(p, α) reaction through the level (J, −) (formation *with* parity change, break-up *without*). Thus angular distributions through isolated levels of the same J but opposite parity will be identical, and this result can be extended to any number of interfering levels providing their relative strengths are given. For example, the interference between two levels (3 2, +) and (1/2, −) will be identical in form with that between (3/2, −) and (1/2, +), and *absolute* parities of compound nuclei in this reaction cannot be determined from the angular distributions, though it is possible to say whether two levels have the same parity or not. Furthermore, it may similarly be proved that the angular distributions expected are independent of the parities of the ^{18}O or ^{15}N nuclei.

4.2. *Detailed Theory*

We shall work out the case of two overlapping levels, one of resonant energy E_1, width Γ_1, spin J_1, formed by protons of orbital momentum l_1 and breaking up to give alpha particles of orbital momentum l_1', and the other level with corresponding quantities, E_2, Γ_2, J_2, l_2 and l_2'. The initial and final spins of the system, j and j', can only take the value 1/2. (For earlier examples of such calculations, see Devons and Hine (1950) or Thomson *et al.* (1952).)

The differential cross section at a given energy E then takes the form :

$$\sigma(\theta,E)\sim\left|\begin{array}{l}\langle l_1\tfrac{1}{2}0\tfrac{1}{2}\,|\,J_1\tfrac{1}{2}\rangle\langle l_1'\tfrac{1}{2}0\tfrac{1}{2}\,|\,J_1\tfrac{1}{2}\rangle\dfrac{Ae^{i\alpha}}{E-E_1+\frac{1}{2}i\Gamma_1}\,Y^0_{l_1'}(\theta,\phi)\\ +\langle l_2\tfrac{1}{2}0\tfrac{1}{2}\,|\,J_2\tfrac{1}{2}\rangle\langle l_2'\tfrac{1}{2}0\tfrac{1}{2}\,|\,J_2\tfrac{1}{2}\rangle\dfrac{Be^{i\beta}}{E-E_2+\frac{1}{2}i\Gamma_2}\,Y^0_{l_2'}(\theta,\phi)\end{array}\right|^2$$

$$+\left|\begin{array}{l}\langle l_1\tfrac{1}{2}0\tfrac{1}{2}\,|\,J_1\tfrac{1}{2}\rangle\langle l_1'\tfrac{1}{2}1\bar{\tfrac{1}{2}}\,|\,J_1\tfrac{1}{2}\rangle\dfrac{Ae^{i\alpha}}{E-E_1+\frac{1}{2}i\Gamma_1}\,Y^1_{l_1'}(\theta,\phi)\\ +\langle l_2\tfrac{1}{2}0\tfrac{1}{2}\,|\,J_2\tfrac{1}{2}\rangle\langle l_2'\tfrac{1}{2}1\bar{\tfrac{1}{2}}\,|\,J_2\tfrac{1}{2}\rangle\dfrac{Be^{i\beta}}{E-E_2+\frac{1}{2}i\Gamma_2}\,Y^1_{l_2'}(\theta,\phi)\end{array}\right|^2$$

plus similar terms for $j_z=-\frac{1}{2}$ where $\langle ljl_zj_z|JJ_z\rangle$ are the appropriate transformation coefficients as listed by Condon and Shortley (1935 *and* 1951)

and the Y's are normalized spherical harmonics. (A, α) and (B, β) refer to the amplitudes and phases of the states of spin J_1 and J_2 respectively, including penetrability effects.

We can simplify the expression if we now put

$$R_1=\{(E-E_1)^2+\tfrac{1}{4}\Gamma_1^2\}^{1/2} \qquad R_2=\{(E-E_2{}^2)+\tfrac{1}{4}\Gamma_2{}^2\}^{1/2}$$
$$\tan\delta_1=\Gamma_1/2(E-E_1) \qquad \tan\delta_2=\Gamma_2/2(E-E_2).$$

A case of especial interest in this experiment is that for which the level 1 is $(1/2, +)$ and the level 2 is $(3/2, -)$. For this

$$\sigma(\theta, E)\sim\frac{A^2}{3R_1{}^2}+\frac{B^2}{R_2{}^2}(1+3\cos^2\theta)$$
$$+\frac{4\sqrt{3}}{3}\frac{AB}{R_1R_2}\cos\theta\cos\{(\alpha-\beta)-(\delta_1-\delta_2)\}.$$

We now put $r(E)=(R_1/R_2)$; $x=(\sqrt{3}B/A)p(E)$, where $p(E)$ is the appropriate ratio of amplitude penetrabilities for incoming protons and outgoing alpha particles and is a slowly varying function of E, so that x may be considered constant. We also put $\{(\alpha-\beta)-(\delta_1-\delta_2)\}=\phi(E)$ where $(\alpha-\beta)$ may be considered constant, and so have

$$\sigma(\theta, E)\sim 1+x^2r^2(1+3\cos^2\theta)+4xr\cos\phi\cos\theta.$$

Thus $x^2r^2=\dfrac{\text{intensity at } 90^\circ \text{ due to state } (3/2, -)}{\text{intensity at } 90^\circ \text{ due to state } (1/2, +)}$.

The phase difference ϕ determining the interference term in $\cos\theta$ is the difference between $(\delta_1-\delta_2)$, which can be calculated as a function of energy, and the unknown phase factor $(\alpha-\beta)$ representing a difference in inherent phases of nuclear levels. The parameter x represents the relative inherent amplitudes of the levels.

Table of Expected Interference Patterns

Interfering levels	Expected Interference Pattern
$\frac{1}{2}+$ and $\frac{1}{2}-$	$1+x^2r^2+2xr\cos\phi\cos\theta$
$\frac{3}{2},\pm$ and $\frac{1}{2},\mp$	$1+x^2r^2(1+3\cos^2\theta)+4xr\cos\phi\cos\theta$
$\frac{3}{2},\pm$ and $\frac{1}{2},\pm$	$1+x^2r^2(1+3\cos^2\theta)+2xr\cos\phi\,(3\cos^2\theta-1)$
$\frac{3}{2},+$ and $\frac{3}{2},-$	$(1+x^2r^2)(1+3\cos^2\theta)+2xr\cos\phi\,(9\cos^3\theta-5\cos\theta)$
$\frac{5}{2},\pm$ and $\frac{1}{2}\mp$	$1+x^2r^2\,(1-2\cos^2\theta+5\cos^4\theta)+2xr\cos\phi\,(5\cos^3\theta-3\cos\theta)$

The angular distribution patterns expected from other pairs of interfering levels may be calculated and are displayed in the table. Each angular distribution pattern is of the form :—

$$F(\theta)+x^2r^2\,G(\theta)+xr\cos\phi\,I(\theta)$$

where $F(\theta)$ and $G(\theta)$ are the angular distributions of the two levels if they were separate, and the integral of the interference term $I(\theta)$ over the whole sphere vanishes. If the two levels are of the same parity, $I(\theta)$ is an even function of $\cos(\theta)$. x, r, and ϕ have a similar significance to those quantities in the previous example.

Because the interference term always depends on xr while the term in $G(\theta)$ varies as x^2r^2, a weakly-excited level may well give rise to an observable interference term when the component $G(\theta)$ of the angular distribution is too low in intensity to be noticed.

We shall finally quote the formula describing the interference of the three levels (a) $(1/2, +)$, (b) $(1/2, -)$, and (c) $(3/2, +)$. Let the phases (α, δ_1), (β, δ_2), (γ, δ_3), refer to these three levels respectively, and let the quantity x^2r^2 measure $(b)/(a)$ and the quantity y^2s^2 measure $(c)/(a)$. Then :—

$$\sigma(\theta, E) \sim 1 + x^2r^2 + y^2s^2(1+3\cos^2\theta) + 2xr\cos\{(\alpha-\beta)-(\delta_1-\delta_2)\}\cos\theta + 4xyrs\cos\{(\beta-\gamma)-(\delta_2-\delta_3)\}\cos\theta + 2ys\cos\{(\gamma-\alpha)-(\delta_3-\delta_1)\}(3\cos^2\theta-1).$$

The same formula applies, *mutatis mutandis*, to the interference of levels of spin $(1/2, -)$ $(1/2, +)$ $(3/2, -)$.

§ 5. Comparison with Experiment

Since there is no sign of a $\cos^2\theta$ term in the angular distribution near the strongly-excited higher resonance, we can conclude that the 850 kev resonance is a level of spin 1/2. Similarly, because the angular distribution between the 640 kev resonance and the 850 kev resonance is predominantly isotropic, the spin of the level or levels giving the greatest contribution to the yield in this region is also 1/2. We shall refer to this broad state or states as ' the background of spin 1/2 '.

Since $\cos^2\theta$ terms are observed near the 640 kev resonance this level presumably has spin 3/2 ; the $\cos^2\theta$ term is of small size because this level is weakly excited. The rapidly-varying strong cosine terms observed near 640 kev suggest that this level is of opposite parity to the background (or possibly to the weakly-excited level at 560 kev, though this alternative would not give rise to such strong cosine terms and may therefore be neglected).

It seems very likely that the broad bump at low energies in the $I_{150^\circ}/I_{90^\circ}$ curve, and the fairly strong cosine terms, are due to interference between the back-ground and a weakly-excited state, presumably that at 560 kev, of opposite parity and of spin either 1/2 or 3/2. The bump in the curve could be taken as further evidence of the existence of a level at 560 kev, though such evidence must be treated with caution.

To fit a curve to the experimental points below 720 kev it is necessary to know the resonant energy and width of each level. We assume that the 560 kev level has a spin 1/2 and a width of 100 kev, that the level at 640 kev has a width of 15 kev, and also that there is one background

level, of spin 1/2, at 680 kev and of 200 kev width. This last assumption is entirely arbitrary ; we do not know the number of background levels, or their positions and widths. This assumed background must have opposite parity to the two other levels, to produce the observed interference effects.

The general formula for three such overlapping levels was quoted earlier. There are four parameters to be found : x and y, and $(\alpha-\beta)$ and $(\beta-\gamma)$. It was first assumed that in the lowest energy regions only the two levels of spin 1/2 were effective. By a method of successive exclusions of ranges of phase-angle, it was possible to locate the phase-difference between these states within a small range. The centre of this was taken as the phase-difference, and a value for the relative excitations was simultaneously obtained. Similarly, in the region of the 640 kev resonance, the weakly-excited level can be neglected as a first approximation, and values of the two other parameters obtained. The four parameters were then used to predict the entire curve, and a better fit achieved by altering the parameters slightly. The curve given in fig. 3 is a result of this process ; it represents a possible fit, but if different assumptions as to the background are made, equally good fits are possible with different parameters. The parameters used predict the right size for the $\cos^2$ component near 640 kev ($\sim 0{\cdot}30$) and also predict a small $\cos^2$ term near 560 kev produced by the interference of this level with that at 640 kev. A critical test to decide whether the spin of the 560 kev level is 1/2 or 3/2 is thus difficult.

It was impossible to fit the curve on such assumptions at the highest energies, for if the level at 850 kev be assumed to have a spin of 1/2 but to be of opposite parity to the background then much stronger cosine terms than those observed would be expected. The assumption that there is only one background level breaks down, and the cosine terms at higher energies must be ascribed to yet another level in the background, which need only be very weakly excited to produce cosine terms of the size observed. The narrow resonance at 850 kev would then presumably have the same parity as the background, but the problem is too complex to be uniquely solved. Thus the parameters used in fitting the curve have no special significance, and the phase angles should not be compared with those predicted by the theory of Wigner and Eisenbud (1947) as can be done in more favourable cases (e.g. Thomson *et al.* 1952).

§ 6. Conclusion

It seems reasonably well established that the spin of the level at 850 kev is 1/2 and that of the level at 640 kev is 3/2 ; the main part of the intermediate ' background ' is due to a level (or possibly levels) of spin 1/2. The weak irregularity at 560 kev, which has been confirmed, may well correspond to a level of spin 1/2 or 3/2 ; one cannot from our results decide between these alternatives. In this reaction it is impossible to determine, from angular distributions, the absolute parity of any

state in the compound nucleus, but one can establish that the levels at both 640 kev and 560 kev have a parity opposite to the background level, whereas the level at 850 kev probably has the same parity as the background. Wigner's criterion of upper limits to reduced widths (see e.g. Wigner and Eisenbud, *loc. cit.*) is not sufficiently strong to enable one to decide the parity of the levels from knowledge of the cross-sections. The parameters used in the detailed explanation of the angular distributions have no real significance, and should not be compared with the predictions of any theory.

There seem to be at least five levels in an energy range of 500 kev, representing an excitation of the compound nucleus ^{19}F of about 8·3–8·8 Mev. This compares with the level spacing of about 130 kev at 10 Mev excitation in this nucleus found in the $^{18}O(p, n)$ reaction.

Acknowledgments

The author wishes to express his thanks to Dr. A. P. French who suggested this problem, and with whom he has had much helpful discussion during the course of this work. He is grateful to Trinity College, Cambridge, for a scholarship, and to the Department of Scientific and Industrial Research for a grant.

References

Bethe, H. A., 1937, *Rev. Mod. Phys.*, **9,** 69.
Burcham, W. E., and Smith, C. L., 1939, *Nature, Lond.*, **143,** 795.
Condon, E. U., and Shortley, G. H., 1937 and 1951, *The Theory of Atomic Spectra* (Cambridge : The University Press).
Devons, S., and Hine, M. G. N., 1949, *Proc. Roy. Soc.* A, **199,** 56.
Freeman, J. M., 1950, *Proc. Phys. Soc.* A, **63,** 668.
Hornyak, W. F., Lauritsen, T., Morrison, P., and Fowler, W. A., 1951, *Rev. Mod. Phys.*, **22,** 291.
Krüger, H., 1938, *Zeit. für Physik*, **111,** 467.
Mileikowsky, C., and Pauli, R. T., 1950, *Nature, Lond.*, **166,** 602 : 1952, *Arkiv för Fysik, Stockholm*, Band 4, No. 13.
Miller, S. L., Javan, A., and Townes, C. H., 1951, *Phys. Rev.*, **82,** 454.
Quenouille, M. H., 1950, *Introductory Statistics* (London : Butterworth-Springer).
Seed, J., 1951, *Phil. Mag.* [7], **42,** 566.
Thomson, D. M., Cohen, A. V., French, A. P., and Hutchinson, G. W., 1952, *Proc. Phys. Soc.* A, **65,** 745.
Wigner, E. P., and Eisenbud, L., 1947, *Phys. Rev.*, **72,** 29.
Wood, R. W., and Dieche, G. H., 1938, *J. Chem. Phys.*, **6,** 908.

LXIV. *The Bauschinger Effect in some Face-centred and Body-centred Cubic Metals*

By R. L. Woolley
Department of Natural Philosophy, St. Andrew's University*

[Revised MS received March 6, 1953]

Summary

The Bauschinger effect has been studied in Cu, Al, Pb, Ni and Fe, after deformations between 1% and 120%. The strain associated with the effect is shown to be approximately proportional to the stress applied to produce work-hardening, divided by the elastic modulus. It is independent of grain size. Its small dependence on temperature is explicable in terms of a thermal component of stress. It is slightly dependent on purity. The results agree with those of other workers, but disagree with the predictions of existing theories. A possible qualitative explanation of the effect is suggested.

§ 1. Introduction

If a work-hardenable metal is deformed plastically by a tensile stress $+\sigma_0$ and unloaded, its mechanical properties become anisotropic; in particular, though its tensile yield stress is now σ_0, it will deform plastically under compression stresses numerically smaller than σ_0. This is known as the Bauschinger effect. During the unloading process a very small plastic deformation usually occurs. When negative stresses are applied the rate of deformation increases steadily and when the stress reaches $-\sigma_0$ the rate of work-hardening is closely equal to that that occurred at $+\sigma_0$ before unloading. The plastic deformation that occurs between 0 and $-\sigma_0$ does not usually exhibit a well-defined compressive yield point. This is shown in fig. 3, curve A, which is a typical stress strain curve. On the other hand, material showing no Bauschinger effect would be isotropic after unloading, and would therefore possess a well-defined compressive yield point at $-\sigma_0$. Figure 3, curve B, represents such an ideal material. The Bauschinger effect is thus not so much a matter of a difference of yield points, but the existence of the non-zero strain β, which may therefore be called the Bauschinger strain.

Though the existence of the Bauschinger effect has long been recognized, comparatively little experimental work has been carried out to elucidate the effect. The effect is likely to depend on various factors, such as composition, grain size, degree of preferred orientation, amount of previous deformation, and temperature, and it is different

* Communicated by the Author.

in metals which deform by slip only, and in those which deform by slip and twinning. The present paper presents the results of a study of the effect in a selection of face-centred and body-centred cubic polycrystalline metals.

One of the factors which has made the Bauschinger effect unattractive for experimental study is the difficulty of measuring the strain. It is obviously desirable to use a homogeneous stress, which necessitates using a specimen suitable for tension and compression. The difficulty of making accurate strain measurements in the compression test is well known ; in the Bauschinger effect the strains are only a small multiple of the elastic strain. Some previous workers used headed specimens with a length/diameter ratio of about two. Under these circumstances there is considerable inhomogeneity of strain for deformations exceeding a few per cent. The advantages of the tension–compression specimen are therefore limited. In the present work the torsion test has been used. The test-piece is a tube with a wall-thickness/diameter ratio of 9. This gives an inhomogeneous strain-distribution but as shown below this is not very serious. The torsion test has the advantage that the shape of the specimen remains unaltered, and the shear strain is easily measured optically. In practice it is difficult to measure β accurately as it depends on extrapolating the initial elastic portion of the unloading curve. The strain γ is what is measured, and the elastic component must be subtracted from this to give β.

§ 2. Apparatus

(i) *Description*

The dimensions of the standard test-piece are shown in fig. 1. The wall-thickness for softer metals (Cu, Al, Pb) was usually $\frac{1}{16}$ in., but was sometimes $\frac{1}{32}$ in. for the harder metals (Fe, Ni) to suit the limited capacity of the testing machine.

The tests were carried out in the simple machine shown schematically in fig. 2. The test-piece is vertical. Its lower end is fixed, and its upper end is twisted about the vertical axis by a horizontal lever loaded by weights attached by flexible steel strip passing over pulleys. The capacity is approximately 1000 cm-kg. It is estimated that the error due to friction is less than 1% of σ_0. It is possible to carry out tests at elevated or reduced temperatures by immersing the specimen in a suitable bath.

The shear strain is measured with a telescope and scale by observing the rotation of a pair of mirrors attached to either end of the test length. The mirrors are fixed to the upper ends of a pair of coaxial nickel silver tubes, separated by a ball race. The lower ends of these tubes each carry a pair of points on one side. These points are pressed into the inner wall of the test piece by two 4 B.A. set screws passing through the wall of the end portion of the specimen. In some experiments the gauge

length was $\frac{1}{2}$ in. and the points were opposite the ends of the reduced centre section of the specimen. In other experiments the gauge length was $\frac{3}{4}$ in. and the points were opposite the 4 B.A. screws ; in this latter case an end correction is applied. The results using the two different gauge lengths were consistent. In no case was any evidence of backlash obtained. The angle between the mirrors can be read to an accuracy of 10^{-4} radian, which corresponds to a shear strain of 0·005%. The dimensions of the specimens can be measured to an accuracy of about 1%.

Fig. 1

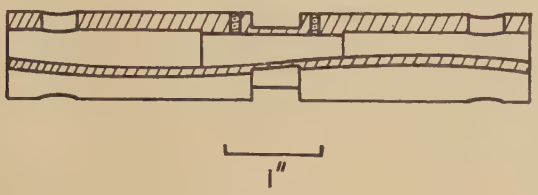

Fig. 2

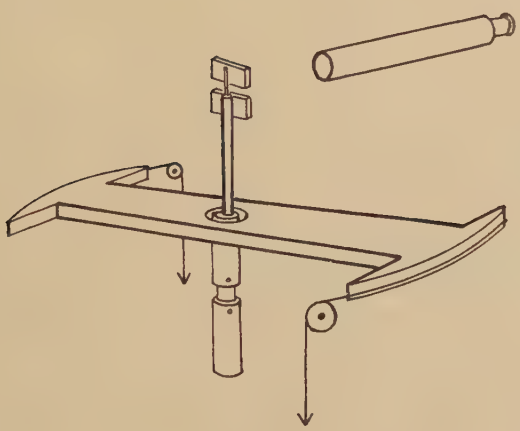

(ii) *Correction for Finite Wall Thickness*

To a first approximation the observed torque-twist diagram (τ. ϕ) with a suitable change of scale is identical with the stress–strain diagram of the metal. Owing to the finite wall thickness a small correction is needed. The exact calculation of this is difficult. But an upper limit can be found as below.

Consider a tube of length l, internal radius a and external radius b. Let $d\tau$ be the torque on an elementary tube of radius r and thickness dr. Suppose that initially during the forward deformation the shear stress is uniform over the cross-section and is σ_0. Let the specimen be unloaded from this point and let the ensuing true stress-strain curve of the metal be $\sigma(\theta)$ where θ is the shear strain. Let c be a mean radius, as yet

unspecified, between a and b. Expanding σ as a Taylor series and neglecting powers higher than the second we then have

$$\tau=\int_a^b 2\pi r^2\left[\sigma_c+(r-c)\frac{d\sigma}{dr}+\tfrac{1}{2}(r-c)^2\frac{d^2\sigma}{dr^2}\right]dr$$

$$\therefore\quad \frac{\tau}{2\pi}=\Delta_3\sigma_c+(\Delta_4-\Delta_3 c)\frac{d\sigma}{dr}+\tfrac{1}{2}(\Delta_5-2c\Delta_4+c^2\Delta_3)\frac{d^2\sigma}{dr^2},$$

where $\Delta_n\equiv(b^n-a^n)/n.$

But $\theta l=\phi r$

$$\therefore\quad d\sigma/dr=(d\sigma/d\theta)\phi/l \quad\text{and}\quad d^2\sigma/dr^2=(d^2\sigma/d\theta^2)\phi^2/l^2.$$

It is convenient to take $c=\Delta_4/\Delta_3=0{\cdot}284$ in. if $a=0{\cdot}250$ in. and $b=0{\cdot}312$ in. (This gives the correct scale for the strain. If some other value is chosen for c then there is a further correction term involving $\phi dT\,d\phi$ which automatically compensates for the difference.) The approximate solution is then $\tau=2\pi\Delta_3\sigma$, which is used to express the correction term as a function of τ, giving

$$\frac{\tau}{2\pi}=\Delta_3\sigma_c+\frac{A}{2\pi}\phi^2\frac{d^2\tau}{d\phi^2}$$

or $$2\pi\Delta_3\sigma_c=\tau-A\phi^2\,d^2\tau/d\phi^2$$

where $$A=(\Delta_5-2c\Delta_4+c^2\Delta_3)/2c^2\Delta_3$$
$$=(b-a)^2/24a^2-(b-a)^3/24a^3+\ldots.$$

This gives the true stress at radius c, the corresponding true strain being given by $\theta=\phi c/l$. If initially during the forward deformation the material is work-hardening, the stress at the outer wall will exceed the stress at the inner wall. In this case it can be shown that the correction term is reduced, and lies between A and $A/2$.

The correction term is very small. For $b/a=5/4$, A has the value 0·002. The correction is negligible unless there is a sharp bend in the stress–strain curve. Figure 3 curve A is a typical stress–strain curve determined experimentally. The correction is too small to be shown. It is of interest to see what would be the effect of finite wall thickness with a specimen possessing zero Bauschinger effect, i.e. whose true stress–strain curve is linear between $+\sigma_0$ and $-\sigma_0$. The extreme case, for a material showing no work-hardening, is easily calculated. Figure 3 curve B shows the $\tau:\phi$ curve for zero wall thickness, and curve C the curve for $b/a=5/4$.

§ 3. Experimental

(i) *Copper: Dependence of Bauschinger Effect on Amount of Previous Cold Work*

The specimens were machined out of 1-in. diameter drawn HC copper rod, and were annealed for 1 hour at 970°C in air at a pressure of 0·1 mm Hg to remove as far as possible all internal stresses and effects due to previous mechanical treatment. After cooling in the furnace

Fig. 3

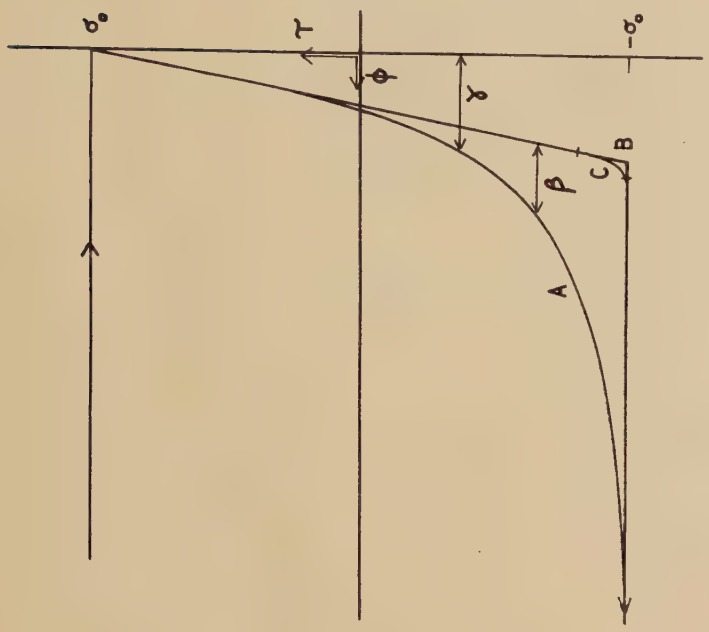
σ₀
τ
φ
γ
−σ₀
β
C
B
A

Fig. 4

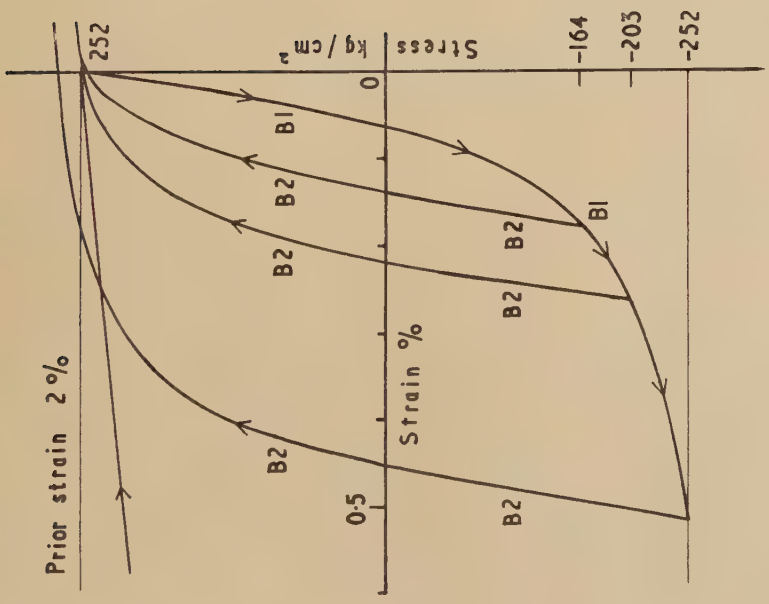
252
kg/cm²
Stress
0
−164
−203
−252
B1
B2
B2
B2
B1
B2
B2
B2
Prior strain 2%
Strain %
0·5

Fig. 5

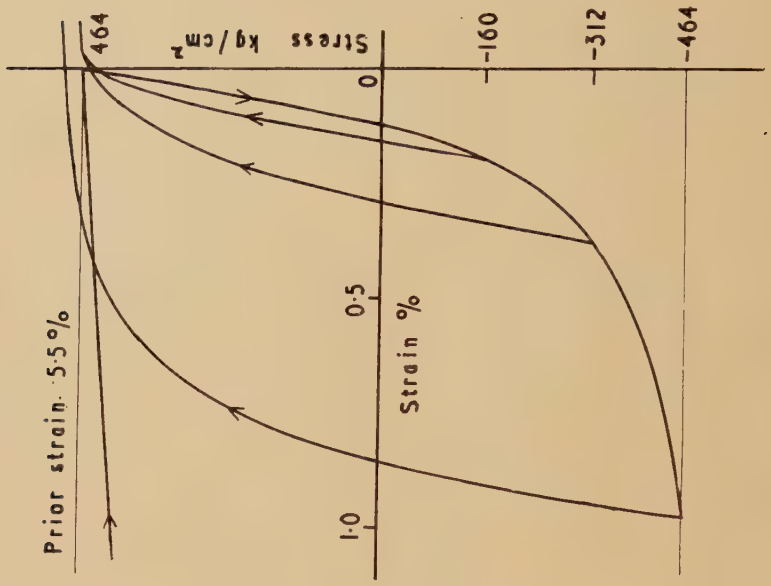
Stress kg/cm²
464
0
-160
-312
-464
0·5
1·0
Strain %
Prior strain 5·5%

Fig. 6

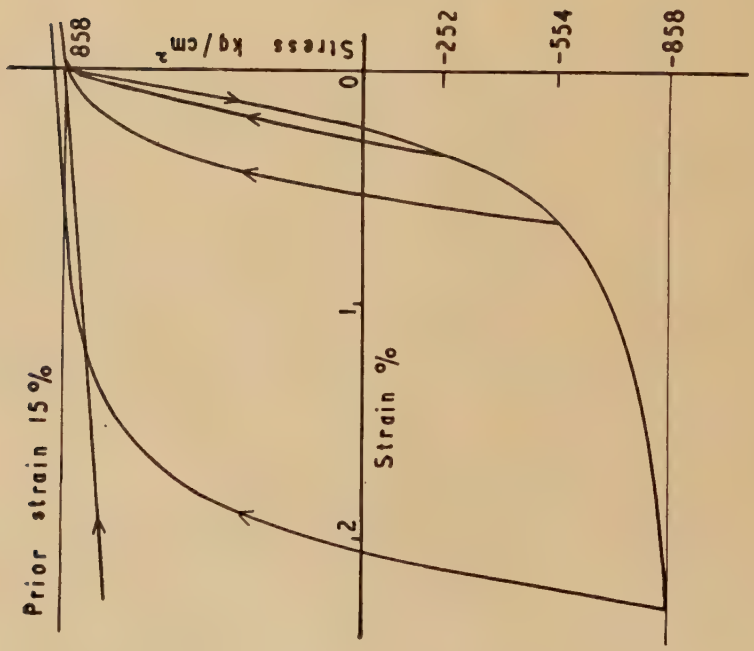
Stress kg/cm²
858
0
-252
-554
-858
1
2
Strain %
Prior strain 15%

they were electrolytically polished and etched. The mean grain size was 147 grains/mm^2, each grain containing an average of three twin elements. Since twin boundaries obstruct slip on at least six out of the twelve possible slip-systems, the effective grain size is taken as the number of twin elements per mm^2, in this case 440 twins/mm^2.

Three specimens were tested by applying a forward shear stress of 252 kg/cm^2 producing a strain of 2%, followed by reverse stresses of 164, 203 and 252 kg/cm^2 respectively, followed by a forward stress exceeding 252 kg/cm^2. The resulting stress–strain curves are shown in fig. 4. In figs. 5 and 6 are shown the results of six other specimens tested at stress levels of 464 and 858 kg/cm^2, the stress level being defined as the forward stress immediately before unloading begins, and denoted by σ_0.

Creep effects are considerable during the forward deformation. The stress was usually changed in steps of about $\sigma_0/10$, and the strain observed after 1 or 2 minutes, when the creep rate had greatly diminished. The observations near $+\sigma_0$ on the unloading curve are a little unreliable as slight creep occurs here. However, along most of the unloading curve, and along the reverse stress curve between zero and about $-3\sigma_0/4$, no creep effects were discernable. Usually a small creep was observed when the stress reached $-3\sigma_0/4$, and this became quite noticeable by $-\sigma_0$.

The curve running from $+\sigma_0$ to $-\sigma_0$ is denoted by B1 (cf. fig. 4). There is a considerable resemblance between the B1 curves at the three stress levels. This is illustrated in fig. 7, which shows the B1 curves of figs. 4, 5 and 6 replotted with the scale of both stress and strain divided by 252, 464 and 858 respectively. The B1 curves now nearly coincide, except near $-\sigma_0$. This strain-difference observed near $-\sigma_0$ corresponds to a relatively small stress-difference. It may be partly due to the larger creep rate associated with the higher stress levels. It is seen that to a good approximation the Bauschinger strain from $+\sigma_0$ to at least $-0{\cdot}9\sigma_0$ can be written

$$\beta=\sigma_0 f(\sigma/\sigma_0) \qquad \text{or} \qquad d\beta/d\sigma=f'(\sigma/\sigma_0).$$

The function f thus provides a measure of the Bauschinger effect independent of σ_0. In practice it is γ rather than β which is directly measured.

In the experiments described below it was found that the results for other metals and other conditions were of the same general character as those shown in figs. 4–6, and by suitable adjustment of the scale could also be made to coincide with the curve of fig. 7, to a first approximation. To obtain a single parameter which would be an experimental measure of the effect in any given test, it was decided to take the strain γ at the stress $\sigma=-0{\cdot}75\sigma_0$ divided by the strain γ at $\sigma=0$. This ratio is denoted by ρ. The value $-0{\cdot}75\sigma_0$ was chosen as this is the largest negative stress at which creep effects can be neglected. For a material with no Bauschinger effect $\rho=1{\cdot}75$. In figs. 4, 5 and 6, ρ has the values 3·47, 3·43 and 3·43 respectively. The accuracy of ρ in any one test is usually ± 2 or 3%.

In the above tests the prior strain was limited to about 20%, because at larger deformations the specimens showed signs of buckling. To overcome this a greased $\frac{1}{2}$-in. diameter rod was inserted in one specimen in place of the mirror assembly, and the specimen was given a preliminary twist of about 120° corresponding to a shear strain of 115%; this effectively prevented buckling. The rod was then withdrawn, the mirror assembly was inserted, and a further strain of $6\frac{1}{2}$% was given, the

Fig. 7

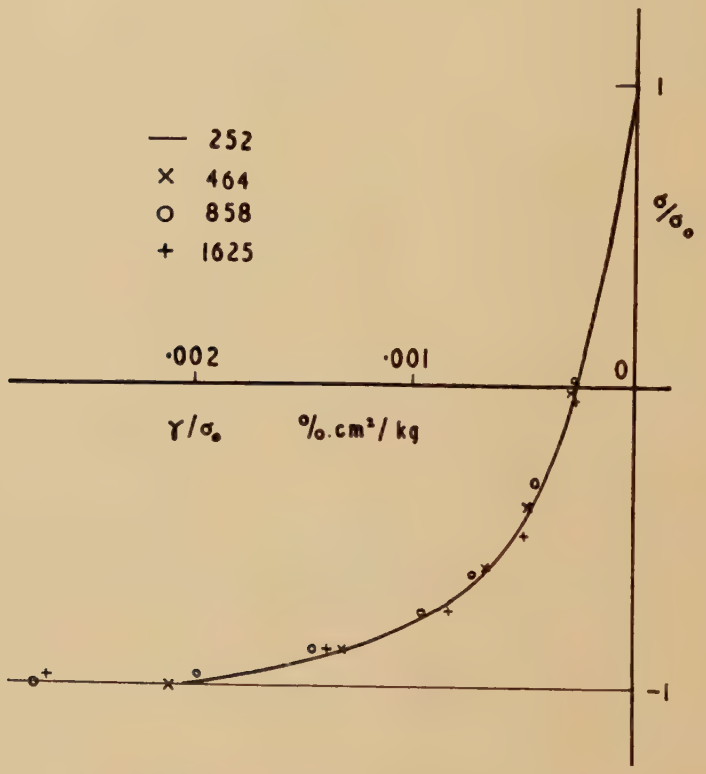

stress level now being 1625 kg cm^{-2}. The B1 curve springing from this point is shown in fig. 7, with the appropriate reduced scale. The effect is relatively slightly smaller than at lower stresses; this difference may not be significant, as the specimen was constrained by the $\frac{1}{2}$-in. rod during its preliminary deformation.

In these tests, and in those described below, the prior strain usually exceeded 1%. With prior strain less than 1% the Bauschinger strain β is less than that given in fig. 7. β of course must tend to zero when the prior plastic strain tends to zero. Thus the region between 0% and about 1% prior plastic strain (the material being initially thoroughly annealed) represents a transition region in which the Bauschinger strain increases

from zero to its normal value as given in fig. 7, this normal value being characteristic up to a prior strain of at least 120%.

In figs. 4–6 it will be seen that the B2 curves to a first approximation are symmetrical to the part of the B1 curve already traversed. The B2 curve springing from $-\sigma_0$, however, does not usually close on the B1 curve at $+\sigma_0$. The strain amplitude of the B2 curve between $-\sigma_0$ and $+\sigma_0$ is approximately 2/3 the amplitude of the B1 curve between $+\sigma_0$ and $-\sigma_0$. The difference between these two curves measured in terms of stress is relatively much smaller, owing to the small value of $d\sigma/d\theta$ and is only two or three times the uncertainty in the stress measurements. A similar difference was however observed in experiments with aluminium and nickel and it does appear to be significant.

Fig. 8

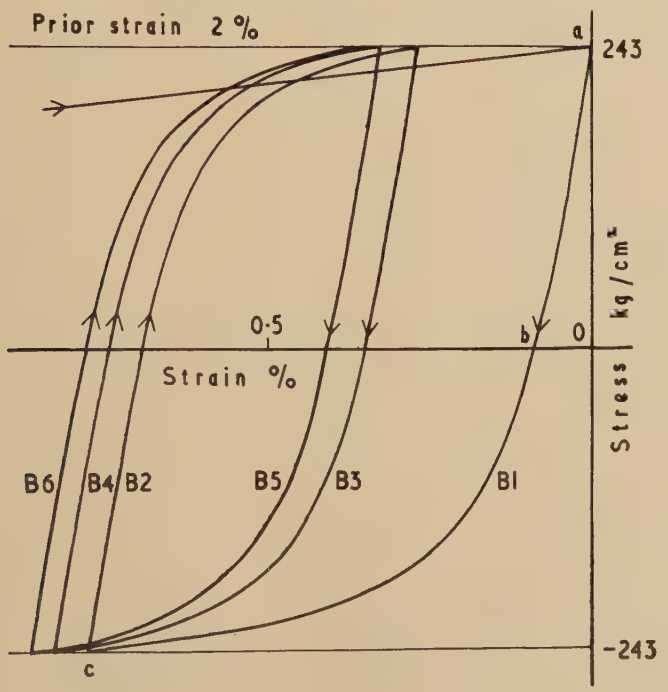

Cycles of stress taken between the limits $+\sigma_0$ and $-\sigma_0$ give further curves which may be denoted by B3, B4, etc. One copper specimen and one aluminium specimen were tested, with similar results. Figure 8 shows the results for aluminium. The curves B2, B3, B4, etc. are to a first approximation equal. The strain-amplitude of B3, however, slightly exceeds that of B2 ; and B5 exceeds B4 ; but this may not be significant, as the corresponding stress-difference is of the same order of magnitude as the accuracy of measurement. It is worth noting that in the test shown in fig. 8 the stress-level was sufficiently low to give no

creep effects ; the difference between the strain-amplitudes of B1 and B2 cannot therefore be attributed to creep.

(ii) *Copper : Effect of Previous Reversal of Direction of Deformation*

In (i) the deformation preceding the B1 curve was entirely in one direction, but it was noted that the B2 curve springing from $-\sigma_0$ was very similar to the B1 curve springing from $+\sigma_0$. This suggested that if a specimen were stressed to $+\sigma_0$, unloaded, stressed to $-\sigma_1$, unloaded, and then stressed to $+\sigma_1$ ($\sigma_1 > \sigma_0$), the B1 curve springing from $-\sigma_1$ would probably be identical with the B1 curve obtained from a specimen stressed to $-\sigma_1$ by unidirectional loading. This was tested on two specimens, Cu 20 with σ_0 and σ_1 equal to 252 and 462 kg/cm². and Cu 21 with values 464 and 728 kg/cm². The resulting reduced B1 curves at stress levels σ_0 and σ_1 all fitted fig. 7 quite well. These observations, together with a more extensive set given below in (iii), show that the ' memory ' of a stress-reversal during deformation may be erased by a further strain of a few per cent.

Table 1

Specimen Cu	11—22	11	12	13	14	17	16	15	19	18
Grains/mm²	147	2	2	2	28	28	28	78	78	78
Twins/mm²	440	105	105	105	170	170	170	310	310	310
σ_0, kg/cm²	252—858	252	464	850	252	464	858	252	464	850
Prior strain, %	2—15	3½	9	21	3	6	17½	2½	6	16
ρ_0	3·40—3·65	3·77	3·77	3·61	3·68	3·37	3·45	3·56	3·42	3·63
$-\sigma_1$, kg/cm²	—	495	655	—	433	720	—	433	729	—
Total prior strain, %	—	9½	15	—	7	14	—	6	13	—
ρ_1	—	3·63	3·39	—	3·45	3·52	—	3·33	3·43	—
Mean ρ	3·49	3·57			3·49			3·47		

(iii) *Copper : Effect of Grain Size*

The specimens used in (i) were annealed again for 1 hour at 970°C. This produced three different grain sizes. These specimens were then tested as in table 1, σ_0 and σ_1 having the same significance as in (ii) above. The first column gives the results from (i). The remaining columns give the results for the recrystallized specimens.

The values of ρ in table 1 agree to within 5%. The variations appear random and there is no significant variation with grain size. The range of grain size used was somewhat limited, but it was quite sufficient to affect the prior forward stress–strain curves, shown in fig. 9. In addition it was later observed with aluminium that specimens with a grain diameter as large as 2 mm and negligible twinning gave the normal Bauschinger effect.

Table 1 also shows clearly that there is no systematic difference between the values of ρ_0 and ρ_1, as mentioned in (ii) above.

(iv) *Other Metals*

Stress–strain curves were taken of the metals listed in table 2. Table 3 gives the summarized results, including the results for copper.

Fig. 9

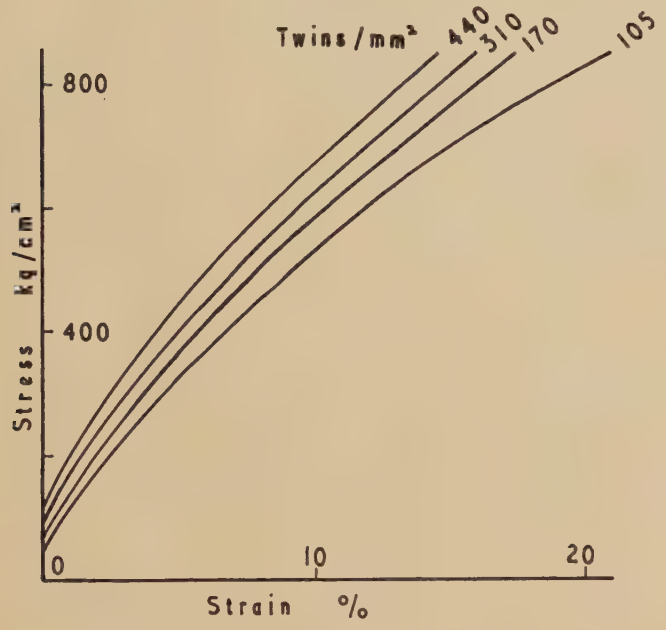

Table 2

Metal	Nominal purity	Heat treatment
Aluminium	99·9%	1 hour at 580°C
Super purity Al	99·99%	1 hour at 580°C
Nickel	99%	1 hour at 1260°C
Lead	99·98%	8 hours at 100°C
Iron	Armco ingot	8 hours at 680°C

Table 3

Metal	Cu	Al	S–P Al	Ni	Pb	Fe
Number of tests	36	20	14	5	7	6
σ_0 kg/cm²	73—1625	110—616	36—251	425—1230	24—73	790—1820
Prior strain, %	½—115	1—21	½—135	1½—16	1—23	1—24
ρ	3·35—3·65	2·85—3·15	3·70—4·30	3·40—3·70	3·15—3·50	3·00—3·50

With nickel, for example, five B1 curves were measured, at stress levels varying from 425 to 1230 kg/cm², corresponding to prior deformations of 1½ to 16%, and the observed values of ρ were between 3·4 and 3·7.

The various values of ρ obtained for any one metal appear to be randomly distributed and not correlated with the stress level, except that ρ is somewhat low when the prior strain is 1% or less, as mentioned in (i) above. The variation is only a little larger than the estimated experimental error. Comparing the various metals, it is seen that the values of ρ are substantially the same, with the exception of S–P Al which is high, and Al which is slightly low.

The fact that ρ is approximately the same for various metals is equivalent to saying that metals give the same Bauschinger strain β when tested at stress levels giving the same elastic strain σ_0/G, where G is the modulus of elasticity. Metals work-hardened by stresses proportional to their respective elastic moduli may thus be regarded as being in corresponding states and thus presumably have similar internal distribution of lattice defects, trapped dislocations, etc.

(v) *Effect of Temperature of Deformation*

Table 4 gives the summarized results of tests carried out at −182°C. It was found that temperature has only a relatively small influence on the Bauschinger effect. The principal difference is that for a given stress level the strain amplitude γ at $-\sigma_0$ is somewhat smaller at −182°C than at room temperature. Figure 10 shows typical results for copper, effective grain size 440 twins/mm².

Table 4

Metal	Cu	Al	S–P Al	Ni	Pb	Fe
Number of tests	5	6	3	3	4	3
σ_0 kg/cm²	152—970	334—970	304—456	729—1700	48—170	2960—3680
Prior strain, %	1—16	2—30	20—34	1—12	1—16½	1—9
ρ	2·9—3·5	2·6—2·9	3·5—3·7	3·1—3·9	3·2—3·3	2·3—2·45

It is reasonable to assume that one effect of temperature is to cause local stress-fluctuations. If these are of mean amplitude S_1 when the temperature is T_1 and the external stress is S, the peak local stress is $S+S_1$. The plastic flow at T_1 produced by the external stress S should therefore be the same as the flow produced at T_2 by an external stress $S+S_1-S_2$. The thermal component of the stress can be estimated by observing the dependence of the yield point on temperature. Thus if an annealed specimen is deformed at −182°C by an external stress 970 kg cm², unloaded, and warmed to room temperature, the yield point in the original direction of loading is found to be 850 kg cm². Figure 10 curve C shows the B1 curve obtained for a room temperature copper specimen at a stress level of 850 kg cm². Its amplitude γ at −850 kg cm² is approximately equal to the amplitude of the curve A at −970 kg/cm². Similar results were obtained in a limited number of experiments with the other face-centred cubic metals. The diminution of the Bauschinger

strain at low temperatures is thus attributed to the reduction of the thermal component of the peak local stress.

Iron is slightly exceptional. At −182°C the prior deformation is accompanied by sharp clicks presumed due to twinning, and the creep component of the extension is jerky. During unloading and reverse loading to $-\sigma_0$ twinning noises are absent, but they recommence when the stress passes $-\sigma_0$. The Bauschinger strain is somewhat reduced in

Fig. 10

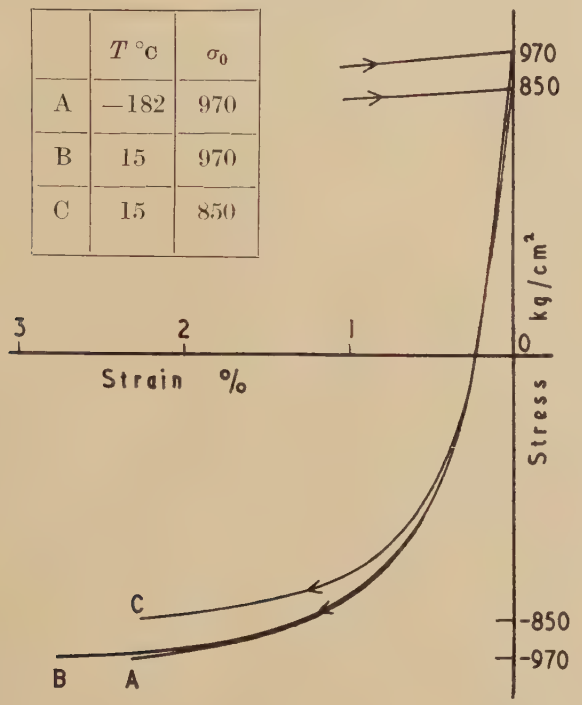

	T °C	σ_0
A	−182	970
B	15	970
C	15	850

amplitude, but its general character is similar to that of the metals which deform by slip only. It differs considerably from the B1 curve for hexagonal metals, which will be discussed elsewhere.

§ 4. Comparison with Previous Work

(i) *Masing and Mauksch* (1926)

These authors carried out a range of tension–compression tests on brass (Cu 58, Pb 2), the prior strain varying from 0·7% to 17·5%. Unfortunately, very little information is given about the portion of the B1 curves between $+\sigma_0$ and 0. From what is given it appears that the B1 curves are very similar to those obtained in the present work on pure metals, the strain being a little smaller, ρ having values between 2·5 and 2·65. Masing and Mauksch' experiments were designed to test

Masing's theory (Masing 1923, 1926) of the Bauschinger effect, which predicts that the B1 curve should be the same as the preceding stress–strain curve from zero to $+\sigma_0$, but with doubled scale and reversed sign. Good agreement between the observed and predicted curves was not obtained; the agreement is even less satisfactory when it is seen that these authors made their computed curve coincide with the beginning of the compression curve, neglecting the plastic deformation that occurred during unloading. Masing's theory can hardly be expected to explain the Bauschinger strain after a prior deformation exceeding 1%, for, as shown in the present paper, the effect in this region is quite unrelated to the prior stress–strain curve. For deformations of order 0·1% Masing's theory probably agrees with experiment; but in this region the Bauschinger effect in any case tends to zero, and is extremely difficult to measure accurately.

A related theory has been discussed by Nabarro (1950). The model used by Polakowski (1951) is in some respects a special case of Masing's model.

(ii) *Rahlfs and Masing* (1950)

These authors examined the Bauschinger effect in torsion, using 1 mm diameter wires of various metals with prior surface strains exceeding 3·5%. The considerable inhomogeneity of strain causes the observed torque-twist curve to deviate a little from the true stress–strain curve, but even so it is interesting to notice that the published curves are very similar to the general curve described by the present author. Values of ρ calculated from Rahlfs and Masing's curves lie between 2·9 and 4·0. Rahlfs and Masing compared their results with Masing's theory and again found that the agreement is not good.

(iii) *Sachs and Shoji* (1927)

These authors studied the Bauschinger effect with brass single crystals (Cu 72) in tension-compression. Figure 5, curve D2, of their paper is practically the same as the general curve obtained by the present author. But figs. 15, 20 and 21 show an effect which is three or four times larger. These however refer to crystals which have received a low-temperature anneal after previous cold-working, so perhaps are not strictly comparable with present results.

Experimental work on the Bauschinger effect has also been described by Polakowski (1951) and Wilson (1952), who are chiefly interested in hardness as a function of strain, and also by Kunze and Sachs (1930), whose experiments were entirely confined to the transition region below 1% prior strain.

§ 5. Discussion

The Bauschinger effect in polycrystalline metals which deform only by slip has been shown to be determined principally by the stress level, and to be largely independent of grain size. The dependence on temperature is small, and for the face-centred cubic metals it is explicable

in terms of a thermal component of stress. The strain associated with the effect in different metals is inversely proportional to the elastic modulus.

There is no adequate theory of the effect. Masing's theory is unsatisfactory for deformations exceeding 1%. The present author (Woolley 1948) suggested an explanation of the effect in terms of an exhaustion theory, but this is not adequate, as on a strict exhaustion theory the B2 curves would be expected to be linear and elastic between $-\sigma_0$ and $+\sigma_0$. The theory of Brandenberger (1947) does not account for the experimental results with pure metals, and is based on somewhat unusual ideas about elasticity and the criterion of yield.

There is lack of experimental results for single crystals. The work of Honeycombe (1951) suggests that during deformation a single crystal may behave more like polycrystalline aggregate with a highly preferred orientation. It is possible that Sachs and Shoji's specimens behaved in this way.

A few conclusions can be drawn from the experimental results presented above. In fig. 8 at the point a there are no dislocations in the specimen capable of being activated or moved by a stress between 0 and $+\sigma_0$. At c, after the strain B1, the number of dislocations capable of being activated and moved by a stress between 0 and $+\sigma_0$ is such that their motion produces the strain B2, which is about $\frac{2}{3}$ of B1. Thus at c either (i) the dislocations which moved during B1 have activated a slightly smaller number of other dislocations, and the B1 dislocations take no further part in the deformation, or (ii) about $\frac{1}{3}$ of the dislocations which moved during B1 have become trapped and the remaining $\frac{2}{3}$ simply move back when the stress is raised to $+\sigma_0$ again. The latter seems the more reasonable explanation. The same argument leads to the conclusion that no further substantial loss of dislocations by trapping occurs, the dislocations responsible for B2 also producing B3, B4, etc. Furthermore, in figs. 4, 5 and 6 it is seen that the B2 curves springing from between 0 and, say, $-\frac{3}{4}\sigma_0$ have the same amplitude as the preceding part of the B1 curve. We infer that in this case there is no loss of active dislocations. The loss of active dislocations which causes the strain amplitude of B2 to be less than that of B1 therefore takes place when the stress is near $-\sigma_0$. This is a reasonable conclusion, as the larger the stress the more easily some dislocations may be pushed into regions of distorted lattice from which they may not easily escape.

The B1 and succeeding B curves to a first approximation form closed hysteresis loops of two-fold rotation symmetry. This implies that the external stress is needed not to activate the dislocations but to move them through a resisting lattice. For suppose that the stress is required merely to activate dislocations, and that the lattice offers no resistance to a dislocation once it is activated and removed a small distance from its original anchorage. During the B1 strain a certain number of dislocations would be activated and would move at once a certain distance,

this giving the B1 strain. Some of these are trapped, as described in the above paragraph. Unloading would be fairly elastic, but as soon as the stress becomes positive the remaining dislocations would immediately move back to their original positions, giving a B2 curve as in fig. 11, curve B2a. Actually internal micro-stresses would probably cause the curve to be more like B2b. But neither of these curves is symmetrical to B1 or resembles the experimental B2 curve.

Fig. 11

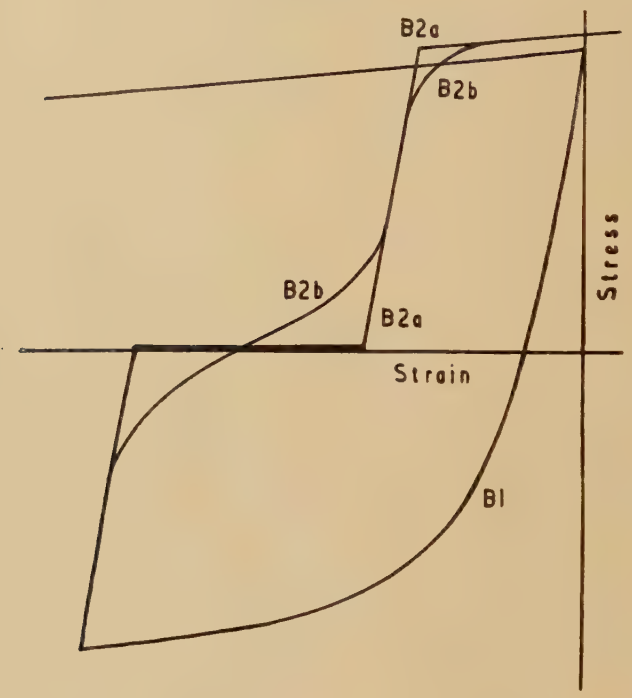

The Bauschinger effect has often been qualitatively attributed to textural stresses, these originating in the fact that the mechanical strength of a grain in an aggregate depends on its orientation. Such stresses were used by Masing (1923) to discuss work-hardening and the Bauschinger effect, and by Greenough (1949) to discuss residual lattice strains measured by x-rays. In Appendix I the contribution of textural stresses has been estimated. It is there shown that the maximum Bauschinger strain produced by these stresses is fairly small compared with that observed. Thus the observed effect is largely a property of the individual grains, and should be shown by single crystals also.

Such an effect in a single crystal must be explained in terms of dislocation theory as a rearrangement of dislocations already present or as a generation of new ones. In Appendix II a semi-quantitative explanation is given in terms of the rearrangement of dislocations present

in the work-hardened lattice. It is not reckoned that the generation of new dislocations contributes largely to the observed effect. An isolated Frank–Read source will generate equally well with positive or negative stresses. If forward deformation exhausts these sources in order of decreasing length, then they produce no Bauschinger effect. But a source very close to an obstacle can generate at least one dislocation loop when the stress is in such a direction as to expand the loop in a direction away from the obstacle, though unable to generate when this stress is reversed. This would give rise to a Bauschinger effect, though the strain-amplitude produced by this mechanism would be small compared with that estimated in Appendix II.

Acknowledgments

Thanks are offered to Professor J. F. Allen and to Professor N. F. Mott for criticism and discussion, and to the British Aluminium Company for supplying super-purity aluminium.

APPENDIX I

Textural Stresses

Masing considered essentially the model shown in fig. 12 (*a*). Each grain is represented by a spring in series with a friction element. The

Fig. 12

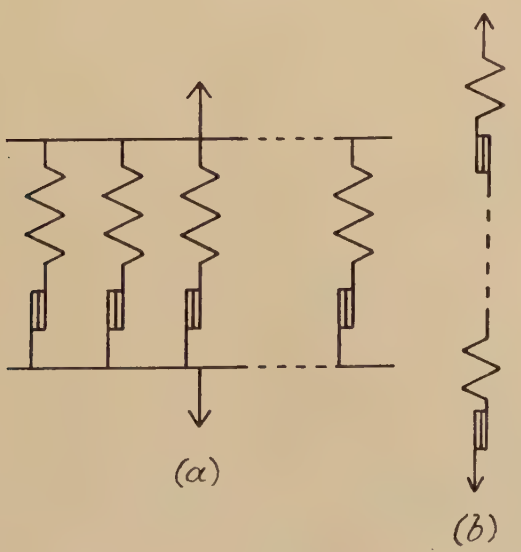

grains are regarded as ideally plastic, showing no hardening and no Bauschinger effect in the region examined, as in fig. 13, curve A.

Experimentally it was reckoned that this was achieved by a plastic strain to produce hardening, followed by a low-temperature anneal to remove textural stresses, the following strain being kept small, usually less than 1%. This model gives a B1 curve ABC (fig. 14) geometrically similar to OA but with the scale of both axes doubled. The continuation CD is identical with AD′. This model is used by Masing to account both

Fig. 13

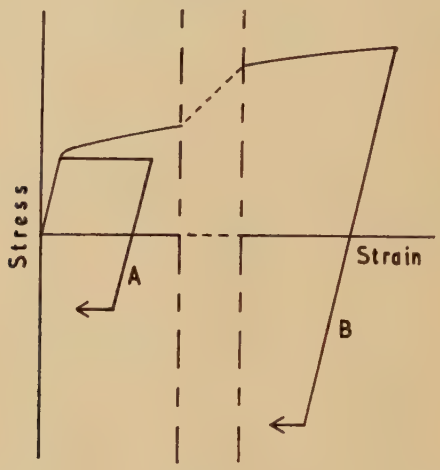

Fig. 14

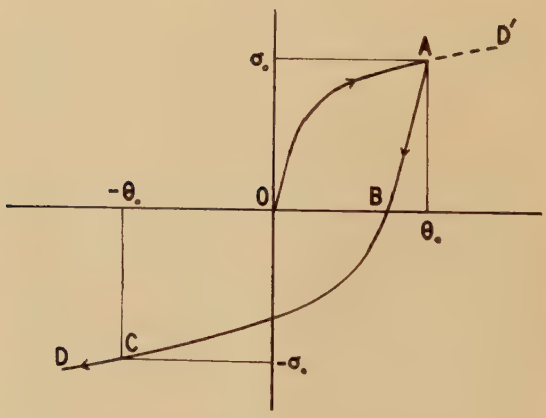

for the beginning of work-hardening and also for the Bauschinger effect. As Masing himself envisaged, it obviously cannot be used to account for work-hardening beyond a plastic strain of say 1%, as in this model the finite slope $d\sigma/d\theta$ of the work-hardening curve is attributed to grains which have not yet reached their yield point and therefore have an elastic strain equal to the overall plastic strain. For finite plastic strain

($>1\%$) there cannot be any direct relation of this type between the Bauschinger strain and the prior strain.

Greenough regarded the grains as work-hardening, and calculated the stresses which would be expected on the basis of the theories of Cox and Sopwith (1937) and of Taylor (1938). His experimental results agree better with Taylor's theory. The exact size and shape of the Bauschinger curve expected on this model can be calculated as below.

Figure 12 (*a*) is again taken to represent the grains of an aggregate extended plastically. During this prior strain the grains have work-hardened. They are regarded as showing no Bauschinger effect and negligible further work-hardening during a subsequent small compression, as in fig. 13, curve B. Let the (work-hardened) tensile yield stress of a given grain be denoted by $\xi\sigma_0$ where $0<\xi<\infty$. Let the total volume of the grains whose yield stress is in the range $\xi\sigma_0$ to $(\xi+d\xi)\sigma_0$ be a fraction $g(\xi)$ of the volume of the specimen. $g(\xi)$ satisfies the equations

$$\int_0^\infty g(\xi)\,d\xi=\int_0^\infty \xi g(\xi)\,d\xi=1.$$

In practice $g(\xi)$ is non-zero only when ξ lies between limits $\xi_{\min}$ and $\xi_{\max}$. Since each grain is regarded as showing no Bauschinger effect, its compressive yield stress is equal to its tensile yield stress. The aggregate, however shows a Bauschinger strain, owing to the range of yield strains present. Taking the origin of stress and strain at the point O, fig. 4, plastic deformation begins at an applied stress $\sigma_0(1-2\xi_{\min})$ and a strain $2\xi_{\min}\sigma_0/G$; the specimen is entirely plastic when the applied stress reaches $-\sigma_0$ and the strain is $2\xi_{\max}\sigma_0/G$. The shape of the B1 curve between these points is calculable in terms of $g(\xi)$, being given by

$$d^2\sigma/d\theta^2=G^2g(\xi)/2\sigma_0 \quad . \quad . \quad . \quad . \quad . \quad . \quad . \quad (1)$$

where

$$\xi=G\theta/2\sigma_0.$$

The theories of Cox and Sopwith, and Taylor, respectively, may be used to calculate $g(\xi)$. The former treat the grains as single crystals, laterally unconstrained. The relation between tensile stress, $\sigma(=\xi\sigma_0)$, and extension, ϵ, $=(l-l_0)/l_0$, for a work-hardening single crystal, may be derived from the equations 26/3, 43/1 and 43/4 cited by Schmid and Boas (1950) in the form

$$\sigma=f(\epsilon)/(\sin\chi_0\cos\lambda_0)^{1+n}$$

where χ_0 and λ_0 specify the initial orientation of the tensile axis, and where $n=\frac{1}{2}$ for a parabolic law of work-hardening. Values of $(\sin\chi_0\cos\lambda_0)^{-3/2}$ are plotted on a stereographic projection at 5° intervals and the mean value M_1 obtained. The ratio $(\sin\chi_0\cos\lambda_0)^{-3/2}/M_1$ is then the value of ξ for the orientation $\chi_0\lambda_0$. $g(\xi)$ is simply the relative frequency of the various values of ξ. The frequency distribution is shown in fig. 15, curve A. It is given as a histogram owing to the limited number of points computed on the stereogram. From this and eqn. (1) the B1 curve can be calculated; this curve is shown in fig. 16, curve A.

The B1 curve may be deduced in a similar way on the basis of Taylor's theory. Greenough writes $\sigma\epsilon = \tau_c \Sigma s$ where τ_c is the resolved shear stress,

Fig. 15

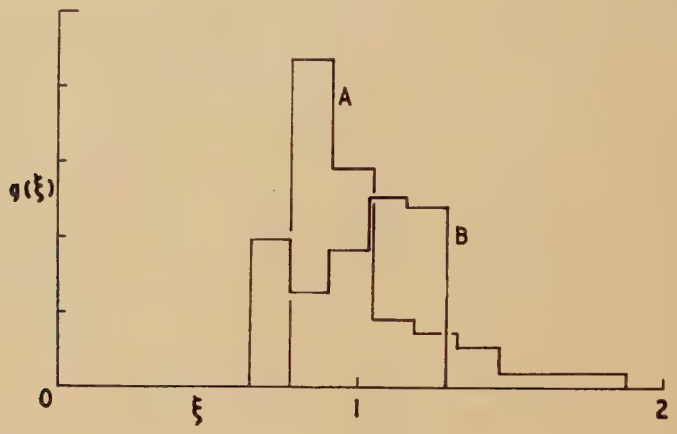

Fig. 16

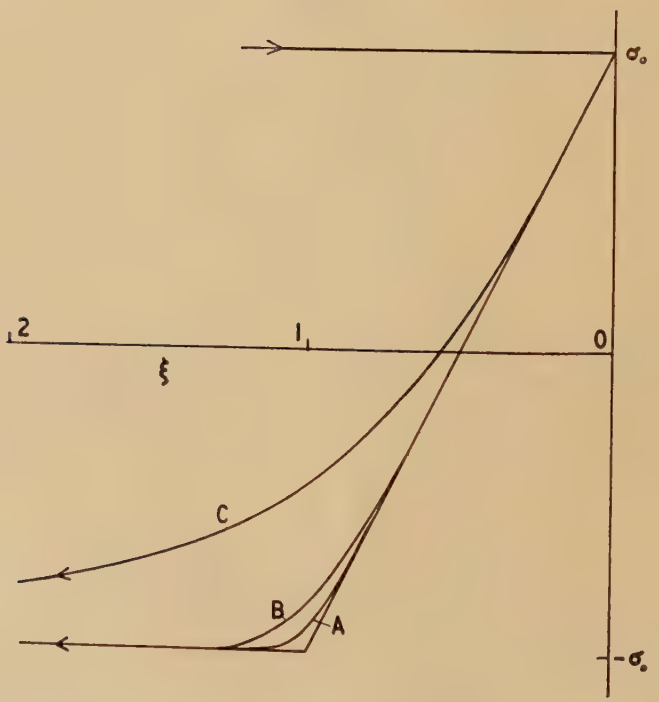

Σs the arithmetical sum of the five shears producing a strain in the grain equal to the overall strain in the specimen, σ the tensile stress and ϵ the extension. For a parabolically work-hardening material $\tau_c \propto \sqrt{\Sigma s}$, so

that $\sigma \propto (\Sigma s)^{3/2}$. Taylor (1938, fig. 13) gives values of Σs computed at 5° intervals over a stereographic projection. These are converted to $(\Sigma s)^{3/2}$ and the mean value M_2 calculated. The ratio $(\Sigma s)^{3/2}/M_2$ is the value of ξ for any given orientation. Figure 15, curve B shows the relative frequency of various values of ξ, and fig. 16, curve B, the stress–strain curve calculated from this with eqn. (1).

These models neglect the continuity of stress between adjacent grains. If we consider the model of fig. 12 (*b*), where stress continuity is preserved at the expense of uniform strain, it is easy to see that here there will be no Bauschinger effect, the B1 curve being linear and elastic between $+\sigma_0$ and $-\sigma_0$, whether the elements be ideal as in fig. 13, curve A, or work-hardening as in fig. 13, curve B. The real state lies between these two extremes, though probably nearer the case of uniform strain than of uniform stress. Thus curves A and B of fig. 16 represent upper limits to the Bauschinger strain.

In comparing the predicted B1 curves with the experimental results, it must be noted that the former refer to tension-compression, while the latter refer to shear. This difference is not likely to affect the order of magnitude of the quantities involved. Figure 16, curve C, shows the observed Bauschinger strain, which is decidedly larger than that calculated. Thus we conclude that textural stresses alone are inadequate to explain the Bauschinger effect.

APPENDIX II

The Role of Dislocations

According to Taylor (1934), work-hardening is attributed to the stress-system set up by dislocations distributed throughout the lattice. If there are N edge dislocations crossing each square centimetre, then these are separated by a mean distance $r=1/\sqrt{N}$ and the yield stress is of order $\sigma_0=Gb/2\pi r=Gb\sqrt{N}/2\pi$, where b is the Burgers vector. If a stress $-\sigma_0$ is now applied, the dislocations should take up new equilibrium positions and in doing so each will move a distance presumably of the same order as their mean distance apart. Thus the Bauschinger strain $\beta(-\sigma_0)$ is given by

$$\beta(-\sigma_0)=Nrb=b\sqrt{N}.$$

Thus β yield strain$=\beta G/\sigma_0=2\pi$. Experimentally this ratio is about 8. This agreement is fortuitously good, as the above theory is only approximate. It does show, however, that this mechanism is capable of contributing to the observed effect.

Mott (1952) has put forward an improved theory of work-hardening in terms of groups of n primary dislocations on slip planes a distance x apart which are terminated by barriers a distance $2L$ apart. If these dislocations are allowed to move a distance $R=\sqrt{Lx}$ during the Bauschinger strain, then the same expression $\beta(-\sigma_0)=2\pi\sigma_0/G$ is obtained.

R is the mean separation of the primary groups of piled-up dislocations, so this motion corresponds to a substantial rearrangement of the primary stress-field. Mott also considers small groups of n' secondary dislocations at a distance r from the primary groups, which relieve local strain by moving from sources a distance l apart ($\sim 10^{-4}$ cm) through a distance l. If these are able to move back when the applied stress is reversed. their contribution to the Bauschinger strain is

$$\beta(-\sigma_0)=\{(n'/l^2)lb\}_{\text{mean}}.$$

Mott gives

$$n'=nl/2\pi r$$

so

$$\beta(-\sigma_0)=nb/2\pi R=\sigma_0/G.$$

Thus the secondary dislocations can contribute to the Bauschinger strain, though rather less than do the primary dislocations.

References

Brandenberger, H., 1947, *Schweiz. Arch. Angew. Wiss. Techn.*, **13,** 232, 268.

Cox, J. L., and Sopwith, D. G., 1937, *Proc. Phys. Soc.*, **49,** 134.

Greenough, G. B., 1949, *Proc. Roy. Soc.*, **197,** 556.

Honeycombe, R. W. K., 1951, *J. Inst. Met.*, **80,** 45.

Kunze, W., and Sachs, G., 1930, *Metallwirtschaft*, **9,** 85.

Masing, G., 1923, *Wiss. Ver. a. d. Siemens-Konzern*, **3,** 231 ; 1926, *Ibid.*, **5,** 135.

Masing, G., and Mauksch, W., 1926. *Wiss. Ver. a. d. Siemens-Konzern*, **5,** 142 ; see also 1925, *Ibid.*, **4,** 74, 244.

Mott, N. F., 1952, *Phil. Mag.*, **43,** 1151.

Nabarro, F. R. N., 1950, *Some Recent Developments in Rheology* (Brit. Rheol. Club).

Polakowski, N. H., 1951, *J. Iron and Steel Inst.*, **169,** 337.

Rahlfs, P., and Masing, G., 1950, *Zeit. f. Metallkunde*, **41,** 454.

Sachs, G., and Shoji, H., 1927, *Zeit. Phys.*, **45,** 776.

Taylor, G. I., 1934, *Proc. Roy. Soc.*, **145,** 362 ; 1938, *J. Inst. Met.*, **62,** 307.

Wilson, D. V., 1952, *Nature, Lond.*, **170,** 30.

Woolley, R. L., 1948, *Rep. Conf. on Strength of Solids, Bristol* (London : Phys. Soc.).

LXV. *Light Pulses from the Night Sky*

By J. V. Jelley and W. Galbraith
Atomic Energy Research Establishment, Harwell*

[Received March 20, 1953]

Abstract

Further experimental results are reported on the phenomenon of light pulses from the night sky associated with cosmic rays. The relative frequency of discharge of G.M. counters with distance from the light receiver, comprising a photomultiplier and a parabolic mirror, has been investigated. The differential height distribution of light pulses has been found to be exponential in form, and the intensity of those pulses detected at the rate of about 1 per minute is, very approximately, 3 photons per cm^2 per pulse.

§ 1. Introduction

We have recently shown (Galbraith and Jelley 1953) that at night in clear weather light flashes can be detected which may probably be ascribed to Čerenkov radiation produced in the atmosphere by cosmic ray showers. The light flashes were detected with a photomultiplier located at the focus of a concave mirror, placed so that rays coming down within 12° of the vertical were focused on the photocathode. The multiplier pulses were fed into an amplifier with equal differentiation and integration time constants of 0·032 μsec. The connection of these pulses with cosmic rays was demonstrated by detecting coincidences between them and discharges in G.M. counters. Some new results have since been obtained and are reported here.

§ 2

With the light receiver previously used, an investigation has been carried out on the relative frequency with which G.M. counters are fired at different distances from, and in coincidence with, the light receiver. The receiver, pointing vertically, was placed at the centre of the air-shower array designed by Cranshaw. In this array there are 4, 8 and 8 G.M. counters, each of area 200 cm^2, at distances of 42, 95 and 126 metres respectively from the light receiver (fig. 1, inset). An additional square tray of counters of total area 700 cm^2 was placed underneath the mirror of the receiver. The hodoscope of the air shower array was triggered by the output of a discriminator following the light pulse amplifier; this discriminator was set at approximately twice the level of the night

* Communicated by W. J. Whitehouse.

sky noise. Figure 1 shows the relative frequency of response of a G.M. counter at different distances from the receiver. The curve is the resultant of three nights of operation, during two of which the central tray was also operating. In reducing the results, the numbers were normalized to take into account the difference in area between the single counter and the tray and also the different number of counters at each distance. It will be seen that there appears to be a maximum in the distribution, the interpretation of which is being studied.

Fig. 1

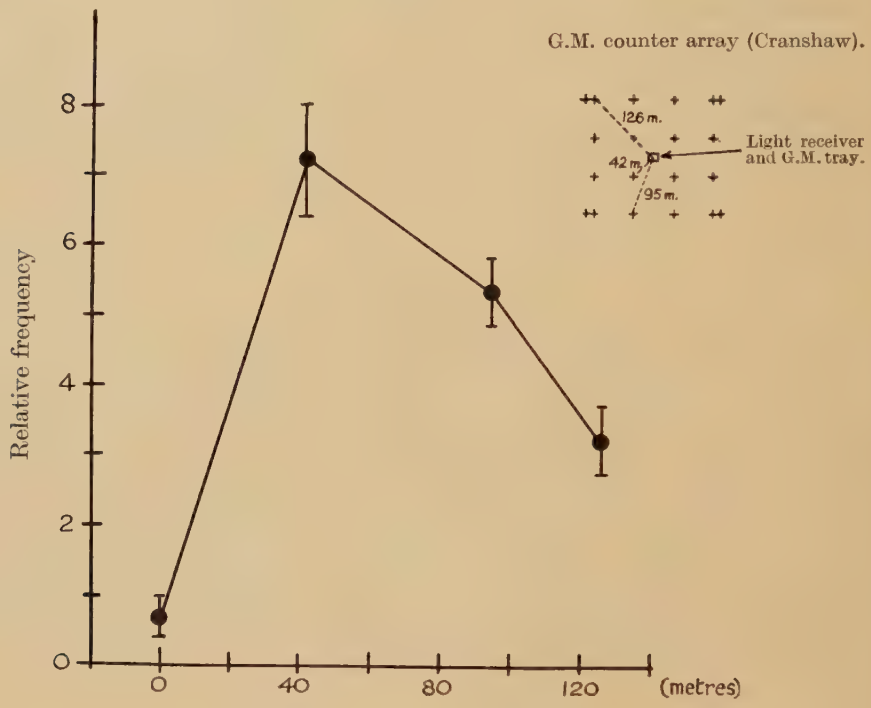

§ 3

Our most recent pulse height distribution was obtained during a run of 3 hours when sky conditions were very clear and remained constant. The distribution is shown in fig. 2 plotted on a logarithmic scale and indicates that the pulse height distribution fits an exponential law. This fit was better than a fit to a power law.

§ 4

The absolute intensity of the light pulses was measured by comparing them with those from α-particles of ^{239}Pu (5·15 MeV) in a pure anthracene crystal placed directly on the photomultiplier. The α-pulses were found

to be approximately five times as big as the smallest light pulses, when the discriminator was set so as to get one pulse a minute. From an absolute calibration by Birks (1950) of the photons emitted by electrons in anthracene and his value for the relative sensitivity of anthracene for electrons and α-particles, Birks (1951), a figure was obtained for the photon flux from the night sky of about 1300 photons per light pulse in the mirror or 3 photons per cm² per light pulse between the wavelength limits of 3000–5500 Å. There was some visible haze in the sky when this calibration was done and we would expect a larger photon flux

Fig. 2

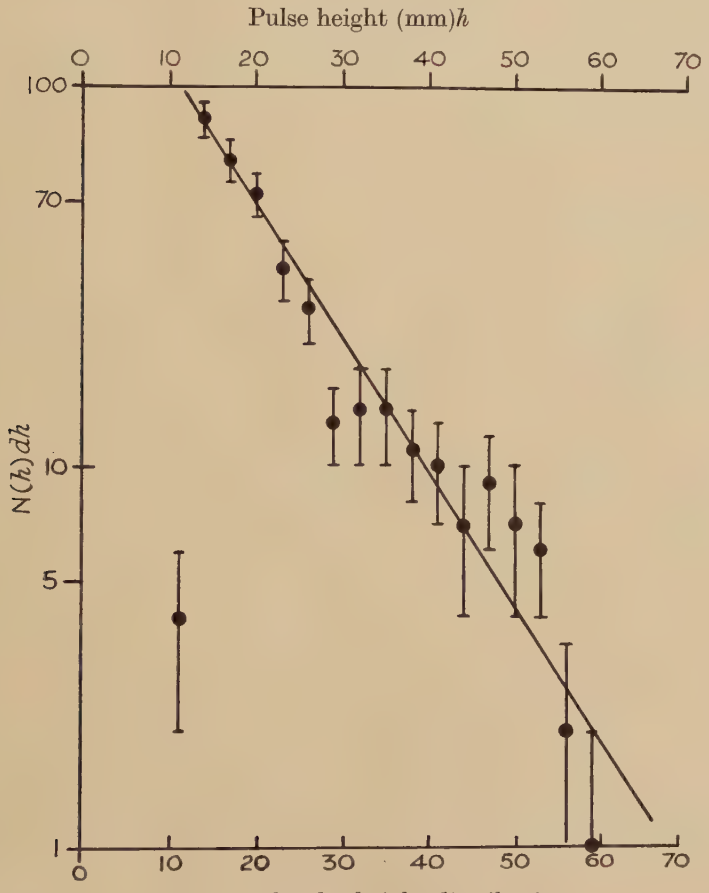

Differential pulse height distribution.

under clearer conditions. It is also felt that an error of ×5 either way would not be unreasonable to assume at this stage, but other methods of absolute calibration are being developed so that this error can be reduced.

In order to verify that these pulses are Čerenkov radiation we intend to check whether they are approximately linearly polarized, as they should be whenever the core of the shower does not aim directly at the

observer. This can be done by using two light receivers with polaroid over the photocathodes. To improve the signal-to-noise ratio one might use an ultra-violet filter to cut down the visible radiation of the night sky (the Čerenkov radiation extends far into the ultra-violet).

A possible application of the light receiver is in finding the direction from which air showers arrive, since Čerenkov radiation in the atmosphere is emitted within a cone of half angle of about 1° along the tracks of the shower particles. It is of direct interest in this connection to determine the variation in intensity and frequency of the light pulses with zenith angle and, also, using the G.M. counter array, the relation between the intensity of the light and the distance of the triggered counter from the receiver. Such a detector, based upon the directional property of the Čerenkov radiation, could then be used to look for localized sources of cosmic rays, and a survey of the known radio stars for these sources immediately suggests itself.

Acknowledgments

We are grateful to Professor O. R. Frisch, for helpful criticism of this note. We wish to thank Mrs. K. M. Glover, Chemistry Division, for the preparation of the plutonium source, Dr. E. Bretscher and Mr. W. J. Whitehouse for their continued interest in these experiments and the Director, Atomic Energy Research Establishment, for permission to publish these results.

References

Birks, J. B., 1950, *Proc. Phys. Soc.* A, **63,** 1294 ; 1951, *Ibid.*, **64,** 874.
Galbraith, W., and Jelley, J. V., 1953, *Nature, Lond.*, **171,** 349.

LXVI. *Cerium Magnesium Nitrate I: The Magnetic Properties and Specific Heat above* 1°K

By A. H. Cooke, H. J. Duffus and W. P. Wolf
The Clarendon Laboratory, Oxford*

[Received February 27, 1953]

Abstract

The magnetic properties and specific heat of cerium magnesium nitrate have been measured at temperatures between 1°K and 4·2°K. The magnetic properties can be described by a highly anisotropic g-tensor, having a very small value along the crystalline axis and a value of 1·84 perpendicular to it. The specific heat is extremely small, being given in this range of temperatures by $C_I = 7{\cdot}5 \times 10^{-6}\, R/T^2$. It is shown that the specific heat can be accounted for almost entirely by magnetic dipole-dipole interaction. The use of the salt for work below 1°K is discussed.

§ 1. Introduction

In this paper we present the results of studies of the magnetic properties and the specific heat of cerium magnesium nitrate, made at temperatures in the helium range by paramagnetic resonance, by susceptibility measurements, and by paramagnetic relaxation. This salt is one of the isomorphous series of rare earth double nitrates which have the formula $A_2B_3(NO_3)_{12} \cdot 24H_2O$, where A is the trivalent rare earth ion and B is a divalent metal, for example magnesium or zinc. Bleaney has pointed out that comparison of the specific heats of different paramagnetic salts shows that exchange interaction between the magnetic ions falls very rapidly with increasing ionic volume, and that as the double nitrates have a particularly large ionic volume, interactions between the ions may be expected to be very small. It follows that adiabatic demagnetization of suitable salts of this series (that is, those in which the magnetic ions have Kramers degeneracy) should yield very low temperatures. Of the different salts, cerium salts are especially interesting since, as the naturally occurring cerium nuclei have no magnetic moment, the electronic states have no nuclear hyperfine structure, and at low temperatures there is no contribution to the specific heat save that due to interaction between the magnetic ions.

The rare earth double nitrates are very soluble in water, from which they crystallize readily in thick plates of trigonal symmetry. Their external morphology has been described by Groth (1908). The crystal structure is not known in detail. We are indebted to Mr. H. M. Powell, who has determined the structure of the lattice formed by the cerium ions in cerium magnesium nitrate. These lie on a rhombohedral lattice,

*Communicated by the Authors.

with a unit cell of side 8·51A, and interaxial angle 79½°. Measurements of the susceptibility and the magnetic anisotropy were made at room temperature on several salts of the series by Krishnan and Mookherji (1938) in their survey of rare earth paramagnetic salts. The only measurements at low temperatures so far reported are those of Becquerel, de Haas, and van den Handel (1931) who measured the Faraday effect when a magnetic field was applied along the trigonal axis of a crystal of cerium magnesium nitrate at temperatures in the helium range. The effect they found was too small to allow an accurate estimate of the magnetic susceptibility to be made; they concluded that the effective magnetic moment of the cerium ion in the direction of measurement was not greater than 0·2 Bohr magnetons.

§ 2. The Measurements

Paramagnetic resonance measurements were made on a small single crystal at a wavelength of 3·33 cm. Resonance was observable only at temperatures below about 10°K, showing that at higher temperatures the spin-lattice relaxation time was so short as to broaden the line beyond the possibility of detection. Measurements at 4·2°K gave a single resonance line, indicating that as in the comparable case of gadolinium magnesium nitrate (Trenam 1953) all the rare earth ions occupy equivalent positions in the crystal. The first measurements were made on a crystal mounted with its trigonal axis horizontal, in a horizontal magnetic field whose direction could be rotated about a vertical axis. The magnetic field at which resonance occurred was strongly dependent on the angle ϕ between the direction of the field and the crystal axis, and was given by the relations

$$h\nu = g\beta H, \quad . \quad . \quad . \quad . \quad . \quad . \quad . \quad . \quad . \quad . \quad . \quad (1)$$

$$g^2 = g_{\parallel}^2 \cos^2\phi + g_{\perp}^2 \sin^2\phi, \quad . \quad . \quad . \quad . \quad . \quad . \quad . \quad (2)$$

where h=Planck's constant, β=the Bohr magneton, ν=resonant frequency in a field H, and $g_{\parallel}$ and $g_{\perp}$ are the values of g with the field respectively parallel and perpendicular to the axis of the crystal. In fig. 1 these results are plotted as a graph of g^2, as derived from the first relation, against $\cos^2\phi$. This gives $g_{\perp}=1{\cdot}84$, and $g_{\parallel}<0{\cdot}3$.* To obtain a more accurate value of $g_{\perp}$, on which the magnetic susceptibility chiefly depends, a second measurement was made with the trigonal axis vertical. Both the radio frequency field and the steady magnetic field then lay in the plane of maximum g-value, increasing the resonance absorption. This measurement also gives $g_{\perp}=1{\cdot}84$. The resonance line was approximately Gaussian in shape, with the width at half power of 40 gauss.

The resonance measurements were supplemented by susceptibility measurements, using a Sucksmith ring balance. A crystal was mounted with its axis horizontal, in the field of an electromagnet which could be rotated about a vertical axis. Measurements at different temperatures

* *Note added in proof.*—Later measurements in fields up to 15 kilogauss give $g_{\parallel}=0{\cdot}25\pm0{\cdot}05$.

in the helium range with the field and the maximum field gradient perpendicular to the crystal axis showed that in this direction the susceptibility per gram is given by

$$\chi = \frac{\lambda}{T} + \alpha,$$

where $\lambda = 4{\cdot}1 \times 10^{-4}$ and $\alpha = 3{\cdot}2 \times 10^{-5}$. The absolute magnitude of the susceptibility, which was obtained by comparison with manganous ammonium sulphate, is accurate only to $\pm 5\%$. Attributing the temperature dependent term to a doublet level gives a g-value of 1·8,

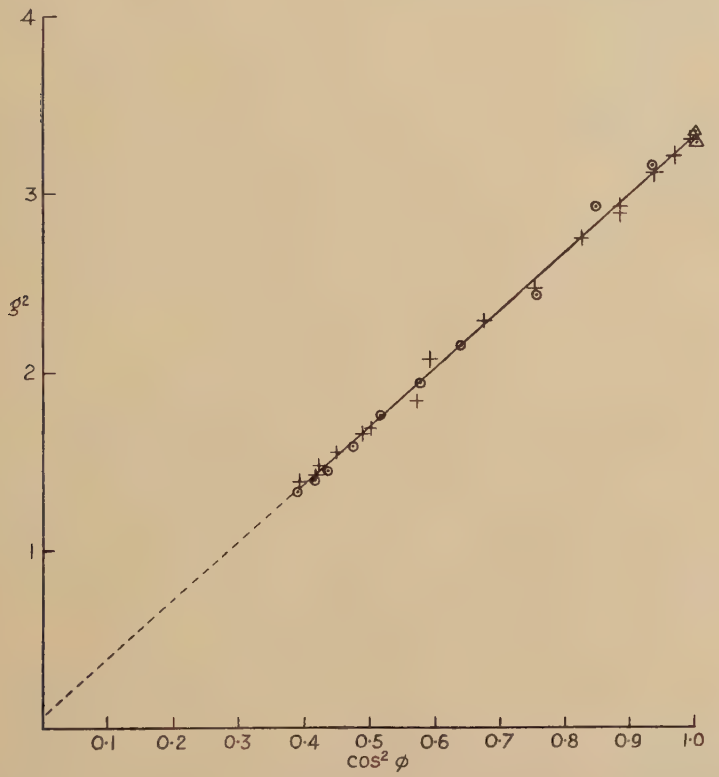

Graph showing the variation of spectroscopic splitting factor, g, with the angle ϕ between the trigonal axis and the magnetic field.

○ Concentrated crystal with the trigonal axis in the plane of the radio frequency and steady magnetic fields.
△ Concentrated crystal with the trigonal axis perpendicular to the fields.
+ Dilute crystal with the trigonal axis in the plane of the fields.

in agreement within the experimental error with the value from resonance. We can conclude that at temperatures in the helium range only one doublet level is appreciably populated. The temperature independent susceptibility is attributable to the second order effect of higher energy levels. With the magnetic field parallel to the crystal

axis the susceptibility proved to be too small to be measured with any accuracy, being masked by interaction of the much greater susceptibility in the perpendicular direction with transverse field gradients.

Paramagnetic relaxation measurements were made by the method of Casimir, Bijl and Du Pré (1941) from which the specific heat and spin-lattice relaxation time of the salt may be calculated (Casimir and Du Pré 1938). The apparatus and experimental method have already been described (Benzie and Cooke 1950 a, b). The specimens used were single crystals cut from a plate 6 cm in diameter and 8 mm thick, which was grown in a period of three weeks in a desiccator over sulphuric acid. In all the measurements the magnetic field was normal to the trigonal axis of the crystal. The spin-lattice relaxation time was found to be highly temperature-dependent. At 4·2°K it was shorter than 10^{-5} sec; at 2·14°K it was 4×10^{-4} sec; at 1·38°K it was 3×10^{-2} sec; and at 1·03°K it was longer than 0·1 sec. In this range then, the relaxation time is varying as T^{-9} or T^{-10}, approximately. At 1·38°K and 1·03°K the specific heat of the salt was determined by measurement of the isothermal and adiabatic susceptibilities in magnetic fields up to 100 gauss. The ratio of the specific heat at constant magnetization C_I to the Curie constant λ was found to be

$$C_I T^2/\lambda = 1970.$$

Taking $g_\perp = 1{\cdot}84$, $\lambda = 0{\cdot}318$ per gram-ion, from which we have $C_I = 7{\cdot}5\times10^{-6}\ R/T^2$, where R=gas constant.

It should be noted that our method of measurement gives only the specific heat due to the magnetic ions, and excludes the lattice specific heat. For most salts this is negligible at a temperature of 1°K, but in this case the magnetic specific heat is so extremely small that this is not so. Observations of the rate of heating of specimens cooled below 1°K by demagnetization indicate that the lattice specific heat becomes comparable with the magnetic specific heat at about 0·5°K.

§ 3. Discussion of the Results

The ground state of the free Ce^{+++} ion is a $^2F_{5/2}$ state, the next lowest level, $^2F_{7/2}$, lying some 2500 cm^{-1} above it. To account for the results we assume that the ground state of the free ion is split by the crystalline electric field into doublets, characterized to a first approximation by the component of angular momentum parallel to the trigonal axis, $J_z = \pm\frac{1}{2}, \pm\frac{3}{2}, \pm\frac{5}{2}$. Assuming that the electric field acting on the cerium ions has the same symmetry as in cerium ethyl sulphate, the work of Elliott and Stevens (1952) shows that the g-values for the state $|J_z=\pm\frac{1}{2}\rangle$ are given by

$$g_\parallel = 2\sin^2\theta, \qquad (3)$$

$$g_\perp = 2\,|\sqrt{(3\sin^2\theta - \sin^2\theta)}\,| \qquad (4)$$

where θ characterizes the admixture of the states $|l_z=0,\ s_z=\frac{1}{2}\rangle$, and $|l_z=1,\ s_z=-\frac{1}{2}\rangle$, in the state $|J_z=\frac{1}{2}\rangle$. From these relations, if

$g_\perp = 1{\cdot}84$, it follows that $g_\parallel$ is either 0·2 or 0·15. It will be seen that both these values lie within our experimental limit for $g_\parallel$, and we may provisionally identify the lowest state of the Ce^{+++} ion in this crystal as the doublet $J_z = \pm\frac{1}{2}$, with no more than a small admixture of other states from the $J = 5/2$ manifold. The susceptibility measurements, which show that Curie's law is obeyed in the helium range, show that the next doublet must be separated from the lowest by at least 10 cm^{-1}.

The specific heat may be compared with the value calculated on the assumption that it arises from dipole–dipole magnetic interaction between the ions. The expression (1) for the splitting of the doublet ground state in a magnetic field is equivalent to the statement that the ions behave like magnetic dipoles

$$\boldsymbol{\mu} = \beta g \,.\, \mathbf{S} \quad . \quad . \quad . \quad . \quad . \quad . \quad . \quad . \quad . \quad (5)$$

where g is a tensor of rank 2, having principal values $g_\parallel$ along Oz, the trigonal axis, and $g_\perp$ along any direction perpendicular to it. As only one level is populated in the temperature range we consider, viz. below 10°K, we can take $\mathbf{S}$ to be the angular momentum of a spin $\frac{1}{2}$, allowing for the proper J value (or admixtures of other levels) via the g tensor.

Following the treatment of Van Vleck (1937) we derive the specific heat from the partition function Z,

$$Z = \sum_\lambda \exp -(W_\lambda / kT), \quad . \quad . \quad . \quad . \quad . \quad . \quad . \quad (6)$$

$$C_I = \frac{\partial}{\partial T}\left[kT^2 \frac{\partial}{\partial T} \log Z\right], \quad . \quad . \quad . \quad . \quad . \quad . \quad . \quad (7)$$

where W_λ is one of the eigen-values of the Hamiltonian $\mathscr{H}$. Expanding in powers of W_λ / kT, and using the fact that

$$\sum_\lambda W_\lambda{}^n = \text{Trace } (\mathscr{H}^n),$$

the specific heat, to terms in $1/T^2$, is

$$C_I = k\left[\frac{\text{Trace } \mathscr{H}}{2kT} + \frac{\text{Trace}(\mathscr{H}^2) - (\text{Trace } \mathscr{H})^2}{8k^2T^2}\right] + . \quad . \quad . \quad (8)$$

From (5), the Hamiltonian for magnetic dipole–dipole interaction is

$$\mathscr{H} = \sum_{j>i} \frac{\beta^2}{r_{ij}{}^3}\left\{(\mathbf{S}_i \,.\, g) \,.\, (g \,.\, \mathbf{S}_j) - \frac{3}{r_{ij}{}^2}[(\mathbf{S}_i \,.\, g) \,.\, \mathbf{r}_{ij}][(\mathbf{S}_j \,.\, g) \,.\, \mathbf{r}_{ij}]\right\}, \quad . \quad . \quad . \quad (9)$$

or in Cartesians

$$\mathscr{H} = \sum_{j>i} \frac{\beta^2}{r_{ij}{}^3}\left\{g_\perp{}^2(S_{xi}S_{xj} + S_{yi}S_{yj}) + g_\parallel{}^2 S_{zi}S_{zj} - \frac{3}{r_{ij}{}^2}[g_\perp(x_{ij}S_{xi} + y_{ij}S_{yi}) + g_\parallel z_{ij}S_{zi}][g_\perp(x_{ij}S_{xj} + y_{ij}S_{yj}) + g_\parallel z_{ij}S_{zj}]\right\}. \quad (10)$$

As in the isotropic case, the trace of this is zero. The trace of $\mathscr{H}^2$ is

$$\text{Tr}(\mathscr{H}^2) = \beta^4 \sum_{j>i} \frac{1}{4r_{ij}{}^6}\left\{g_\perp{}^4\left[\left(1 - \frac{3x_{ij}{}^2}{r_{ij}{}^2}\right)^2 + \left(1 - \frac{3y_{ij}{}^2}{r_{ij}{}^2}\right)^2\right] + g_\parallel{}^4\left(1 - \frac{3z_{ij}{}^2}{r_{ij}{}^2}\right)^2 + 18g_\perp{}^4 \frac{x_{ij}{}^2 y_{ij}{}^2}{r_{ij}{}^4} + 18g_\parallel{}^2 g_\perp{}^2 \frac{(x_{ij}{}^2 + y_{ij}{}^2)z_{ij}{}^2}{r_{ij}{}^4}\right\}. \quad . \quad . \quad . \quad (11)$$

Summing over i, and writing (x_j, y_j, z_j) for the co-ordinates of the jth ion relative to any one fixed ion

$$\mathrm{Tr}(\mathscr{H}^2)=\frac{n}{2}\beta^4\sum_j\frac{1}{4r_j^6}\left\{g_\perp^4\left[2-\frac{6(x_j^2+y_j^2)}{r_j^2}+\frac{9(x_j^4+y_j^4)}{r_j^4}\right]\right.$$
$$\left.+g_\parallel^4\left[1-\frac{6z_j^2}{r_j^2}+\frac{9z^4}{r_j^4}\right]+18g_\perp^4\frac{x_j^2y_j^2}{r_j^4}+18g_\parallel^2g_\perp^2\frac{(x_j^2+y_j^2)}{r_j^4}z_j^2\right\}. \quad (12)$$

On account of axial symmetry, this may be expressed in terms of ρ_j, the distance of the jth ion from the z-axis :

$$\rho_j=x_j^2+y_j^2\,; \qquad r_j^2=\rho_j^2+z_j^2. \quad . \quad . \quad . \quad . \quad . \quad (13)$$

Then

$$\mathrm{Tr}(\mathscr{H}^2)=\frac{n}{2}\beta^4\sum_j\frac{1}{4r_j^6}\left\{g_\perp^4\left(2-\frac{6\rho_j^2}{r_j^2}+\frac{9\rho_j^4}{r_j^4}\right)\right.$$
$$\left.+g_\parallel^4\left(1-\frac{6z_j^2}{r_j^2}+\frac{9z_j^4}{r_j^4}\right)+18g_\parallel^2g_\perp^2\frac{\rho_j^2z_j^2}{r_j^4}\right\}. \quad . \quad . \quad . \quad (14)$$

To obtain the specific heat per gram-ion, the summation over i must be taken over $n=N$ ions, where $N=$Avogadro's number. The lattice sum over j in eqn. (12) need in practice be taken only over relatively close neighbours, since it converges rapidly, its terms being of order $1/r^6$. In this particular case, inclusion of the 326 nearest neighbours gives a result accurate to better than 1%. Further, because of the uncertainty in the value of $g_\parallel$, we neglect the terms in $g_\parallel^2g_\perp^2$ and $g_\parallel^4$, retaining only the term in $g_\perp^4$. On account of the great anisotropy, the resulting uncertainty in the value of the specific heat is less than 3%. The expression for the specific heat is then

$$C_I=\frac{N\beta^4g_\perp^4}{32kT^2}\sum_j\frac{1}{r_j^6}\left(2-\frac{6\rho_j^2}{r_j^2}+\frac{9\rho_j^4}{r_j^4}\right). \quad . \quad . \quad . \quad . \quad (15)$$

Summing over the 326 nearest neighbours then gives $C_I=6{\cdot}75\times10^{-6}\,R/T^2$, accounting for almost the whole of the observed specific heat. Exchange interaction must then be very small.

This specific heat is much smaller than that of any other paramagnetic salt so far reported. For example the specific heat of chromium potassium alum is 2300 times greater, and that of copper potassium sulphate is 85 times greater than that of cerium magnesium nitrate at the same temperature. From the practical point of view, the chief interest of the comparison lies in the use of the salts for obtaining very low temperatures by adiabatic demagnetization. A useful figure is the ratio of the specific heat constant b, given by $C_I=b/T^2$, to the Curie constant λ, since in demagnetization from moderately high magnetic fields the ratio of the final temperature T_f to the initial temperature T_i is given by $T_f^2/T_i^2=b/\lambda H^2$. The value of b/λ for cerium magnesium nitrate is 380 times smaller than for chromium potassium alum, and 60 times smaller than for copper potassium sulphate.

The properties of cerium magnesium nitrate below 1°K have been investigated by Daniels and Robinson (1953), whose experiments,

reported in the following paper, show that the susceptibility obeys Curie's law within an accuracy of 2% down to 0·006°K, and that this temperature may be reached by demagnetization from a field of 7·13 kilogauss at 1°K. As in the comparable case of cerium ethyl sulphate (Cooke, Whitley and Wolf 1953) the salt lends itself to experiments requiring the application of a magnetic field after demagnetization, since by applying the magnetic field along the axis of low susceptibility the temperature is raised by only a small amount. In an experiment on the alignment of ^{60}Co nuclei reported by Ambler, Grace, Halban, Kurti, Durand, Johnson and Lemmer (1953), using cerium magnesium nitrate as a cooling agent, a field of 430 gauss was applied at a temperature of 0·007°K, producing a 50% anisotropy in the gamma-radiation.

Acknowledgments

We wish to express our gratitude to Professor F. E. Simon for his interest and encouragement, and to Dr. B. Bleaney, Dr. J. M. Daniels, Dr. N. Kurti, Mr. F. N. H. Robinson, and Dr. K. W. H. Stevens for their cooperation. We are especially indebted to Mr. H. M. Powell for his work on the cerium ion lattice structure. This work was carried out during the tenure of an Overseas Research Scholarship awarded by the National Research Council of Canada (H. J. D.) and a Department of Scientific and Industrial Research Award (W. P. W.).

References

Ambler, E., Grace, M. A., Halban, H., Kurti, N., Durand, H., Johnson, C. E., and Lemmer, H. R., 1953, *Phil. Mag.*, **44,** 216.

Benzie, R. J., and Cooke, A. H., 1950 a, *Proc. Phys. Soc.* A, **63,** 201 ; 1950 b, *Ibid.*, **63,** 213.

Becquerel, J., de Haas, W. J., and van den Handel, J., 1931, *Proc. K. Acad. Wet. Amst.*, **34,** 1231.

Casimir, H. B. G., Bijl, D., and Du Pré, F. K., 1941, *Physica*, **8,** 449.

Casimir, H. B. G., and Du Pré, F. K., 1938, *Physica*, **5,** 507.

Cooke, A. H., Whitley, S., and Wolf, W. P., 1953, *Proc. Phys. Soc.* (to be published).

Daniels, J. M., and Robinson, F. N. H., 1953, *Phil. Mag.*, **44,** 630.

Elliott, R. J., and Stevens, K. W. H., 1952, *Proc. Roy. Soc.* A, **215,** 437.

Groth, P., 1908, *Chemische Krystallographie*, **2,** 156.

Krishnan, K. S., and Mookherji, A., 1938, *Phil. Trans. Roy. Soc.* A, **237,** 135.

LXVII. *Cerium Magnesium Nitrate II: Determination of the Entropy–Absolute Temperature Relation below* 1°K

By J. M. Daniels and F. N. H. Robinson
The Clarendon Laboratory, Oxford*

[Received February 27, 1953]

Abstract

The entropy of cerium magnesium nitrate as a function of absolute temperature and the relation between the magnetic temperature and absolute temperature below 1°K have been determined by adiabatic demagnetization experiments. The absolute temperature is almost constant and equal to 3·08 millidegrees for $S/R<0{\cdot}45$. Above 6 millidegrees $T=T^{\star}$. The results for lower temperatures are given in the form of a table.

§ 1. Introduction

In some experiments on the alignment of atomic nuclei by Bleaney's method (Daniels, Grace and Robinson 1951), we used the Tutton salts, because they form an isomorphous series whose thermal and magnetic properties can be varied widely by changing the proportions of the isomorphous constituents. The advantages of such a series for this purpose have been described elsewhere (Daniels *et al.* 1953). In our search for other suitable isomorphous series of salts, our attention was drawn to the double nitrates of the rare earths and the iron transition series, whose suitability for nuclear alignment experiments had been suggested by Bleaney (1953). A complete investigation of the thermal and magnetic properties of one of these salts was thought desirable, and cerium magnesium nitrate was chosen. Because Ce^{+++} is the only paramagnetic ion with Kramers degeneracy yet no hyperfine splitting of the ground state which can be introduced into this series, it is to be expected that lower absolute temperatures can be attained by demagnetizing this salt, rather than any of the others. The results of measurements in the liquid helium range of temperatures reported in the preceding paper lent support to this view.

§ 2. Experimental Procedure

A piece was cut from a single crystal and shaped into an approximate prolate spheroid. It was 6 cm long and 1 cm diameter, and the long axis of the spheroid was perpendicular to the crystallographic trigonal axis (i.e. in the plane of the crystal plate). This was the same specimen as was used by Cooke and Wolf for their specific heat measurements reported in the preceding paper. Magnetizing and measuring fields were applied along this axis. The magnetic temperature, T^{*}, was measured in the usual way with a mutual inductance surrounding the

* Communicated by the Authors.

specimen, and a ballistic galvanometer. Using the g-values quoted in the preceding paper, and assuming that the specimen is a spheroid, we get $T^\star = T^* + \Delta$°K where $\Delta = 0{\cdot}0027$°K, and $T^\star$ is the magnetic temperature for a specimen of spherical shape, as defined by Kurti and Simon (1938). The value of Δ actually taken was $0{\cdot}00265$°K since this is in better agreement with the observed entropy T^* curve as will be described later.

The entropy–magnetic temperature (S–$T^\star$) relation was constructed as follows. A number of demagnetizations were made, and the values of T^* obtained immediately after demagnetization, $T_f{}^*$, were obtained by extrapolating the observed values of T^* back to the time of demagnetization. The entropy of the specimen at each value of $T_f{}^*$, which is the same as before the magnetizing field is turned off, is obtained from the values of the magnetizing field and the initial temperature using the tables of Hull and Hull (1941). Values of magnetic temperature $T_f{}^*$ corresponding to different values of entropy S are thus obtained. At temperatures just below 1°K, where $T = T^\star$ and $S'/R \equiv \{\ln 2 - S/R\} \propto 1/T^2$, a graph of $(R/S')^{1/2}$ against $T_f{}^*$ is a straight line which, when extrapolated to cut the $T_f{}^*$ axis, makes an intercept of $-\Delta$. The value of Δ so obtained was $0{\cdot}00265$°K, and this was assumed to be the appropriate value of Δ for our specimen. This graph is shown in fig. 1. From the slope of this graph, it is found that $S'T^2/R = 3{\cdot}2 \times 10^{-6}$. A graph of S/R against $T^\star$ for low values of $T^\star$ is shown in fig. 2. It is noticed that S/R is proportional to $1/T^{\star 2}$ for values of $T^\star$ from 1 degree down to $0{\cdot}0035$ degrees, where $S/R = 0{\cdot}43$. For values of S/R between $0{\cdot}1$ and $0{\cdot}28$, $T^\star$ is constant to within the accuracy of our measurements.

The 'magnetic specific heat', $C^\star$, was obtained in the usual way by heating with γ-rays, and the results are shown in fig. 3, where $\log C^\star$ is plotted against $\log T^\star$. It is seen that $C^\star$ is proportional to $1/T^{\star 2}$ for values of $T^\star$ above $0{\cdot}01$ degrees, and at $T^\star = 0{\cdot}0032$ degrees $C^\star$ becomes infinite.

The absolute temperature is obtained from the thermodynamic relation $T \,.\, dS = dQ$, which can be written in the form

$$T = \frac{C^\star/R}{(d/dT^\star)(S/R)}.$$

Hence it is seen that above $0{\cdot}01$ degrees, where both S'/R and $C^\star$ are proportional to $1/T^{\star 2}$, $T = T^\star$. The sloping line in fig. 3 is a line of slope -2 through the centroid of the points A, for which $T^\star > 0{\cdot}008$ degrees. The centroid of the points B, indicated by the vertical cross in fig. 3, lies very near the sloping line. Assuming this value of $C^\star$, and also using the fact that S'/R is still proportional to $1/T^{\star 2}$, we find that for $T^\star = 0{\cdot}00573$ degrees, $T = 0{\cdot}00563$°K.

Below this temperature, measurements of $C^\star$ are not sufficiently accurate to apply this method; and at $T^\star = 0{\cdot}0032$ degrees, $T^\star$ is no longer a useful thermometric parameter, since both $C^\star$ and $(d/dT^\star)(S/R)$ are infinite.

Fig. 1

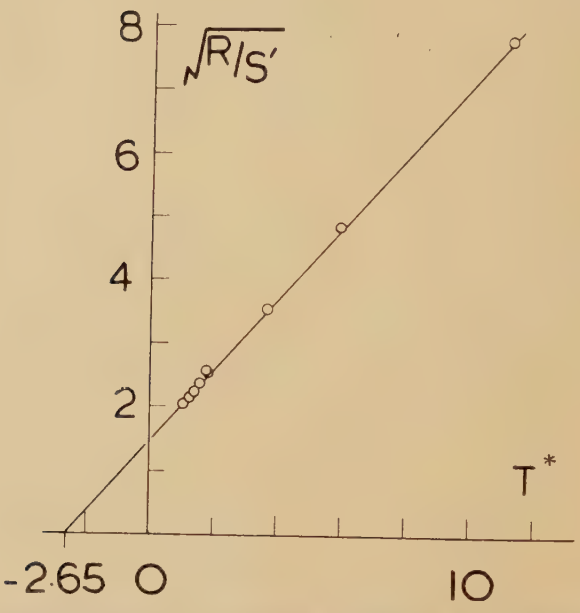

Entropy of cerium magnesium nitrate as a function of magnetic temperature, plotted to show the demagnetizing correction temperature $\Delta = 0{\cdot}00265°$K.

The units of T^* are degrees $\times 10^{-3}$.

Fig. 2

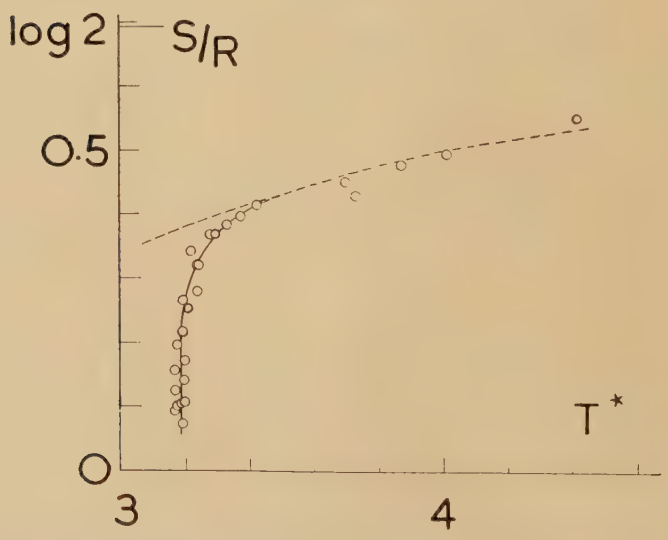

Entropy of cerium magnesium nitrate as a function of magnetic temperature $T\star$. The units of $T\star$ are degrees $\times 10^{-3}$. The dashed line represents $\ln 2 - \frac{S}{R} = \frac{3{\cdot}2 \times 10^{-6}}{T\star^2}$.

In this region, T was obtained by constructing a Q–S curve; the slope of this curve, $dQ/dS=T$. This was done as follows. Immediately after demagnetization from known initial conditions, which define S, the specimen was subjected to a strong source of γ-radiation for a fixed

Fig. 3

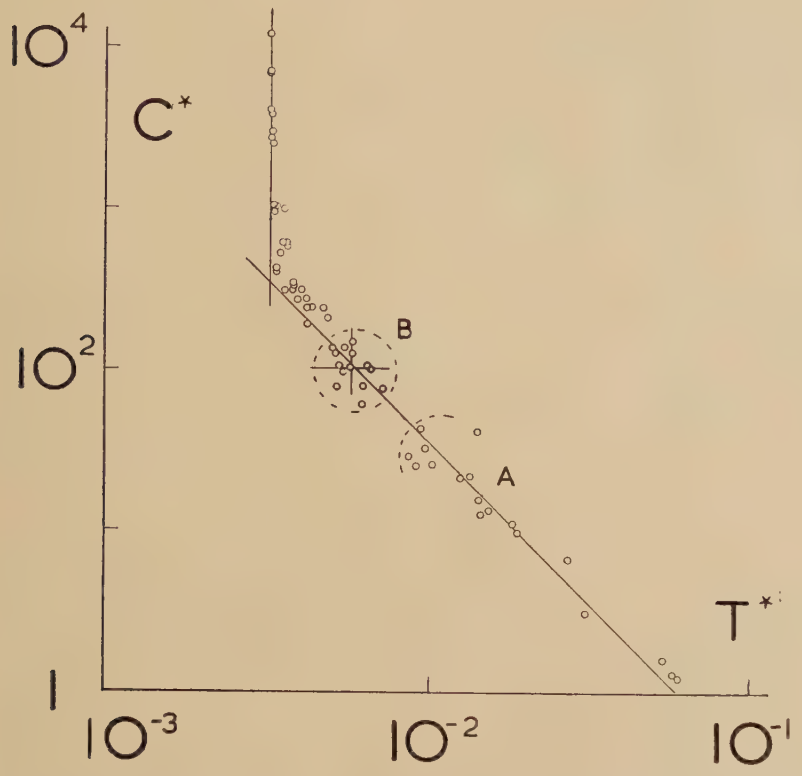

The magnetic specific heat $C^\star$ of cerium magnesium nitrate as a function of magnetic temperature $T^\star$. $C^\star$ is in arbitrary units, $T^\star$ in degrees. The sloping line is a line of slope -2 through the centroid of the points A. The vertical cross marks the centroid of points B.

time, supplying a quantity of heat Q_1. The magnetic temperature was then measured for a few minutes, and extrapolated back to zero time to allow for stray heating. The time of application of γ-rays is adjusted so that the extrapolated value of $T^\star$ lies in the range 0·01 degrees to 0·3 degrees, where $C^\star=A/T^{\star 2}$. Hence the amount of heat Q_2 required to warm the specimen up to some convenient reference temperature can be easily calculated. The value of A, $6{\cdot}4\times10^{-6}R$, was taken from the slope of fig. 1. Then

$$Q=Q_1+Q_2 \quad \text{and} \quad dQ/dS=dQ_1/dS+dQ_2/dS.$$

If it is arranged that, for a series of measurements, the time of γ-ray heating, and hence Q_1, is not varied,

$$T=dQ/dS=dQ_2/dS.$$

Figure 4 incorporates the results of four separate series of experiments. In each of these series the slope $dQ/dS=T$ appeared to be constant below $S/R=0{\cdot}5$. The line shown in fig. 4 is constructed by fitting a line by

Fig. 4

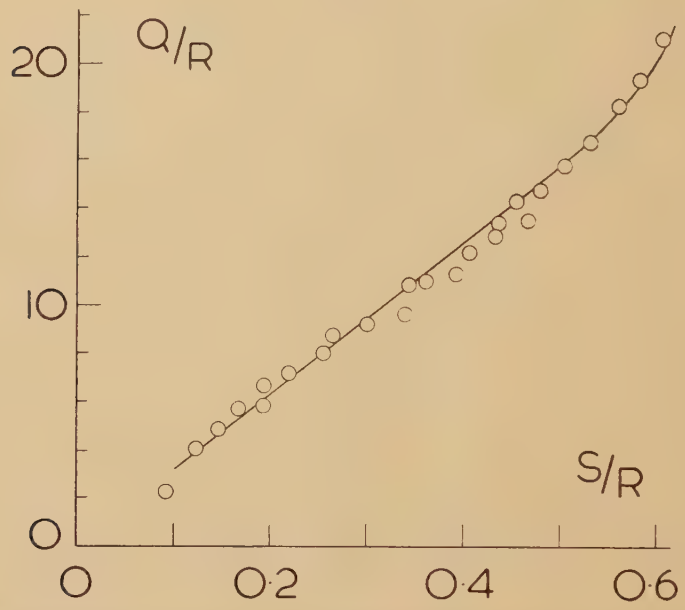

The gram ionic heat content Q of cerium magnesium nitrate as a function of entropy S. The units of $\frac{Q}{R}$ are degrees $\times 10^{-4}$; the zero of $\frac{Q}{R}$ is arbitrary.

least squares to the points below $S/R=0{\cdot}506$. (Since the amount of γ-ray heating was different in each series of measurements, the zero of Q has had to be adjusted for each series. This was also done by least squares.) This straight line, $10^4Q/R=30{\cdot}8S/R$; $T=3{\cdot}08\times10^{-3}$°K, is then taken to be a faithful representation of the points below $S/R=0{\cdot}4$. The line is continued above $S/R=0{\cdot}4$ by seeking a power series

$$10^4Q/R=a+b(S/R-0{\cdot}4)+c(S/R-0{\cdot}4)^2+\ldots.$$

which fits smoothly on to the straight line at $S/R=0{\cdot}4$ and gives

$$T=dQ/dS=T^\star=0{\cdot}00586 \text{ at } S/R=0{\cdot}6.$$

The curve shown in fig. 4 is

$$10^4Q/R=30{\cdot}8S/R+0{\cdot}087(10S/R-4)^4,$$

from which

$$T=dQ/dS=3{\cdot}08+0{\cdot}348(10S/R-4)^3 \text{ millidegrees.}$$

(Above $S/R=0{\cdot}6$, T and $T^\star$ are identical.) The table giving T and $T^\star$ for various values of S/R is constructed using this formula. It is seen that T is constant at 0·00308°K for a considerable range of values of S/R.

The value of $T=0{\cdot}00570°\text{K}$ at $T^{\star}=0{\cdot}00573$ is slightly different from the value of $T=0{\cdot}00563°\text{K}$ obtained from the specific heat measurements. The values in this table are, however, accurate only to two significant figures, the third is included for ease in interpolation.

§ 3. Conclusion

We find that the entropy diminution, S', of cerium magnesium nitrate, is proportional to $1/T^2$ down to $0{\cdot}01°\text{K}$, and that the deviation from the $1/T^2$ law at $0{\cdot}006°\text{K}$ is probably not more than 2%. Below this temperature, the entropy as a function of absolute temperature is as given in the table. For values of S/R between 0·1 and 0·425, the absolute temperature is almost constant at $0{\cdot}0031°\text{K}$. Cerium magnesium nitrate can thus be used to provide a constant temperature bath at this temperature.

The constant of proportionality between S'/R and $1/T^2$, $3{\cdot}2\times10^{-6}\,\text{deg}^{-2}$, is seen to be rather different from the value $3{\cdot}75\times10^{-6}\,\text{deg}^{-2}$ quoted in the preceding paper. No explanation can at present be offered for this discrepancy, except to stress the difficulties of measuring such a small specific heat, which may be compared with one of the lowest values previously measured, that of copper caesium sulphate for which $S'T^2/R=1{\cdot}26\times10^{-4}$, about 300 times as large.

S/R	T millidegrees	$T^{\star}$ millidegrees	S/R	T millidegrees	$T^{\star}$ millidegrees	S/R	T millidegrees	$T^{\star}$ millidegrees
0·100	3·08	3·20	0·450	3·12	3·66	0·560	4·50	4·90
0·300	3·08	3·20	0·475	3·23	3·88	0·570	4·79	5·09
0·350	3·08	3·28	0·500	3·43	4·09	0·580	5·12	5·32
0·400	3·08	3·38	0·525	3·76	4·35	0·590	5·46	5·56
0·425	3·08	3·49	0·550	4·25	4·72	0·600	5·86	5·86

Acknowledgments

We wish to acknowledge gratefully the unstinted assistance in the experimental work given us by Dr. N. Kurti; the cooperation of Dr. Cooke, Mr. Duffus and Mr. Wolf in this project, and the continued encouragement given to us by Professor F. E. Simon.

This work was carried out during the tenure of an I.C.I. Research Fellowship (J.M.D.) and a Nuffield Research Fellowship (F.N.H.R.).

References

Bleaney, B., 1953, private communication.
Daniels, J. M., Grace, M. A., and Robinson, F. N. H., 1951, *Nature, Lond.*, **168**, 780.
Daniels *et al.*, 1953, to be published.
Hull, J. R., and Hull, R. A., 1941, *J. Chem. Phys.*, **9**, 465.
Kurti, N., and Simon, F. E., 1938, *Phil. Mag.*, **26**, 849.

LXVIII. *The Specific Heat of Beryllium at Low Temperatures*

By R. W. Hill and P. L. Smith
Clarendon Laboratory, Oxford*

[Received March 3, 1953]

Abstract

Measurements have been made in the temperature range 4 to 300°K. The results obtained are consistent with the most recent high temperature data, but are markedly different from existing low temperature ones. In particular, no trace of anomalous behaviour near 11°K was found, and the low temperature results have been analysed to yield an electronic specific heat of $5{\cdot}4\times10^{-5}T$ cal deg^{-1} g atom^{-1}, in good agreement with theoretical predictions. The Debye characteristic temperature is constant at 1160° below 20°K, but falls with increasing temperature to 925° at 300°K; this behaviour is believed to be characteristic of the close-packed hexagonal lattice. Values are also given for the heat capacity of a bakelite varnish used in these experiments.

§ 1. Introduction

Before this work was undertaken, the only measurements of the specific heat of beryllium at low temperatures were those of Cristescu and Simon (1934), who reported a small anomaly around 11°K. The magnitude of this anomaly was comparable with that found in superconductors at their transition points, and it was suggested that the anomaly was electronic in origin. More recently, Buckingham (1951) has shown that the type of electron-lattice interaction which gives rise to superconductivity (Fröhlich 1950) can also cause an appreciable anomaly in the electronic specific heat of those non-superconductors whose behaviour can adequately be represented in terms of the free electron model. While beryllium can scarcely be included in this category, a new investigation seemed worthwhile, particularly since the beryllium obtainable at the time of the older measurements must have been very impure by modern standards. This latter point was considered important, since small amounts of impurity are well known to produce disproportionately large effects in the behaviour of some metals, particularly superconductors.

When measurements were made between 4 and 20°K, the results obtained differed greatly from those of Cristescu and Simon, and the measurements were therefore extended up to room temperature, where comparison with the recent high temperature values of Ginnings, Douglas and Ball (1951) becomes possible.

* Communicated by Professor F. Simon, F.R.S.

§ 2. Experimental

Due to the extreme smallness of the specific heat of beryllium, it is impracticable to enclose a specimen in a calorimeter in the normal way. Instead, a cylindrical block of the metal must be used, the electrical heater and resistance thermometers being wound onto the block using bakelite varnish to ensure good thermal contact. The beryllium used in these experiments was a bullet-shaped piece, weighing 127 g (14 moles), which had been prepared from powder by a high temperature extrusion process. This specimen was kindly supplied by Dr. Blainey of A.E.R.E., Harwell, whose analysis shows it to have been 99·5% beryllium by weight, the major impurities being chlorine (0·15%) and oxygen (0·1%). Small amounts (0·05%) of several other elements were also detected.

The method of mounting the specimen is shown in fig. 1 ; the low temperature apparatus closely resembles that described by Parkinson, Simon and Spedding (1951). For the temperature range 4° to 25°K a thermometer of 47 S.W.G. constantan (1000 ohms) was used, and at higher temperatures a platinum thermometer (120 ohms at 20°C). The heater consisted of 700 ohms of 44 S.W.G. constantan.

In a normal calorimeter, calibration of the thermometers is carried out by measuring the vapour pressure over a small quantity of liquid condensed into the calorimeter. This method is impossible here, and the procedure adopted was to put the liquid in the space A ; helium was liquefied by the Simon method in B when necessary. With exchange gas in the shield C, and with the jacket D highly evacuated, the specimen E reached temperature equilibrium with the liquid in a few minutes below 20°K, the corresponding time in the range 60 to 90°K being about one hour. For the constantan thermometer, the hydrogen boiling and triple points and the helium boiling point were taken as fixed points, the known behaviour of the constantan (Parkinson 1950) permitting accurate interpolation. An estimate was made of the extent of the ortho-para conversion in the liquid hydrogen, and the appropriate boiling and triple points taken.

The platinum thermometer was calibrated at the hydrogen and ice points, and also between 60 and 90°K. In this latter range the calibration was constructed from the nitrogen and oxygen vapour pressures, pure gas being condensed into A, with the appropriate commercial liquid in the Dewar vessel. The resistance values at the oxygen boiling point and the nitrogen boiling and triple points were readily obtained, and intermediate values were found by controlled pumping of the pure liquids, a high vacuum being maintained in the jacket D throughout.

The specific heat measurements were made in a conventional manner, no difficulty having been experienced in obtaining adequate thermal insulation except at the lowest temperatures, where, in order to remove the exchange gas used for cooling to 4°K, it was found necessary to pump for at least two hours.

It has been mentioned that varnish was used to bond the thermometer and heater wires to the specimen.—These wires, and an aluminium radiation shield used at the higher temperatures, do not contribute appreciably to the total measured heat capacity, but consideration of Simon's (1922) values for a cement 'Ketonharz' indicated that a correction of about 10% might have to be made for the heat capacity of

Fig. 1

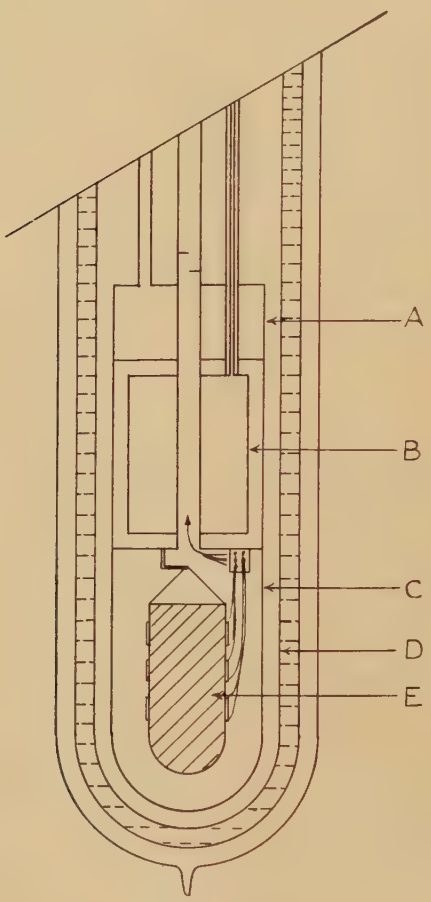

The apparatus.

the varnish at 20°K. It was therefore decided to measure the heat capacity of the varnish between 4 and 90°K, at which temperature the correction was expected to be negligible. A specimen was prepared by coating thin aluminium foil with the varnish, which was subsequently baked to the manufacturer's specification. The results obtained are given in table 1; the magnitude of the correction to be applied to the beryllium results nowhere exceeds 10% and is less than 0·5% above 90°K.

§ 3. Results

Over 150 measured points were obtained between 4° and 300°K. In this temperature range the specific heat changes by a factor of 10^4, and an adequate graphical representation of the results is therefore difficult.

Table 1. The Specific Heat of Bakelite Varnish*

T°K	C_p (cals deg^{-1} g^{-1})
4	0·0011
10	0·0046
15	0·010
20	0·017
30	0·029
40	0·043
50	0·057
60	0·068
70	0·082
80	0·099
90	0·105

* Formite Bakelite Varnish V11105.

Fig. 2

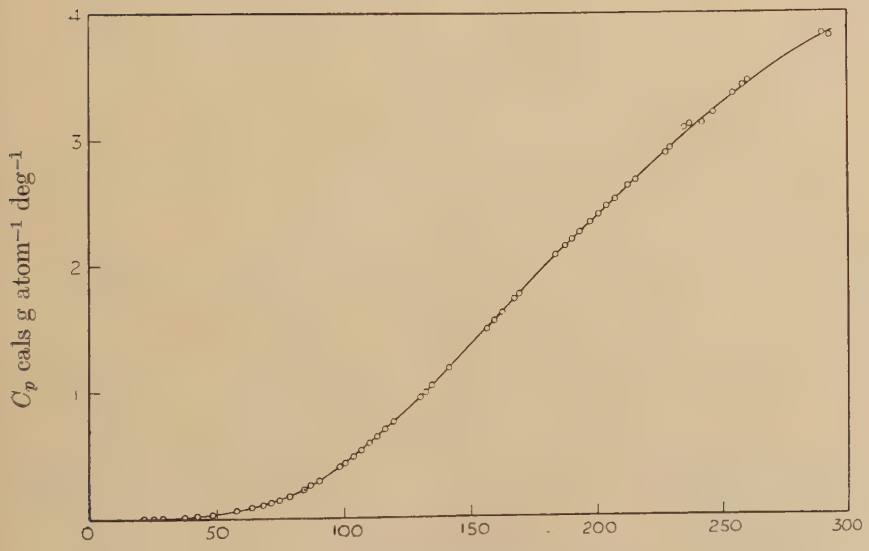

The specific heat of beryllium above 20°K.

The results obtained at the higher temperatures are therefore shown in fig. 2, and those below 20°K in fig. 3. It is evident from these graphs that the results show little scatter except at the very highest and lowest

temperatures. The high temperature scatter is due primarily to the difficulty of keeping a sufficiently high vacuum in an apparatus of the type used when the temperature of the walls approaches room temperature and out-gassing becomes appreciable. The scatter at the lowest temperatures reflects the difficulty inherent in measuring very small heat capacities.

Fig. 3

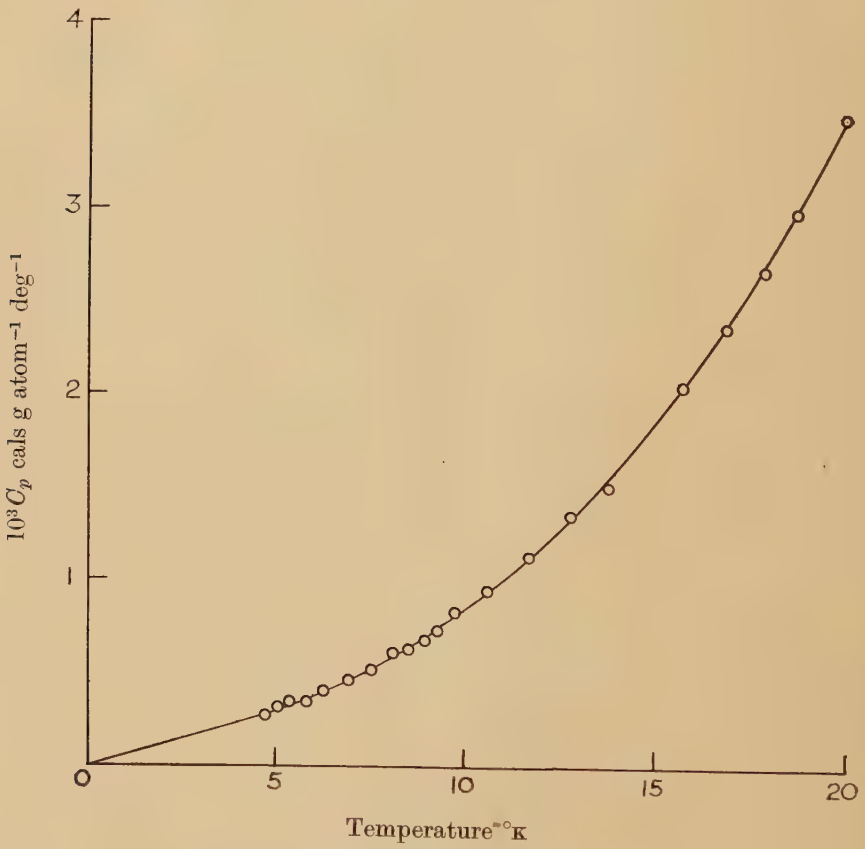

The specific heat of beryllium below 20°K.
○ experiment. —— equation (1).

Smoothed values of the specific heat C_p are given in table 2, together with the values for the enthalpy H, the entropy S and the Gibbs' free energy G which may be calculated from them. Before the behaviour of the specific heat itself may be analysed, the values of C_p must be reduced to C_v; the relation used for this was,

$$C_p - C_v = 1{\cdot}11 \times 10^{-5} C_p^2 T,$$

where the coefficient is the one obtained by Ginnings *et al.* from the thermal expansion and compressibility near room temperature. Having

derived C_v, it is next necessary to separate the lattice and the electronic contributions. Analysis of the low temperature results shows them to fit the formula

$$C_v = 5{\cdot}4 \times 10^{-5} T + 464(T/1160)^3 \text{ cals g atom}^{-1} \text{ deg}^{-1}, \quad . \; . \quad (1)$$

this being the full line in fig. 3. The former term gives the electronic contribution, and may be expected to be valid throughout the temperature range of the present experiments. After this term has been subtracted from C_v, the lattice contribution remains, and this may now be used to derive the Debye characteristic temperature θ. Values of C_v (total) and θ are included in table 2.

Table 2. The Specific Heats and Thermodynamic Functions of Beryllium

T°K	C_p	C_v	θ	S	$H-H_0$	$-(G-G_0)$
5	0·00031		1160			
10	0·00083		1160			
20	0·00345		1160			
40	0·0216		1155	0·009	0·2	
60	0·0734		1145	0·027	1·2	
80	0·195		1070	0·063	3·7	1·3
100	0·437		1015	0·130	9·8	3·2
120	0·762		995	0·237	21·8	6·6
150	1·37		970	0·439	53·6	16·8
200	2·40	2·39	950	1·01	148	54
250	3·31	3·28	925	1·64	292	119
300	3·95	3·90	925	2·30	475	216

The thermal unit is the calorie per g atom throughout.

The significance of these results will be discussed in the next section ; for the moment we shall be concerned only with their relation to those obtained by other workers. In the case of Cristescu and Simon's results a direct comparison may be made, and the most striking difference is the complete absence of the anomalous behaviour around 11°K reported by the older authors. The two sets of results also differ at other temperatures by amounts which vary between plus and minus 10%. Compared with the remarkable range of values which have been reported at higher temperatures (Ginnings, Douglas and Ball, *loc. cit.*), this disagreement is not particularly great, and the different purities of the specimens seems to be its only possible cause.

Since the present measurements do not overlap those of Ginnings *et al.*, a comparison can best be made from the values of Debye θ deduced from them. Using the present value of the electronic specific heat, the older results have been recalculated and θ values obtained which decrease slowly with temperature ; these, together with those listed in table 2,

are plotted in fig. 4. The agreement is seen to be very satisfactory, though it appears that our present values near 250°K are a little high, the error being too small to affect appreciably the thermodynamic functions listed above.

Fig. 4

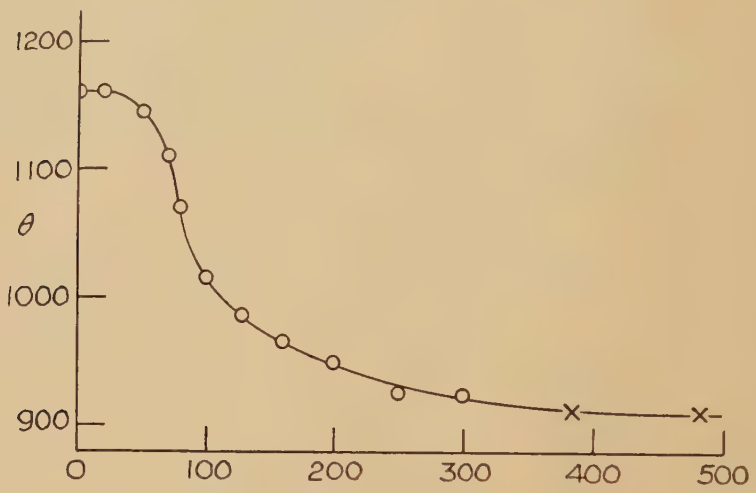

The Debye characteristic temperature of beryllium.
× Ginnings, Douglas and Ball. ○ this research.

§ 4. Discussion

(*a*) *The Electronic Specific Heat*

The specific heat of the conduction electrons in a metal depends on $n(\epsilon')$, the density of electronic energy levels per electron at the Fermi surface,

$$C=\gamma T=\frac{\pi^2 k^2 T}{3}n(\epsilon').$$

For perfectly free electrons, this relation takes the simple form

$$\gamma=3{\cdot}26\times10^{-5}\,n^{1/3}(A/\rho)^{2/3}\text{ cal deg}^{-2}\text{ g atom}^{-1}$$

where n is the number of conduction electrons per atom, A the atomic weight and ρ the density of the metal. It is usually found that the measured value of γ exceeds that calculated from the free electron model, but in the case of beryllium the reverse is true, the calculated value being $1{\cdot}18\times10^{-4}$ cal deg^{-2} g atom^{-1} compared with the experimental value of $0{\cdot}54\times10^{-4}$. The same result is expressed in the statement that the ratio of effective to real electron mass of the conduction electrons $m^*/m=0{\cdot}46$.

An explanation of this curious result can be obtained from band theory, according to which a divalent metal like beryllium is an electron conductor only by virtue of the overlapping of the s and p bands. In the present

case, Herring and Hill (1940) have shown that this overlapping occurs in such a way that the density of states curve passes through a minimum in the vicinity of the Fermi surface. The value of γ cannot immediately be deduced from these calculations, but the same results have been given in a more convenient form by Seitz (1940); from these a value of $\gamma = 5{\cdot}5 \times 10^{-5}$ cal deg^{-2} g atom^{-1} is obtained. This agreement with the experimental value is most satisfactory.

It is interesting to compare the present case with that of magnesium, where the energy of the Fermi surface is appreciably greater than that at which the minimum in the density of states occurs (Mott and Jones 1936), so that the value of γ should be roughly the free electron value. This has been shown to be the case by Estermann, Friedberg and Goldman (1951), who give a value of m^*/m of 1·33.

Fig. 5

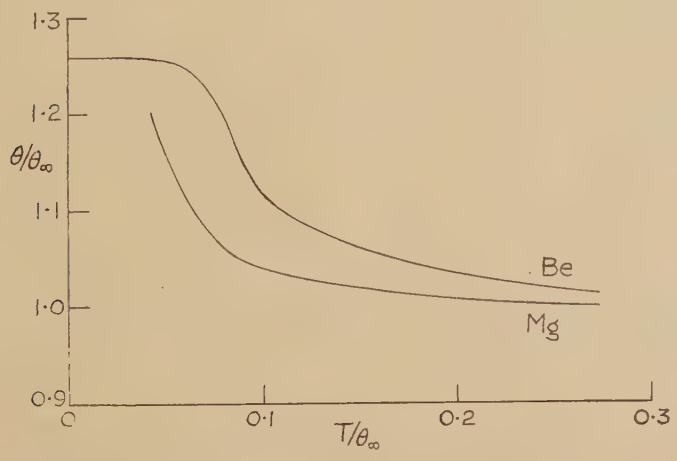

The reduced Debye characteristic temperature of beryllium and magnesium as a function of reduced temperature.

(*b*) *The Lattice Specific Heat*

The temperature variation of the Debye θ, which must be considered only as a convenient parameter, has been given in table 2. This variation may be compared with that shown by magnesium (Clusius and Vaughen 1930) which has the same hexagonal close-packed structure with a similar axial ratio. A comparison may most easily be made if a reduced form of θ is studied; in the present cases it is found that θ is virtually constant at the higher temperatures, and this value, denoted by θ_∞, has been used as a convenient reducing parameter. Using $\theta_\infty = 920°$ for beryllium and 327° for magnesium, curves of θ/θ_∞ as a function of T/θ_∞ have been constructed (fig. 5). The θ values for magnesium have been calculated after making due allowance for the electronic contribution. At a given T/θ, the electronic contribution is roughly six times larger in

magnesium than in beryllium, and the accuracy of the θ values consequently lower, though the effect of this is serious at the lowest temperatures only.

Comparing the two curves of fig. 5, it is seen that there is a marked similarity between them, though they do not coincide. Coincidence would require the ratios of the force constants between various types of neighbour to be the same in the two metals, in addition to the necessity of identical axial ratios. Since the axial ratios differ by about 5^{0}_{0}, and the equality of the force constant ratios is *a priori* improbable, the failure of the curves to coincide is not surprising. Indeed, when this case is compared with that of the diamond structure elements (Hill and Parkinson 1952) it is the similarity of the curves, rather than their difference, which is remarkable.

Acknowledgments

The authors are indebted to Professor F. E. Simon, F.R.S., for suggesting this investigation, and for valuable advice and encouragement. They are also indebted to the University of Oxford for the award of an I.C.I. Fellowship, and the Directorate of Scientific and Industrial Research for a grant respectively. This work was supported by a grant from Industrial Distributors, Ltd.

References

Buckingham, M. J., 1951, *Nature, Lond.*, **168,** 281.
Clusius, K., and Vaughen, J. V., 1930, *J. Amer. Chem. Soc.*, **52,** 4686.
Cristescu, S., and Simon, F. E., 1934, *Z. phys. Chem.* B, **25,** 273.
Estermann, I., Friedberg, A. A., and Goldman, J. E., 1952, *Phys. Rev.*, **87,** 582.
Fröhlich, H., 1950, *Phys. Rev.*, **79,** 845.
Ginnings, D. C., Douglas, T. B., and Ball, A. F., 1951, *J. Amer. Chem. Soc.*, **73,** 1236.
Herring, C., and Hill, A. G., 1940, *Phys. Rev.*, **58,** 132.
Hill, R. W., and Parkinson, D. H., 1952, *Phil. Mag.*, **43,** 309.
Mott, N. F., and Jones, H., 1936, *Theory of the Properties of Metals and Alloys* (Oxford).
Parkinson, D. H., 1950, *Thesis*, Oxford.
Parkinson, D. H., Simon, F. E., and Spedding, F. H., 1951, *Proc. Roy. Soc.* A, **207,** 137.
Seitz, F., 1940, *Modern Theory of Solids* (New York : McGraw-Hill).
Simon, F. E., 1922, *Ann. Phys., Lpz.*, **68,** 241.

LXIX. *The Thermal and Electrical Conductivities of Beryllium*

By R. W. Powell
Physics Department, National Physical Laboratory, Teddington*

[Received February 17, 1953]

Abstract

Several samples of metallic beryllium have been studied. Heat treatment to temperatures of the order of 700°C invariably caused increases in the thermal and electrical conductivities and determinations of these two properties have been made for both as received and heat treated states. For the most part the thermal conductivity measurements were limited to the range 50° to 350°C, but in one instance these measurements were extended to 700°C.

The thermal conductivity is found to have a large negative temperature coefficient, in contrast to the only previous measurements recorded above room temperature which had yielded a positive temperature coefficient. Much of the abnormal nature of the temperature variation of the Lorenz function of beryllium which these results of Lewis (1929) had indicated now disappears.

Analysis of the present results suggests that beryllium, on account of its high characteristic temperature, possesses a considerable lattice component of thermal conduction, K_g, which can be represented over the range 50° to 400°C by the equation

$$K_g = \frac{268}{T} - 0{\cdot}151,$$

where K_g is in joule cm/cm² sec°C and T is in °K.

The electronic component K_e is represented over the same range by the equation

$$K_e = 2{\cdot}57 \times 10^{-8} \frac{T}{\rho} - \frac{249 \times 10^{-8}}{\rho},$$

where ρ is the electrical resistivity in ohm cm²/cm.

Hence the equation suggested for the derivation of the thermal conductivity of a sample of beryllium from a knowledge of its electrical resistivity is :—

$$K = 10^{-8} \frac{T}{\rho}\left(2{\cdot}57 - \frac{249}{T}\right) + \frac{268}{T} - 0{\cdot}151.$$

This equation fits the present results to within −6 to +5%. It could probably be applied to temperatures above 400°C, but not below 0°C, where further investigation is considered necessary.

---

* Communicated by the Author.

§ 1. Introduction

The writer's interest in the thermal conductivity of beryllium was first aroused when Lewis (1929) published a paper dealing with several properties of this metal over the range −170° to 180°C. Lewis found that the Lorenz function was far from constant but increased rapidly over the temperature range studied. He remarked that for the Wiedemann–Franz–Lorenz Law to hold for beryllium its thermal conductivity would need to decrease instead of increase with rise of temperature.

Figure 1 contains some typical curves showing the variation of the Lorenz functions of metals and alloys with temperature and includes Lewis' curve for beryllium. This emphasizes the abnormal nature of the beryllium results. A somewhat unusual behaviour might be associated with beryllium having a characteristic temperature of about 1000°K,

Fig. 1

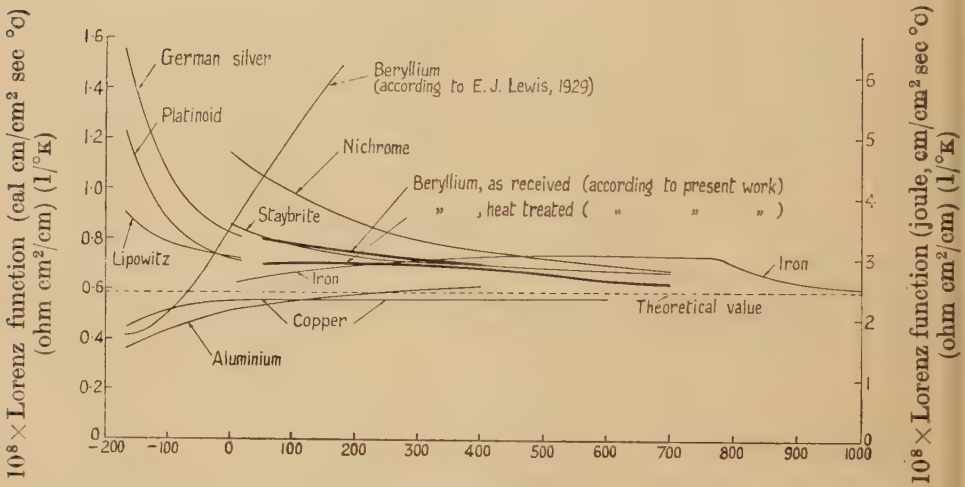

Temperature variation of Lorenz functions of metals and alloys.

which is several times greater than the absolute temperature of the experiments, but the course of the Lorenz function curve over the range −170° to 180°C was so anomalous that it was felt highly desirable for an independent investigation to be undertaken and a wider range of temperatures covered. The specimens provided for the present investigation were, however, the first samples of beryllium which had become available to the writer in a form suitable for these experiments.

In the meantime the reliability of Lewis' results does not appear to have been questioned. Seitz (1940) includes Lewis' curve for beryllium in a diagram showing the Wiedemann–Franz ratio for several metals plotted against temperature, and suggests in a footnote that the large deviation in the case of beryllium is probably associated with the assumption that the electrons are perfectly free.

More recently Estermann and Zimmerman (1952), in the course of a discussion of their own results on heat conduction in alloys at low temperatures, refer to Seitz's suggestion that in the case of beryllium and β-manganese, the large values of the Wiedemann–Franz ratio may be explained on the basis that the electrons are not perfectly free. This suggestion does not seem to be borne out by their own experiments, although they say it might still apply to the cases considered by Seitz, as the anomalous behaviour of beryllium takes place at high temperatures and is of quite a different nature.

The present work shows that the thermal conductivity of beryllium does indeed decrease with increase in temperature and it would seem that Lewis' thermal conductivity results must have been subject to serious errors. The thick lines included in fig. 1 indicate the mean values obtained for the Lorenz function of beryllium in the course of the present investigation. Much of the anomaly has disappeared, and the curves tend towards the theoretical value at high temperatures in the usual way.

§ 2. Results of Other Investigators

In order to facilitate comparison, the previously published values for the electrical resistivity and thermal conductivity of beryllium are collected together in table 1.

It will be seen that higher resistivity values were obtained from most of the earlier determinations and that for those cases where low-temperature measurements were made the residual resistance was also high. These results can no doubt be explained by the lower purity of the specimens and by the omission of a heat treatment which appears to be essential. Lewis showed that heat treatment at about 700°C lowers the resistivity. Denton confirmed this and showed that the heat treatment also produces a considerable reduction of the residual resistivity which remains on cooling to liquid hydrogen temperatures. Still lower residual resistivities are obtained for some of the single crystals examined by Grüneisen and his collaborators, and it is significant that these crystals have about the lowest resistivity values so far obtained at 0°C. Apart from Lewis, these are the only workers who have made measurements of the thermal conductivity of beryllium. Actually they studied the effect of magnetic fields on the conductivities of beryllium crystals, and only the values corresponding to zero field have been included in table 1. Two points are of interest in connection with this German work. Firstly, they comment on the very high conductivity attained by beryllium, remarking that at −195°C the electrical conductivity of beryllium is four to five times that of copper and the thermal conductivity of beryllium is three times that of copper. Secondly, they deduce from their magnetic field experiments that at these low temperatures the lattice component of the thermal conductivity is appreciable. For instance, at −193°C the lattice components for the directions perpendicular and parallel to the crystal axis are respectively

Table 1. Existing Data for the Electrical Resistivity and Thermal Conductivity of Beryllium

Electrical resistivity values are expressed in microhm cm²/cm units; thermal conductivity values are expressed in joule cm/cm² sec °c units and should be divided by 4·1855 to convert to cal cm/cm² sec °c units. The temperatures, °c, to which the values relate follow in brackets.

Author	Details of Samples	Electrical Resistivity	Thermal Conductivity
Bridgman (1927)	Cast rod, length 9 cm Diameter 0·46 cm Density 1·82	$9·6_5$ (0) 10·6 (30) 12·0 (75)	
McLennan and Niven (1927)	From Beryllium Corporation of America	17·6 (20) 13·7 (−192) 13·6 (−252) 13·6 (−269)	
Lewis (1929)	From Beryllium Corporation of America. About 99·5% Be — As received Traces of Al, Mn, and Cr, smaller traces of Fe, Si and Mn — After 700°c heat treatment	23 (22·5) Sample 1 / Sample 2 1·50 (−189) / 1·56 (−191) 3·22 (−77) / 3·33 (−77) 6·45 (21) / 6·76 (22) 9·75 (108·5) / 9·83 (97) 14·64 (223) / 14·85 (212) 18·60 (315) / 19·05 (305) 22·45 (401) / 23·90 (403) 27·55 (512) / 29·00 (504) 32·45 (607) / 34·55 (604) 39·00 (700) / 40·00 (690)	0·971 (−176·2) 1·36 (−65·0) 1·64 (9·4) 1·91 (105·2) 2·13 (190·4)
Meissner and Voigt (1930)	Two samples of Siemens and Halske Be Be 2 :—98% Be, electro deposited, 1·5 × 0·18 × 0·15 cm Be 3 :—99·5% Be, a rod, cast from molten state, 0·8 × 0·15 × 0·15 cm	Be 2 / Be 3 7·9* (0) / 7·9* (0) 2·55 (−191·4) / 3·34 (−187·0) 2·43 (−252·7) / 3·29 (−194·7) 2·43 (−270·8) / 3·20 (−252·7) 2·43 (−271·8) / 2·96 (−269·0) 2·96 (−271·7) *Mean of values for the two	
Losana (1939)	Three samples prepared by heating in vacuo Be to which Zn had been added Sample 1, stated as 99·58% Be Sample 2, stated as 99·781% Be Sample 3, stated as 99·962% Be	Sample 1 / 2 / 3 19·4 / 17·1 / 12·2 (0) 19·6 / — / 12·6 (100) 19·9 / 17·6 / 13·0 (200) 20·3 / — / 13·4 (300) 20·7 / 18·2 / 13·9 (400) 27·2† / — / 14·4 (500)	

	Length 1·55 cm, area 0·00648 cm² Density 1·84		0·0454 (−194·13) 0·00458 (−252·82)	16·3 (−192·8) 28·3 (−249·8)
	Be 1 :—Smaller, but similar crystal Same ρ_0 assumed		3·58 (0) 0·047 (−194·63) 0·00616 (−252·83)	
Grüneisen and Erfling (1940)	Three crystals having their lengths perpendicular to the hexagonal axis	Be 3	3·12 (0) 0·0755 (−182·98) 0·0452 (−195·15) 0·0078 (−252·79)	 $14{\cdot}9_3$ (−192·6) 31·0 (−250·0)
		Be 4	3·13 (0) 0·0868 (−182·8) 0·0537 (−195·32) 0·0124 (−252·78)	 $11{\cdot}0_4$ (−182·6) $14{\cdot}6_8$ (−194·2) 25·3 (−250·5)
		Be 8	3·12 (0) 0·0770 (−183·29) 0·0473 (−195·1) 0·0076 (−252·81)	 $12{\cdot}2_7$ (−182·3) $14{\cdot}4_2$ (−193·5) 38·4 (−250·6)
Erfling and Grüneisen (1942)	Further measurements on Be 2 and on another crystal Be 6, in a direction parallel to the hexagonal axis	Be 2	3·58 (0) 0·0763 (−183·03) 0·0450 (−194·2)	 14·61 (−181·1)
		Be 6	3·56 (0) 0·0728 (−183·03) 0·0404 (−194·86)	
Denton (1947)	Rods 3·5 cm long, 0·3 cm diameter, from block of American G.E.C. sintered beryllium	As received	5·86 (0) 2·64 (−183) 2·52 (−253)	
		After 715°C heat treatment	3·50 (0) 0·297 (−183) 0·21 (−253)	
Kaufmann, Gordon and Lillie (1950)	Several samples cast by the Brush Company and extruded as ¼″ rods by the Univ. of Chicago Group	As extruded	3·88 to 4·11, mean 4·02 (room)	
		Annealed at 1000°C	3·90 to 4·02, mean 3·95 (room)	
		Quenched from 1000°C	4·01 to 4·19, mean 4·08 (room)	
	Two samples vacuum melted at M.I.T., and extruded at Detroit. Annealed at 1000°C		4·28 (room) 4·31 (room)	

2 and 3·6 joule cm/cm² sec °C, or, about 15 and 22% of the total heat conductivity.

Returning to the tabulated data, the resistivity values obtained by Losana form an anomalous group from which it would seem that the samples to which they relate were of much lower purity than claimed by Losana.

MacDonald and Mendelssohn (1950) have also measured the electrical resistivity of beryllium to low temperatures. Their data have not been included in table 1, as the values were only given in terms of R_0, the resistance at 0°C. From the fact that at the temperature of liquid helium the resistances of the two samples tested were large, $0{\cdot}38_4\,R_0$ and $0{\cdot}27_6\,R_0$, it seems likely that the samples had not been heat treated in the aforementioned manner. From their results they derived a characteristic temperature of 650°K.

Alekeyevsky and Migunov (1947) have found that beryllium does not become superconducting when cooled to between 0·06° and 0·15°K.

§ 3. Description of Samples Tested

In the course of this investigation measurements have been made on twelve beryllium specimens, of which five were prepared and supplied by the Metallurgy Division of the National Physical Laboratory, one was from a block of American G.E.C. ' sintered ' beryllium, and the remaining six, which were also of American origin, were stated to be samples of ' Process Q ' beryllium. No detailed chemical analyses were made on the samples. The reference numbers and other details relating to these specimens are given below :—

(*a*) *Samples prepared at the N.P.L.*

(i) *Specimen No. B.7(D)* :—A bar 13·1 cm long by 0·5 cm square section machined from a chill cast bar prepared from the Brush Beryllium Company's crude reactor product.* Density $1{\cdot}82_6$.

(ii) *Specimen No. B.26(1)* :—A bar 7·7 cm long by 2·25 cm diameter machined from a chill cast bar prepared from the Brush Beryllium Company's crude reactor product. Density $1{\cdot}84_2$.

(iii) *Specimen No. B.26(2)A* :—A bar 1·884 cm long by 0·865 cm diameter. This had come from the same casting as specimen No. B.26(1), but after an attempt had been made to extrude the metal at 1000°C. Only a short length had formed in the die and the metal had been squashed, the length being reduced by 22% and the area increased by 28%. Subsequently the metal had been heated in vacuum for 1 hour and furnace cooled. Specimen No. B.26(2)A was then cut and ground from the treated metal. Density 1·84.

---

* Analysis of this product gave the following percentage composition: Be 96·5, Mg 1·81, F 1·52, Fe 0·55, Al 0·06, Ca 0·035, Cu 0·008, Mn 0·005 and C 0·032. The cast beryllium should be of higher purity due to distillation of MgF_2.

(iv) *Specimen No. B.28(2)* :—A bar 11·1 cm long by 2·23 cm diameter machined from a chill cast bar prepared from German flake beryllium.* Density $1{\cdot}82_3$.

(v) *Specimen No. B.47B* :—A bar 15·72 cm long by 2·287 cm diameter machined from a chill cast bar prepared from the Brush Beryllium Company's crude reactor product. Density 1·84.

(*b*) *First American Beryllium*

(vi) *Specimen cut from Sample 2(b)* :—A bar 6·6 cm long of 1·0 cm square section, prepared from sample 2(b) of Report 1304 Metallurgy Division, N.P.L. This was a block of beryllium prepared by the 'sintering' process by the American G.E.C. A number of small transverse cracks could be observed along the edges of this bar. Density 1·83. Spectro analysis gave Mg, Ca, Ba, Si, Fe, Cu, Ti, Al and Mn as present.

(The Beryllium specimens used by W. H. Denton (1947), were prepared from the same supply.)

(*c*) *Process Q Beryllium*

(vii) *Slice cut from 2 in. disc* :—A slice approximately 5 cm long, 0·33 cm thick and 0·62 cm wide which had been cut from the centre of a disc of nominal diameter 2 in. and thickness $\frac{1}{8}$ in. Density 1·85.

(viii) to (xii) 1 *inch diameter bars* :—Five bars, numbered 1 to 5, each 1 in. in diameter and 6 in. in length. Density $1{\cdot}86_5$. Spectro analysis indicated Mg and C as the main impurities, with more than a trace of Ca, Al and Mn. Chemical analysis gave 0·34% Mg, presumably as MgF_2.

§ 4. Experimental Procedure

The electrical resistivity of each sample was first determined at room temperature. In the case of the five 1 inch diameter bars of the Process Q Beryllium, samples (viii) to (xii), these values agreed so closely with one another that it was considered unnecessary to carry out the further tests on more than one of the bars. Bar No. 4, sample (xi), was the one chosen.

Sample (i), was the first for which electrical resistivity determinations were made over an extended range of temperature. The measurements showed that heat treatment to a temperature of about 700°c produced an appreciable reduction in the resistivity. In view of this the procedure followed for all specimens which were suitable for thermal conductivity as well as electrical resistivity measurements has been first to determine the thermal conductivity up to a temperature of 300 to 400°c for the

---

* Analysis of a sample of flakes had given the following percentage composition :—Total Be 98·5, Be insoluble in HCl 0·18, Al 0·13, Fe 0·18, Cu 0·03, Cl 0·05, excluding insoluble matter which consisted of BeO containing about 3% of Al_2O_3.

Table 2. Electrical Resistivity (microhm cm²/cm) of Beryllium Samples Tested in the As Received (A.R.) State and after Heat Treatment (H.T.) at about 700°C

Sample	(i)		(ii)		(iii)		(iv)		(v)		(vi)		(vii)		(xi)	
Condition	A.R.	H.T.	A.R.	H.T.	A.R.	H.T.	A.R.	H.T.	A.R.	H.T.	A.R.	H.T.	A.R.	H.T.	A.R.	H.T.
Temperature (°C)																
20	7·2	5·1	7·1	4·1	6·7	3·2	8·0	5·6	5·8	4·2	5·2	4·1	6·3	5·1	4·3	3·8
50	8·4	6·2	8·0	5·1	7·7	4·1	8·9	6·7	6·7	5·0	6·2	5·0	7·2	6·1	5·2	4·6
100	10·4	8·2	9·6	6·7	9·2	5·3	10·5	8·4	8·2	6·6	7·7	6·6	8·8	7·7	6·6	6·1
200	14·8	12·4	12·9	10·2	12·3	8·1	13·8	11·9	11·3	9·9	10·9	9·9	12·1	11·0	9·6	9·1
300	19·2	16·7	16·3	13·9	15·5	11·1	17·3	15·5	14·6	13·3	14·5	13·5	15·5	14·5	12·8	12·4
400	24·0	21·3	19·9	17·8	19·2	13·5	21·1	19·4	18·1	16·9	18·2	17·1	19·2	18·3	16·2	16·0
500	29·2	26·3	23·8	21·9		16·7	25·1	23·6	21·8	20·7	22·2	20·9	23·0	22·2	20·0	19·8
600	33·5	31·8	27·8	26·3		20·4	29·4	27·9	25·6	24·4	26·4	25·2	27·3	26·5	24·0	23·8
700	38·5	37·6	31·8	30·9			33·9	32·8	29·2	29·2	30·8	29·9	32·0	31·6	28·3	28·3

specimen in its as received condition. Next the specimen was mounted up in an evacuated furnace tube and a study made of the effect of heat treatment on the electrical resistivity. Finally, a repeat determination has been made of the thermal conductivity of the heat treated sample. Specimens described under (ii), (iv), (v), (vi) and (xi) have been examined in this complete manner.

Fig. 2

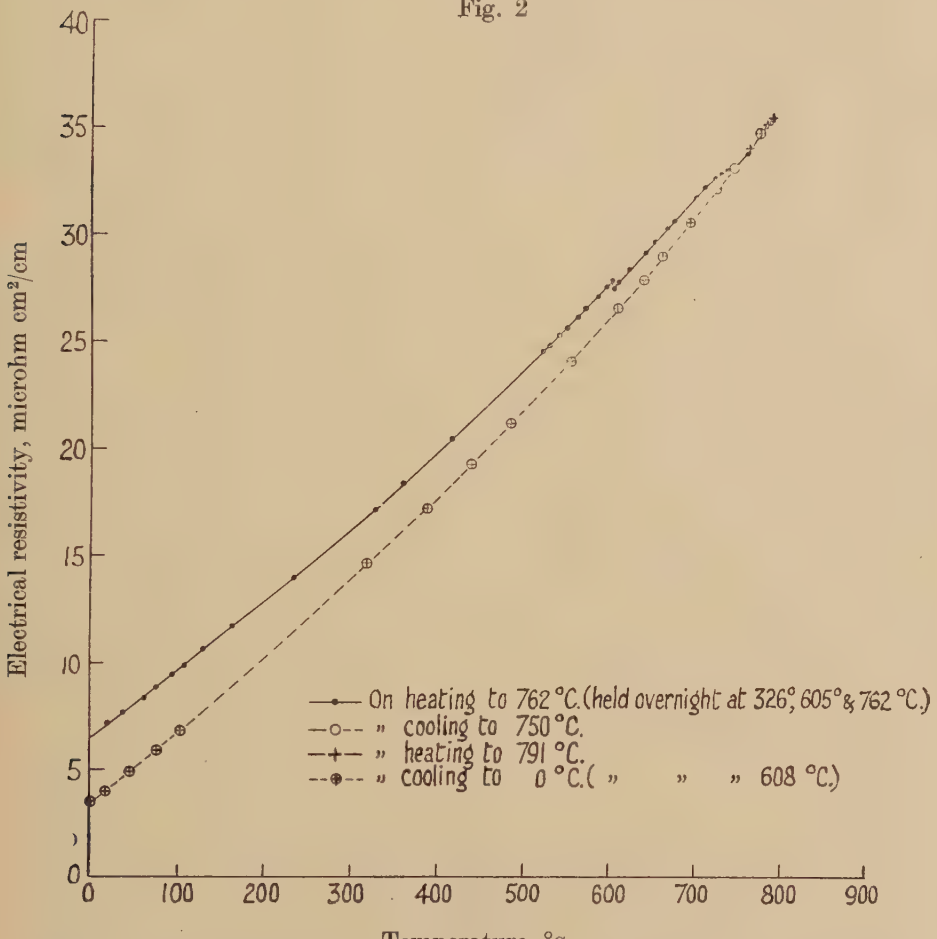

Effect of heat treatment on electrical resistivity of beryllium (Sample (ii)).

§ 5. Electrical Resistivity Measurements and Discussion

Figure 2 shows the effect of heat treatment on the electrical resistivity of sample (ii). Very similar curves were obtained for each sample and the complete resistivity results are illustrated and described more completely elsewhere (Powell 1952). In the example shown, a small drop in resistivity is seen to have occurred on holding overnight at 605°C and the change appeared to have reached completion after a similar period at 762°C.

Table 2 contains values of the electrical resistivity of each sample tested which have been read at temperatures of 20°, 50°, 100°C and then at 100°C intervals from the smooth curves drawn through the experimental points obtained for the as received and heat treated states. The change in resistivity due to the heat treatment is seen to be greatest for sample (iii) and least for sample (xi). The reason for the change is still the subject of a certain amount of conjecture. Lewis had suggested that an allotropic change occurred in the metal. Jaeger and Zanstra (1933) and Kosolapov and Trapeznikov (1936) also claim to have found evidence for the occurrence of a β-form of Be on heating to temperatures of at least 600°C. It has an hexagonal lattice with the constants $a=7{\cdot}1$ Å, $c=10{\cdot}8$ Å.

At the time that our measurements were made the X-ray tests referred to by Denton (1947) were carried out at room temperature in the Metallurgy Division of the Laboratory. No major difference in the structure of the metal before and after heat treatment to 715°C could be observed. There were indications that some slight residual strain had been removed by the heat treatment.

Gordon (1949) has determined expansion coefficients by X-ray methods and has found that the hexagonal close-packed lattice persists to 1000°C with no indication of the transformation claimed by others. It may, however, be significant that his sample had been annealed at 600°C before the X-ray tests were made.

More recently, Sidhu and Henry (1950) have reported that the volume of the unit cell of β-Be is about 29 times that of α-Be, so that it seems possible that the prominent lines of the β-modification which would occur at relatively small Bragg angles might have been beyond the range of X-ray measurements employing the back-reflection method. They find $a=6{\cdot}93$ Å, $c=11{\cdot}35$ Å, a cell-size which bears some resemblance to that originally obtained by Jaeger and Zanstra.

A point of some general interest is that at normal temperatures beryllium, in the heat treated condition, undergoes a greater increase in resistivity with temperature than any other metal. The mean value of the temperature coefficient for the range 20° to 100°C given by the data in table 2 is 0·0075. For their single crystal Grüneisen and Adenstedt obtained a coefficient of 0·010 over the range 0° to 20°C. The high temperature coefficient of beryllium is no doubt associated with its large characteristic temperature, for which Cristescu and Simon (1934) obtained values from specific heat measurements increasing from about 800° at normal temperatures to 1040°K at 40°K, and MacDonald and Mendelssohn (1950) a value of about 650°K from resistivity measurements. Lindemann's melting point formula gives a value of 940°K.

§ 6. Thermal Conductivity Measurements and Results

The thermal conductivity determinations were made in the usual manner by joining the specimen under test to a bar of metal of known thermal conductivity and establishing a temperature gradient over the

lengths of the two bars, lateral interchange of heat being reduced to a minimum by surrounding the bars by a guard tube furnace and packing the interspace with a powder of low conductivity. For measurements at temperatures below about 200°C the beryllium was in the lower position so that the heat in-flow was measured in terms of the gradient set up in the bar of known conductivity, and the heat out-flow was measured in terms of the rate of flow and rise in temperature of the cooling water supplied to the base. For measurements above 200°C, the positions of the two bars were reversed and only the heat out-flow from the beryllium sample measured.

The thermal conductivity values obtained for the five samples tested are plotted in fig. 3. In each instance the conductivity determinations to temperatures of 300 or 400°C were made for the as received condition and measurements over the same range were repeated after the heat treatment. For sample (v) the latter measurements were extended to over 700°C. The heat treatment is invariably seen to produce an increase in the thermal conductivity.

Fig. 3

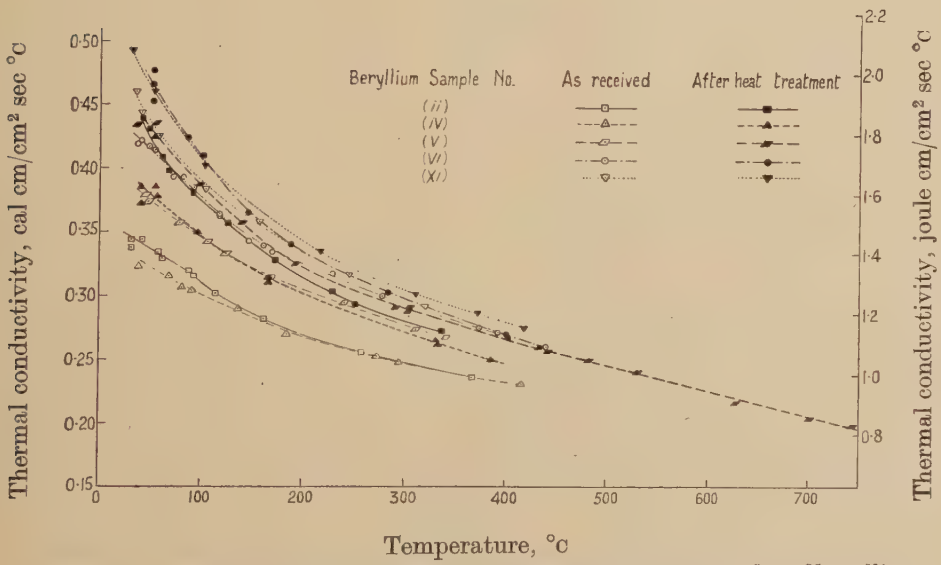

Variation of thermal conductivity with temperature for five samples of beryllium in as received and heat treated states.

It will also be seen that in no instance is the positive temperature coefficient claimed by Lewis observed, indeed, the thermal conductivity of beryllium invariably decreases over the range studied, and, particularly for the heat treated samples, possesses one of the largest negative coefficients of all metals.

Table 3 contains thermal conductivity values which have been read from the curves plotted in fig. 3. The values at 50°C are seen to range from 1·35 to 1·95 joule cm/cm² sec °C which suggests that impurities or

imperfections may have been present in some of the samples; the highest values were obtained for the two samples of American original samples (vi) and (xi). The differences decrease at higher temperatures and at 400°C are only about half as large as at 50°C.

Table 3. Thermal Conductivity (joule cm/cm² sec °C) of Beryllium Samples tested in the As Received (A.R.) State and after Heat Treatment (H.T.) at about 700°C

(Divide by 4·1855 to convert to cal. cm/cm² sec °C)

Sample	(ii)		(iv)		(v)		(vi)		(xi)	
Condition	A.R.	H.T.	A.R.	H.T.	A.R.	H.T.	A.R.	H.T.	A.R.	H.T.
Temperature °C										
50	1·41	1·76	1·35	1·58	1·56	1·80	1·73	1·95	1·81	1·93
100	1·30	1·55	1·26	1·44	1·44	1·61	1·57	1·70	1·63	1·70
200	1·13	1·31	1·12	1·26	1·28	1·35	1·36	1·40	1·40	1·43
300	1·04	1·17	1·04	1·13	1·16	1·21	1·23	1·25	1·25	1·27
400			0·97	1·03		1·11	1·13	1·13		1·17
500						1·03				
600						0·95				
700						0·86				

§ 7. Correlation of Thermal Conductivity and Electrical Resistivity Data

The usual way of correlating the above data for various temperatures is in terms of the Lorenz function, $K\rho/T$, where K is the thermal conductivity, ρ the electrical resistivity and T the absolute temperature. When the units of thermal conductivity are joule cm/cm² sec °C and those of electrical resistivity are ohm cm²/cm, the theoretical value which results when both conduction processes are electronic is $2{\cdot}45\times10^{-8}$. At temperatures sufficiently high for the resistance to be mainly due to thermal agitation the relation is normally only valid for temperatures exceeding the characteristic temperature θ_D. For pure metals the function usually falls well below the theoretical value as the temperature becomes appreciably less than θ_D. (See fig. 1.)

As already stated, θ_D is of the order of 1000°K for beryllium so most of the present work has been carried out at temperatures well below θ_D, and this increases the interest in the analysis of the results.

The values obtained for the Lorenz function in the course of the present investigation are set out in table 4.

Mean curves for the as received and heat treated states are included in fig. 1. It will be seen that neither curve shows any resemblance to that of Lewis, and that the original markedly anomalous behaviour of beryllium has disappeared.

Table 4. Lorenz Function $\times 10^8$ (joule cm/cm^2 sec °C) (ohm cm^2/cm) (1/°K) of Beryllium Samples Tested in the As Received (A.R.) State and after Heat Treatment (H.T.) at about 700°C

Sample	(ii)		(iv)		(v)		(vi)		(xi)	
Condition	A.R.	H.T.	A.R.	H.T.	A.R.	H.T.	A.R.	H.T.	A.R.	H.T.
Temperature °C										
50	3·48	2·78	3·71	3·27	3·24	2·78	3·32	3·02	2·92	2·75
100	3·34	2·78	3·55	3·25	3·17	2·85	3·24	3·01	2·89	2·77
200	3·08	2·84	3·27	3·16	3·05	2·82	3·13	2·93	2·84	2·75
300	2·95	2·84	3·13	3·05	2·95	2·82	3·12	2·93	2·79	2·75
400			3·06	2·98		2·79	3·05	2·87		2·79
500						2·76				
600						2·64				
700						2·59				

On the other hand it will now be noticed that instead of the values of the Lorenz function being less than $2{\cdot}45\times10^{-8}$ and increasing towards it as θ_D is approached, as is more generally the case, the experimental values are all above the theoretical and mostly decrease. The first impression is that the Lorenz functions of these beryllium samples are indeed comparable with those of many steels and other alloy groups, for which a fair correlation has been obtained by plotting the thermal conductivity against the product of the electrical conductivity and the absolute temperature, Powell (1951).

All the results given in tables 2 and 3 are plotted in an analogous way to this in fig. 4, but in this instance the thermal conductivity divided by the absolute temperature is plotted against the electrical conductivity, that is against the reciprocal of the electrical resistivity. The correlation obtained in this way for the beryllium samples is relatively poor. Taking both as received and heat treated conditions together the points all lie within about $\pm16\%$ of the line

$$\frac{K}{T}=\frac{3{\cdot}35\times10^{-8}}{\rho}-2{\cdot}09\times10^{-4} \quad . \quad . \quad . \quad . \quad . \quad . \quad (1)$$

(shown as a series of long dashes in fig. 4).

Somewhat better correlations can be obtained by considering the two conditions separately. The points for the as received condition lie within $\pm13\%$ of the line

$$\frac{K}{T}=\frac{3{\cdot}43\times10^{-8}}{\rho}-2{\cdot}09\times10^{-4} \quad . \quad . \quad . \quad . \quad . \quad . \quad (2)$$

(shown as a series of dashes of medium length in fig. 4), and the points for the heat treated condition lie within $\pm10\%$ of the line

$$\frac{K}{T}=\frac{3{\cdot}14\times10^{-8}}{\rho}-2{\cdot}09\times10^{-4} \quad . \quad . \quad . \quad . \quad . \quad . \quad (3)$$

(shown as a series of short dashes in fig. 4). Not only is the correlation poorer than with other groups of alloys, but this treatment of the results is seen to lead to a negative thermal conductivity instead of a positive one for zero electrical conductivity. The indications are that this correlation fails in the case of beryllium owing to the presence of an unusually large lattice component of the thermal conductivity which increases in magnitude as the temperature is decreased. The presence

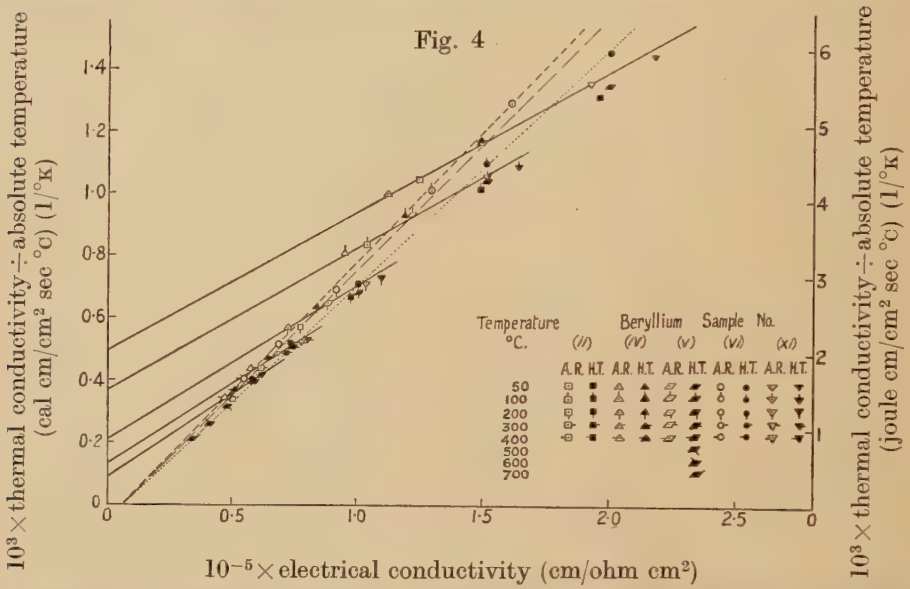

Thermal conductivity divided by absolute temperature against electrical conductivity for five samples of beryllium in as received and heat treated states.

of this component becomes evident when consideration is given to the results obtained at any one temperature for the different samples and conditions. This has been done for the points plotted in fig. 4, where the best straight lines have been drawn through each of the groups of points obtained at temperatures of 50, 100, 200, 300 and 400°C. These groups of points are marked in the figure by distinctive tags, and the equations of the straight lines drawn as full lines through the various groups are

$$\text{at } 50^\circ\text{C}, \ (T=323^\circ\text{K}), \quad \frac{K}{T} = \frac{1{\cdot}84\times10^{-8}}{\rho} + 2{\cdot}06\times10^{-3}, \quad . \ . \quad (4)$$

$$\text{at } 100^\circ\text{C}, \ (T=373^\circ\text{K}), \quad \frac{K}{T} = \frac{1{\cdot}88\times10^{-8}}{\rho} + 1{\cdot}54\times10^{-3}, \quad . \ . \quad (5)$$

$$\text{at } 200^\circ\text{C}, \ (T=473^\circ\text{K}), \quad \frac{K}{T} = \frac{2{\cdot}03\times10^{-8}}{\rho} + 0{\cdot}88\times10^{-3}, \quad . \ . \quad (6)$$

$$\text{at } 300^\circ\text{C}, \ (T=573^\circ\text{K}), \quad \frac{K}{T} = \frac{2{\cdot}13\times10^{-8}}{\rho} + 0{\cdot}54\times10^{-3}, \quad . \ . \quad (7)$$

$$\text{at } 400^\circ\text{C}, \ (T=673^\circ\text{K}), \quad \frac{K}{T} = \frac{2{\cdot}21\times10^{-8}}{\rho} + 0{\cdot}37\times10^{-3}. \quad . \ . \quad (8)$$

Treated in this way no point departs from the appropriate line by more than 6·5%.

These equations can be reduced to show the thermal conductivity at each temperature as the sum of two components, the electronic K_e, and the lattice K_g, i.e. $K=K_e+K_g$.

Then, at 50°C, $$K=1{\cdot}84\times10^{-8}\frac{T}{\rho}+0{\cdot}665, \quad . \quad . \quad . \quad . \quad (9)$$

at 100°C, $$K=1{\cdot}88\times10^{-8}\frac{T}{\rho}+0{\cdot}575, \quad . \quad . \quad . \quad . \quad (10)$$

at 200°C, $$K=2{\cdot}03\times10^{-8}\frac{T}{\rho}+0{\cdot}415, \quad . \quad . \quad . \quad . \quad (11)$$

at 300°C, $$K=2{\cdot}13\times10^{-8}\frac{T}{\rho}+0{\cdot}31, \quad . \quad . \quad . \quad . \quad (12)$$

and at 400°C, $$K=2{\cdot}21\times10^{-8}\frac{T}{\rho}+0{\cdot}25. \quad . \quad . \quad . \quad . \quad (13)$$

In these equations the numerical coefficient of the first term is the true Lorenz function, as derived from the electronic component of the thermal conductivity and the electrical resistivity. It will be seen to have the expected low value, at temperatures well below θ_D, and more nearly to approach the theoretical value as the temperature is increased. The second term is the lattice component of the thermal conductivity which is seen to be extraordinarily large and to decrease rapidly as the temperature increases. No other metal has shown any similar behaviour at comparable temperatures.

Some years ago Grüneisen and Goens (1927) treated several samples of copper, aluminium, gold, platinum, tungsten and iron in an analogous way by plotting the thermal resistance (reciprocal of thermal conductivity) against the electrical resistivity divided by the absolute temperature. For each of the temperatures 18°, −190° and −252° different straight lines were necessary to fit the results for the various metals. Thus the type of behaviour which they found for these metals at very low temperatures has now become evident over the range 50° to 400°C in the case of beryllium.

In view of the magnitude of the lattice conductivitiy term it seems not unlikely that this may vary from sample to sample and so account for some of the scatter of the experimental results. Sample (vi) might, for instance, have a higher lattice conductivity. On the other hand the fairly consistent displacement of the points for this sample may be due to the transverse cracks observed along its length having a greater influence on the electrical conductivity than on the thermal. Therefore, in deriving a general equation to fit the present results and which might serve for the estimation of the thermal conductivities of other beryllium samples from electrical resistivity measurements, no allowance is made for any possible variation in lattice conductivity from sample to sample.

Table 5. Comparison of Thermal Conductivity Values read from Experimental Curves with those Calculated from eqn. (16) (thermal conductivities expressed in joule cm/cm² sec °c)

Sample	(ii)			(iv)			(v)			(vi)			(xi)		
Temperature °c	Observed	Calculated	Difference %	Observed	Calculated	Difference %	Observed	Calculated	Difference %	Observed	Calculated	Difference %	Observed	Calculated	Difference %
As received condition :—															
50	1·41	1·41	0	1·35	1·33	−1	1·56	1·55	−1	1·72	1·62	−6	1·81	1·80	−1
100	1·30	1·31	+1	1·26	1·24	−2	1·45	1·43	−1	1·57	1·49	−5	1·63	1·64	+1
200	1·13	1·17	+4	1·12	1·12	·0	1·28	1·27	−1	1·36	1·30	−4	1·40	1·42	+2
300	1·04	1·07	+3	1·04	1·02	−2	1·16	1·15	−1	1·23	1·16	−6	1·25	1·27	+2
400		0·99		0·97	0·95	−2		1·06		1·13	1·06	−6		1·16	
500		0·93			0·89			0·99			0·98			$1·06_5$	
600		0·87			0·83			0·93			0·91			0·99	
Heat treated condition :—															
50	1·76	1·82	+3	1·58	1·55	−2	1·80	1·84	+2	1·95	1·84	6	$1·92_5$	1·94	+1
100	1·55	1·63	+5	1·44	1·41	−2	1·61	1·64	+2	1·70	1·64	−4	$1·69_5$	1·73	+2
200	1·31	1·36	+4	1·26	1·23	−2	1·35	1·39	+3	1·40	1·39	−1	1·43	1·48	+3
300	1·17	1·20	+3	1·13	1·11	−2	1·21	1·24	+2	1·25	1·22	−2	1·27	1·30	+2
400		1·08		1·03	1·01	−2	1·11	1·12	+1	1·13	1·11	−2	1·17	1·17	0
500		0·99			0·93		1·03	1·04	+1		1·03			$1·07_5$	
600		0·91			0·87		0·95	0·97	+2		0·95			$0·99_5$	
700		0·85			0·81		0·86	$0·89_5$	+4		0·88			0·92	

In fig. 5 the derived values for the lattice conductivity are plotted against the reciprocal of the absolute temperature. The points are found to be satisfied over the range 50° to 400°C by the straight line

$$K_g = \frac{268}{T} - 0{\cdot}151. \quad . \quad . \quad . \quad . \quad . \quad . \quad . \quad (14)$$

The values derived for the Lorenz function from the slopes of the lines in fig. 4 are also plotted against the reciprocal of the absolute temperature in fig. 6. They are fairly well satisfied over the same temperature range by the straight line

$$L_e = \frac{K_e \rho}{T} = 2{\cdot}57 \times 10^{-8} - \frac{249 \times 10^{-8}}{T}. \quad . \quad . \quad . \quad . \quad (15)$$

Hence the present results indicate that within the range 50° to 400°C, K, the thermal conductivity of a beryllium sample at the absolute

Fig. 5

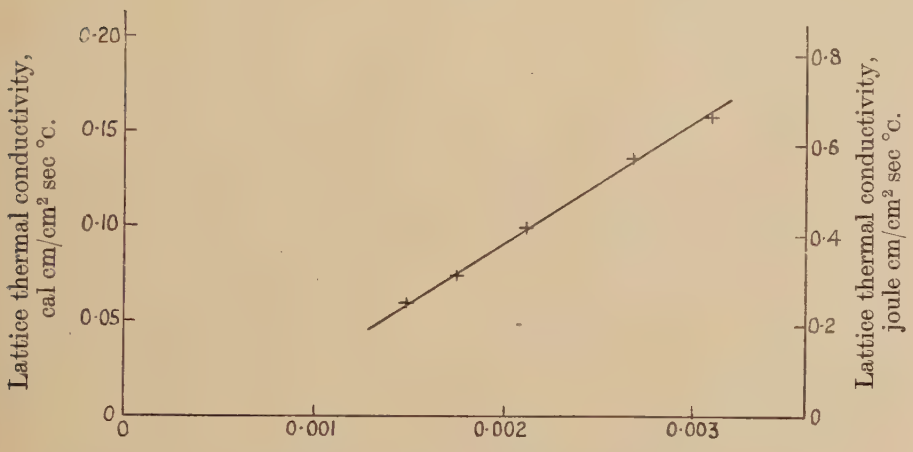

Reciprocal of absolute temperature, 1/°K.

Derived values for the lattice thermal conductivity of beryllium plotted against reciprocal of absolute temperature.

temperature, T, can be derived from its electrical resistivity at that temperature, ρ, by means of the equation

$$K = 10^{-8} \frac{T}{\rho} \left(2{\cdot}51 - \frac{249}{T}\right) + \frac{268}{T} - 0{\cdot}151, \quad . \quad . \quad . \quad (16)$$

where K is expressed in joule cm/cm² sec °C and ρ in ohm cm²/cm.

In table 5 a comparison is made between the observed values of the thermal conductivity as read from the curves fitted to the experimental points and values calculated from the eqn. (16) using the electrical resistivity values given in table 2. The differences between observed and calculated values range from −6 to +4% for the as received condition and from −6 to +5% for the heat treated condition. It is of interest that when

the equation is applied to give values at 500°, 600° and 700°C in the case of sample (v) the differences in this range are comparable with those for the same sample over the lower range. This suggests that the equation could be used to derive values above 400°C in other instances. Such values are included in table 5 for those samples for which the electrical resistivity had been observed. It is unlikely that eqn. (16) can be applied to temperatures much below those covered in the present experiments. In fact the results obtained at low temperatures by Grüneisen and others are quite inconsistent with this equation.

On the other hand, the lattice conductivity components which these workers derived from measurements made in magnetic fields, agree fairly well with the predictions of eqn. (14). For instance, at 80°K, eqn. (14) gives $K_g = 3{\cdot}20$ joule cm/cm² sec °C, compared with Grüneisen and Erfling's values of about 2 for the direction normal to the axis and

Fig. 6

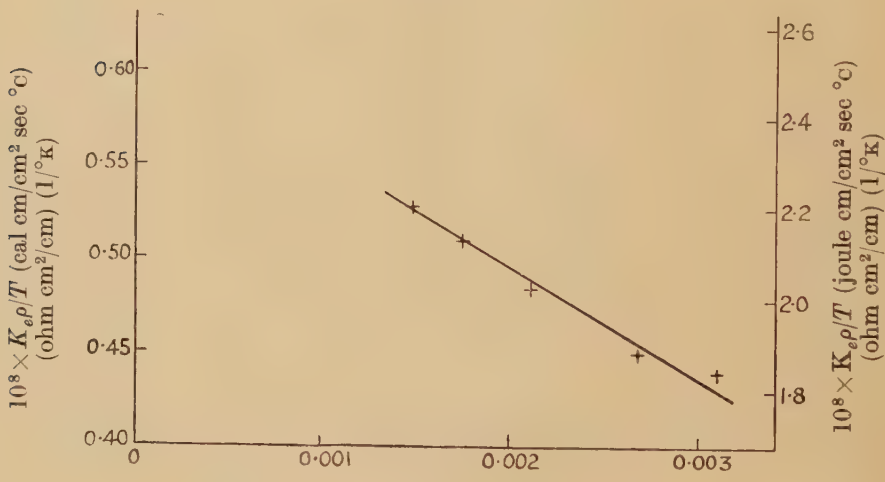

Reciprocal of absolute temperature, 1/°K.

Lorenz function of beryllium as given by the electronic component, $K_e\rho/T$, against the reciprocal of the absolute temperature.

Grüneisen and Adenstedt's value of 3·6 for the parallel direction. At 23°K their value is only about 0·07 for the normal direction and 0·1 for the parallel direction, so it seems likely that the value at 80°K is below the maximum of the K_g versus T curve. Grüneisen and Erfling's data at about 90°K would appear to support this conclusion, but were not analysed in a similar manner to those at 80°K in their published paper. From their data for a sample in the perpendicular direction a value of about 3·35 joule cm/cm² sec °C can be deduced for K_g which may be compared with a value of 2·83 derived from eqn. (14). It is therefore of interest that as regards the lattice component of thermal conductivity there seems to be agreement between the conclusions of these low temperature

observations of the conductivities of beryllium single crystals under the influence of magnetic fields and the present observations of the conductivities of polycrystalline samples of beryllium at temperatures above normal.

There is clearly need for an extension of this investigation to lower temperatures than those covered by the present work.

Acknowledgements

The work has been carried out in the Physics Division of the National Physical Laboratory and formed part of an investigation undertaken on behalf of the Atomic Energy Research Establishment. The author is indebted to Mr. T. H. Schofield of the Metallurgy Division for providing the specimens and to Mr. R. P. Tye of the Physics Division for assistance with some of the experimental work.

The paper is published with the approval of the Director of the Atomic Energy Research Establishment and the Director of the National Physical Laboratory.

References

Alekeyevsky, A., and Migunov, L., 1947, *J. Phys., U.S.S.R.*, **11,** 95.
Bridgman, P. W., 1927, *Proc. Amer. Acad. Arts Sci.*, **62,** 207.
Cristescu, S., and Simon, F., 1934, *Z. f. Phys. Chem.*, **25B,** 273.
Denton, H. W., 1947, *A.E.R.E. Report*, No. G/R. 101, 20th Feb.
Erfling, H. D., and Grüneisen, E., 1942, *Ann. d. Phys.*, **41,** 89.
Estermann, I., and Zimmerman, J. E., 1952, *J. Appl. Phys.*, **23,** 578.
Gordon, P., 1949, *J. Appl. Phys.*, **20,** 908.
Grüneisen, E., and Adenstedt, H., 1938, *Ann. d. Phys.*, **31,** 714.
Grüneisen, E., and Erfling, H. D., 1940, *Ann. d. Phys.*, **38,** 399.
Grüneisen, E., and Goens, E., 1927, *Z. f. Phys.*, **44,** 615.
Jaeger, F. M., and Zanstra, J. E., 1933, *Proc. Amst. Acad.*, **36,** 636.
Kaufmann, A. R., Gordon, P., and Lillie, D. W., 1950, *Trans. Amer. Soc. Metals*, **42,** 785.
Kosolapov, G. F., and Trapeznikov, A. K., 1936, *J. Exptl. and Theor. Phys. (U.S.S.R.)*, **6,** 1163.
Lewis, E. J., 1929, *Phys. Rev.*, **34,** 1575.
Losana, L., 1939, *Aluminio*, **8,** 67.
MacDonald, D. K. C., and Mendelssohn, K., 1950, *Proc. Roy. Soc.* A, **202,** 523.
McLennan, J. C., and Niven, C. D., 1927, *Phil. Mag.*, **4,** 386.
Meissner, W., and Voigt, B., 1930, *Ann. d. Phys.*, **7,** 782.
Powell, R. W., 1951, Inst. Mech. Engrs. and Amer. Soc. Mech. Engrs., *General Discussion on Heat Transfer*, p. 290 ; 1952, *Report to A.E.R.E.* Ref. B.C. 24, 20th Oct.
Seitz, F., 1940, *The Modern Theory of Solids*, p. 177 (fig. 11).
Sidhu, S. S., and Henry, C. O., 1950, *J. Appl. Phys.*, **21,** 1036.

LXX. *The Thermal Conductivity of Solid Helium at High Densities*

By F. J. Webb and J. Wilks
Clarendon Laboratory, Oxford *

[Received March 6, 1953]

Abstract

Earlier measurements of the thermal conductivity of solid helium (Webb, Wilkinson and Wilks 1952) have been extended to higher densities by using pressures up to 1800 atmospheres. Values of the conductivity are now available for densities from 0·19 to 0·35 g/cm³, corresponding to a range of Debye characteristic temperatures (24° to 90°) which is sufficient to cause the measured conductivities at a given temperature to vary by a factor of over 300. Below a density of 0·28 g/cm³ the present results are in substantial agreement with the discussion given previously ; at higher densities the results are irregular.

§ 1. Introduction

During the past few years several dielectric crystals such as diamond, quartz and artificial sapphire have been examined to discover how their thermal conductivities vary with temperature (e.g. Berman, Simon and Wilks 1951). Solid helium, however, is unique ; its compressibility is so high that one can readily measure the variation of conductivity with density, as well as the variation with temperature. We have recently shown (Webb, Wilkinson and Wilks 1952) that an increase of density from 0·194 g/cm³ to 0·218 g/cm³ is sufficient to increase the thermal conductivity by as much as a factor 15. The two processes which are responsible for the characteristic shape of the conductivity temperature curve of an ideal dielectric are most simply interpreted in terms of the mean free path λ defined by the usual expression $K=1/3\ \lambda\ Cv$. On the low temperature side of the maximum the mean free path is limited by boundary scattering and tends to a value of the order of the diameter of the specimen (Casimir 1938) ; the thermal conductivity thus falls off at about the same rate as the specific heat. At higher temperatures the position is of interest as the conductivity throws light on the mutual scattering of the lattice waves (Umklapp processes). In particular we showed that at temperatures between about $\theta/10$ and $\theta/20$ (where the conductivity is increasing rapidly with falling temperature) the mean free path λ is determined by Umklapp processes, and at different densities and temperatures is given by the relation $\lambda=A\ \exp\ (\theta/2{\cdot}3T)$, in agreement with Peierls' theory (1929, 1935).

It is interesting to speculate how the conductivity would behave if the density were increased still further. We have estimated the thermal

* Communicated by Professor F. Simon, F.R.S.

conductivities at higher densities by assuming that the mean free path λ continues to be the same function of θ/T as it is in the lower range of densities. As the conductivity at the lowest temperatures depends on the size of the specimen, these estimates were made for helium in a tube of the same internal diameter (0·5 mm) as was used in making the previous

Fig. 1

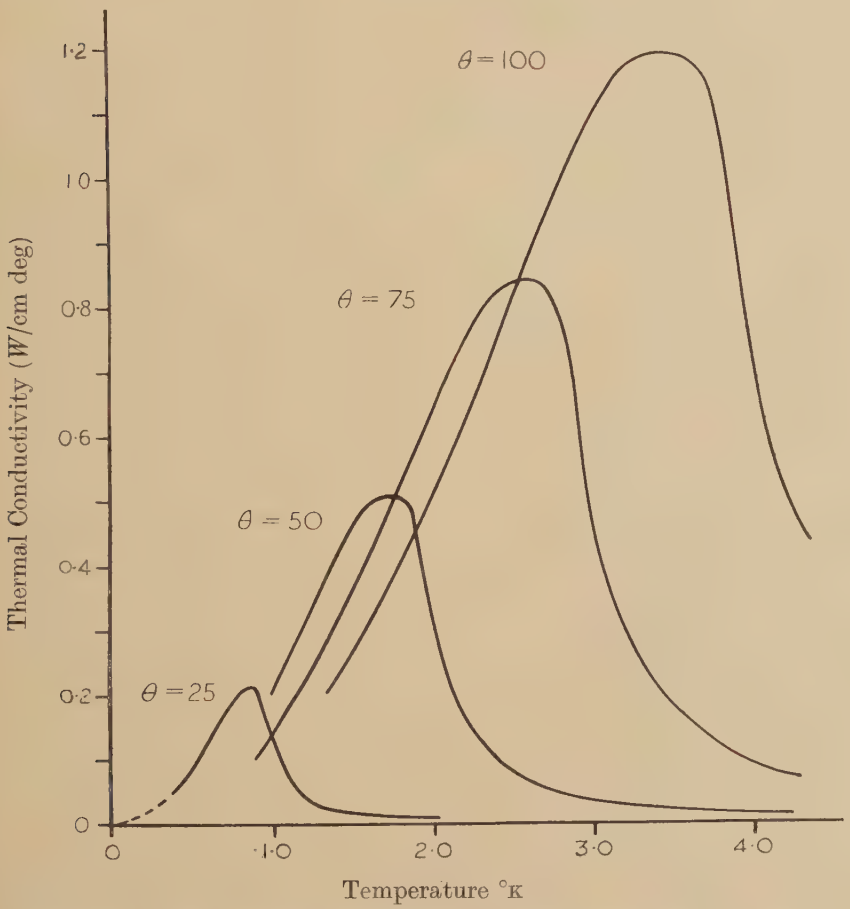

An estimate of the thermal conductivity of solid helium as a function of the Debye θ. (An extrapolation of our previous results.)

measurements at the lowest temperatures. Thus the values of λ corresponding to a given value of θ/T were taken from fig. 6 of our previous paper. Estimates for four different values of θ (corresponding to four different densities) are given in fig. 1 and indicate that very striking changes in the conductivity are to be expected. The recent work of Dugdale and Simon (1953) on the equation of state of solid helium shows that to obtain such high values of θ, pressures of the order of 2000 atmospheres are required. Although the helium must therefore be contained

in extremely thick walled tubes, its enhanced conductivity ensures that the heat flow in it is still large compared with that in the metal. Unfortunately the data on the specific heat of helium at high densities is not very complete and this inevitably introduces some uncertainty into the interpretation of the conductivity measurements. However, the predicted conductivities were so very large compared with our previous results (where the greatest value was 0·2 watt units) that it seemed worth while to see whether they could be realized.

§ 2. The Apparatus

As the measurements were made in a standard helium expansion liquefier, some compromise was necessary in designing the apparatus. In fact two apparatuses were used (figs. 2 (*a*) and (*b*)) : " *a* " was designed primarily to cover as wide a range of temperatures as possible, while " *b* " was designed so that the density of the helium could be obtained as accurately as possible. In both cases the helium specimen was enclosed in a U shaped tube whose ends were joined to capillaries, one leading to a high pressure pump and the other to a Bourdon gauge. Thus it was possible to observe that the pressure from the pump was transmitted to the specimen and to ensure that the requisite pressures were obtained in the filling process ; this precaution was all the more important as the pump was not in the same room as the liquefier and was connected to the specimen by a pipeline of 1/4 mm capillary 40 metres long. A heater H was soldered to the bottom of the U-tube and carbon resistance thermometers R were mounted symmetrically, two on each limb. (For clarity, two thermometers and the copper radiation shield have been omitted from fig. 2 (*a*), and neither thermometers nor heater are shown in fig. 2 (*b*). In the latter arrangement the heater was attached to the copper block E.) The electrical equipment was similar to that in our previous experiments.

In the first apparatus, the U-tube was of I.D. 0·5 mm and O.D. 2·4 mm, the distance between the thermometers being 4 cm. The ends of the U-tube were joined to capillaries by hard-soldered couplings, which were then Woods-metalled and clamped inside the copper blocks C. These blocks were joined by a copper bar to the cryostat B, suspended below the expansion vessel A of the helium liquefier. The capillaries themselves were Woods-metalled to the expansion vessel before passing out of the vacuum jacket. As the density of fluid helium is known accurately only along the melting curve, the tube was filled by first adjusting the pressure at a given temperature until it was just a little lower than the melting pressure ; then the capillary was blocked by cooling the expansion vessel. To obtain the requisite high densities, filling temperatures from 9° to 20°K had to be employed and the following procedure was adopted. The expansion vessel was cooled to the required temperature and held there until the helium in the specimen was in equilibrium at the correct temperature and pressure, as shown by the thermometers and gauge. The capillary was then blocked so that the bulk of the helium in

Fig. 2

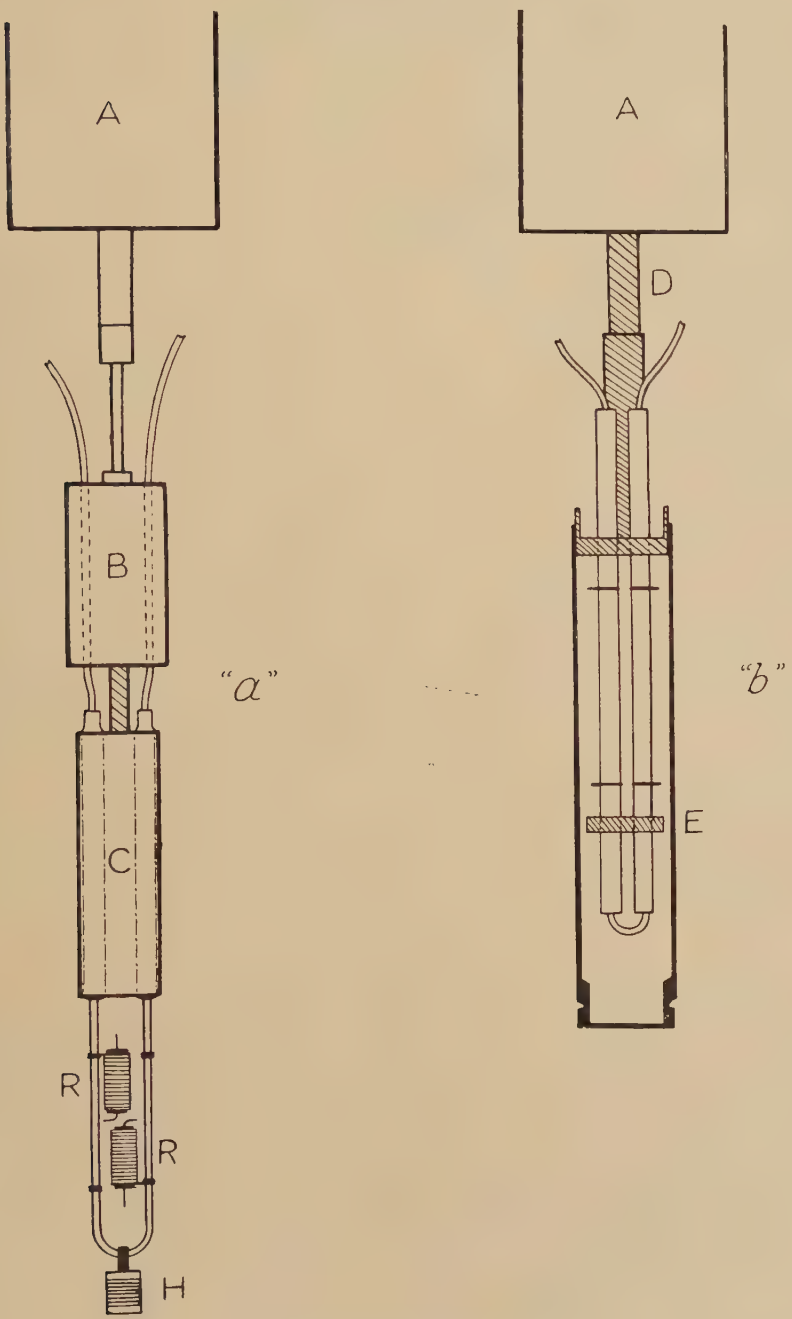

The Apparatuses.

the U-tube would subsequently cool and solidify at constant volume. Finally the expansion vessel was cooled to about 9°, the helium liquefied by expansion, the cryostat B filled with liquid helium and measurements made. As previously, the correction for the heat flow in the metal tube was small and was taken into account by using the results of a blank run. In practice the fluid helium in the specimen took a very long time to reach temperature equilibrium during the filling process, because the only effective thermal contact between it and the expansion vessel was via the capillary tubes. Therefore we generally blocked the capillaries when the temperature of the lower thermometers was within about 2° of that of the expansion vessel. The true density was then estimated from the isotherms of the fluid (Buchmann 1933), but the correction is not very satisfactory as Buchmann's data does not agree on the melting curve with the work of Dugdale and Simon (1953). A correction was also applied on account of the comparatively large ' dead volume ' in the capillaries between the specimen and the expansion vessel; because the helium was cooled from the top, this dead volume would result in the density at the bottom of the specimen being appreciably lower than that at the top of the capillary.

In arrangement "*b*" the specimen tube was considerably larger (2·6 mm I.D., 6·3 mm O.D., 6 cm long) and was surrounded by a copper jacket into which exchange gas could be introduced during the filling process. The copper jacket itself was maintained in thermal contact with the expansion vessel A via the thick copper rod D, and so both the jacket and the specimen tube within it quickly attained temperature equilibrium. Thus it was possible to fill the specimen tube with fluid helium at an exact temperature and pressure corresponding to conditions near the melting curve. The new arrangement also ensured that the ' dead ' volume in the capillaries was negligible relative to the size of the specimen; thus the density of the helium is known more accurately. After filling the specimen, the expansion vessel was cooled to 9°, the helium in it liquefied and measurements made using the expansion vessel as a cryostat.

§ 3. The Results

All the measurements at densities below about 0·28 g/cm^3 gave results that were in agreement with one another and were similar in magnitude to the values previously estimated. At higher densities the interpretation of the measurements is more difficult and it is convenient to discuss the results for the two ranges of density separately. Figure 3 shows the conductivities of helium at the lower densities as measured in both the large and small tubes. One run was made at a very low density (0·218 g/cm^3) by filling the specimen at 4·0° and this gave good agreement with our previous measurements at a similar density. The other two runs with tube "*a*", for which the densities are estimated as 0·262 and 0·282 g/cm^3, show that the conductivities have increased more or less as was expected. The measurements using arrangement "*b*" (0·262 g/cm^3) gave results similar to the highest curve in "*a*"; as mentioned above this second set up will give a more reliable value for the density.

Figure 4 shows the conductivities at higher densities together with one curve from fig. 3 for purposes of comparison. Using the narrow specimen tube the observed value of the conductivity is substantially *less* at a density of 0·289 than at 0·282 g/cm³. After this unexpected

Fig. 3

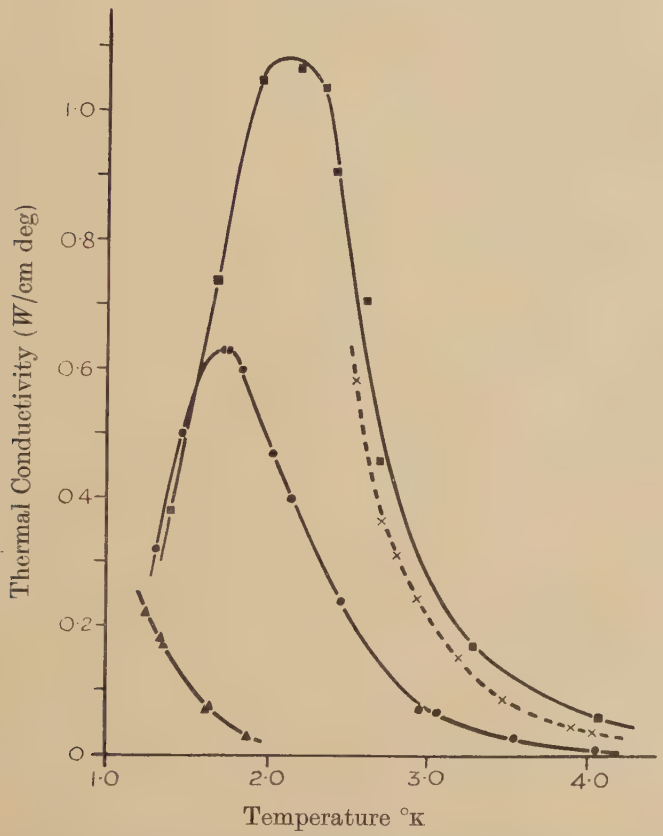

The thermal conductivity of solid helium at densities up to 0·28 g/cm³.

▲ 0·218 g/cm³
● 0·262 g/cm³ } Apparatus "*a*"
■ 0·282 g/cm³
× 0·276 g/cm³ Apparatus "*b*"

decrease, the conductivity again rises with increasing density although it remains less than our estimate by a factor of over 2. As the measurements were made in random order, it is unlikely that the discontinuity was due to an undetected change in the apparatus which occurred during the measurements. Experiments made in apparatus "*b*" with its much wider specimen tube provided a check as to whether these observed values were a function only of the helium itself; these subsequent results are shown by the dashed curves in fig. 4. Except at about 4°, the new curves lie higher than the earlier ones for corresponding densities but they are still somewhat

irregular ; for example the upper pair of curves look as if they were going to cross on the high temperature side of the maximum. Thus although these curves serve to indicate a minimum value for the conductivity the true values may be still higher.

Fig. 4

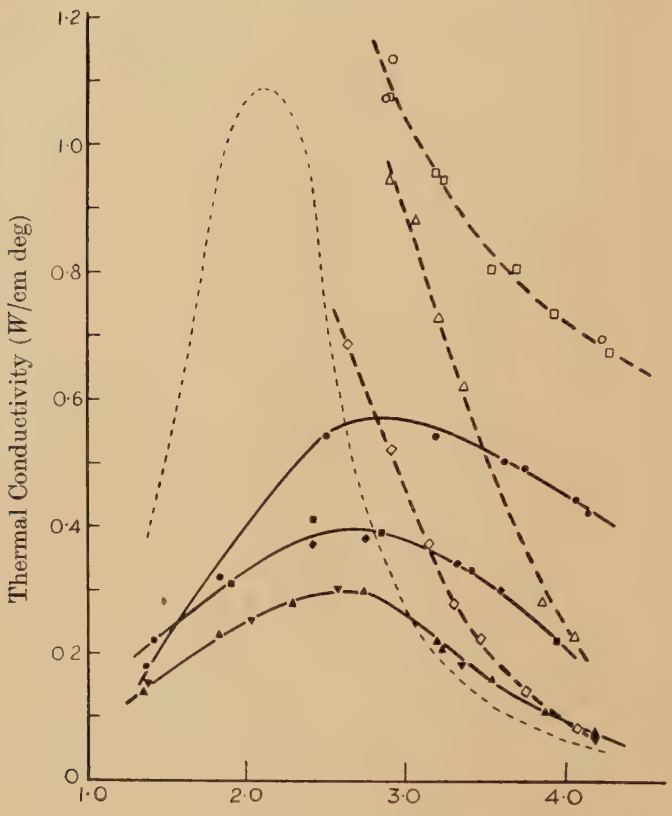

The thermal conductivity of solid helium at densities above 0·28 g/cm³.

▲ ▼ 0·289 g/cm³
■ ♦ 0·316 g/cm³ } Apparatus "*a*"
● 0·336 g/cm³
◊ 0·294 g/cm³
△ 0·308 g/cm³ } Apparatus "*b*"
□ ○ 0·345 g/cm³

§ 4. Discussion

Our chief concern is whether the conductivity in the temperature region where mutual scattering predominates ($\theta/10$ to $\theta/20$) is such that the mean free path λ is the same function of θ/T as at the lower densities. We therefore require values of θ as a function of temperature and density, but the data are not at all complete. Dugdale and Simon (1953), who

measured the specific heat at high densities down to about 5°, found that for a given density θ is almost constant below 10°, and at first sight it might seem reasonable to extrapolate this constant value to lower temperatures. However, these authors proceeded differently by showing that the specific heat over their wide range of densities could be expressed as a function of T/ϕ, where ϕ is a reducing parameter characteristic of each density. This suggested the possibility of such a function being applicable to all densities and it was in fact found that with suitable values of ϕ the specific heats at lower densities (Keesom and Keesom 1936, Webb, Wilkinson and Wilks 1952) are in rough agreement with it. As the measurements at the low densities extended to the lowest values of the reduced temperature (T/ϕ) Dugdale and Simon used an extrapolation based on them when evaluating entropies. However, these authors were interested principally in the entropies at higher temperatures where the contribution of the extrapolated specific heats is not very important, whereas for our purpose the values of θ are much more critical. Actually the specific heats at a given reduced temperature T/ϕ are systematically less for the low densities than for the high ones. (This is associated with the fact that Keesom and Keesom's values for θ are nowhere independent of temperature.) Thus it is not clear whether one should extrapolate Dugdale and Simon's results by assuming that θ remains constant below 5° or by assuming that it increases in a similar way to that observed by Keesom and Keesom. As these two assumptions lead to values of θ which may differ by as much as 15% at 2°K, it does not seem profitable to analyse our results by calculating the mean free path as we did for measurements at lower densities. Therefore we proceed by estimating θ from the thermal conductivity and seeing if we obtain reasonable values.

We first consider the curves in fig. 3, which have substantially the same form as our estimates. The conductivity maxima occur at temperatures in agreement with the estimates but their actual magnitudes are about 20% larger. This is of no great significance as the available data for the mean free path is much less complete in this temperature range ($\theta/T>20$). Moreover the results were obtained in capillaries, where as we have previously noted there is a possibility of obtaining poor crystals. At lower temperatures the conductivity falls off as expected and the curves cross over so that the helium with the lower specific heat has the lower conductivity.* The temperature region $\theta/10$ to $\theta/20$ corresponds approximately to the region 2° to 4° at a density of 0·262 g/cm³, and to the region

* At the lowest temperatures the conductivity should be proportional only to the velocity of sound and the specific heat ; that is, at a given temperature the conductivity should be proportional to θ^{-2}. The present results do not extend to sufficiently low temperatures to observe this relation. However, in our earlier experiments below 1° a few measurements were made at $\rho=0{\cdot}214$ g/cm³ besides the complete set at $\rho=0{\cdot}194$. The conductivities at the two densities were the same at 0·5°, but at 0·2° the higher density had a conductivity only half that of the lower density.

above 3° for the higher densities. If we assume that over this range the value of θ appropriate to each density is approximately constant, then by using the expression for the mean free path as a function of θ/T which was valid at lower densities, we can find the value of θ which would give rise to the observed thermal conductivity. The best fit is obtained by taking $\theta=58°$ and $\theta=70°$ for the lower and higher densities respectively. The values of θ for these densities obtained from the specific heats at 5° are 45° and 55° respectively ; at the lower temperatures with which we are concerned they may be considerably higher. However the discrepancy is sufficiently large to suggest that the conductivity itself may have increased more than was expected. This might well occur if the reduced compressibility of the helium at higher densities led to a reduction in the anharmonicity of the interatomic forces, for there would then be fewer of the Umklapp processes which limit the mean free path. Although such an explanation is difficult to investigate theoretically, it would be consistent with the fact that the most compressible dielectric crystal so far examined —helium—has the shortest mean free path for a given value of θ/T (Berman, Simon and Wilks 1951). It would be very interesting to know the value of the specific heats below 5°, both to clear up these points concerning the thermal conductivity and for the sake of the Debye θ values themselves.

The results shown in fig. 4 are for higher densities (θ values up to 90°): except at 4° the conductivities are all smaller than was expected. The results obtained from apparatus "*b*" are, however, consistently higher than those from "*a*" ; since any imperfections in the helium will give rise to too small a conductivity, it is clear that the "*a*" set of curves are not a function of the helium alone but have been influenced by the experimental arrangement. Although the values obtained in the wider tube "*b*" are considerably larger, the three curves are irregular and the true conductivity may be still greater. Whereas all the experiments at densities of 0·282 g/cm^3 or less gave consistent and regular results, the conductivities at higher densities were always anomalous. Above a certain density the helium appears less ready to solidify as a perfect crystal : possibly there is a tendency to form a microcrystalline structure. This behaviour, which is most marked in the narrower tube, recalls our earlier work where we showed that in order to obtain consistent results it was necessary to anneal helium which had solidified in narrow capillaries. In the present experiments the specimens spent almost an hour at temperatures between 9° and 12° while the expansion vessel was cooled prior to liquefaction, and one would have expected some annealing to take place there. Although there is no satisfactory explanation for this irregular behaviour it may be remarked that specimens at the highest densities will be cooled through the transition in the solid state discovered by Dugdale and Simon (1953). This, however, can hardly be the explanation as besides giving the wrong value for the critical density, the transition is perfectly reversible.

§ 5. Conclusion

The great compressibility of solid helium has enabled us to measure the conductivity of a material whose density could be almost doubled. Throughout this range the *true* conductivity of the helium at a given temperature always increases with increasing density. At 2° for example it increases by a factor of over 300. Up to densities of 0·28 g/cm³ the

Fig. 5

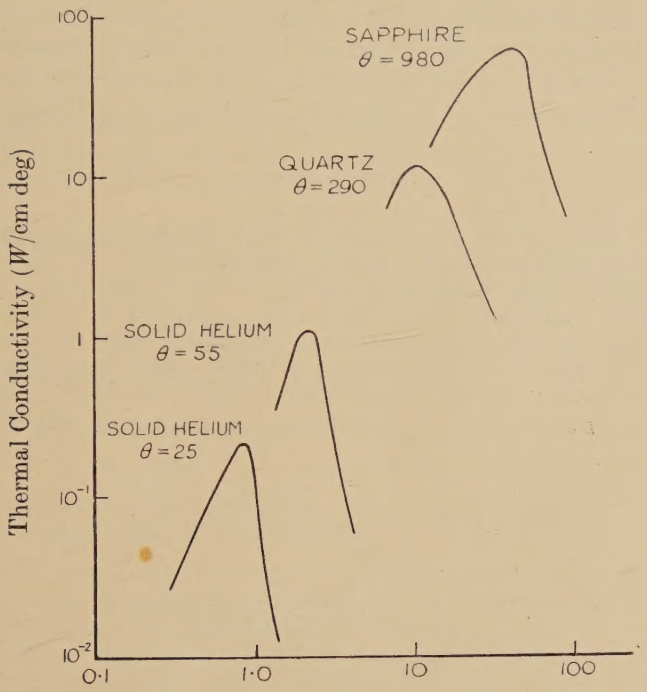

The thermal conductivities of various dielectric crystals.

results are in broad agreement with the picture we have given previously, namely, that the mean free path is essentially a function of θ/T. It may be that because of the reduced compressibility of the helium the conductivity has in fact increased more than would be indicated by θ values alone, but a decision must await further specific heat measurements. At the higher densities the conductivity is still increasing but it becomes difficult to obtain consistent results, presumably because the helium less readily solidifies as a perfect single crystal.

The results give further support to Peierls' theory of thermal conductivity (1929) and show that the essential parameter governing the thermal conductivity of dielectric crystals is the Debye θ. Indeed, the very different conductivities observed in various dielectric crystals are

largely due to their very different values of this parameter. Figure 5 shows the conductivities of helium at two densities, together with those of quartz and sapphire due to Berman (1951) ; these curves are similar in shape and their positions vary regularly with the values of θ.

Acknowledgments

We wish to thank Professor Simon for his continued interest in these experiments ; also Dr. J. S. Dugdale, Dr. D. W. Robinson and Mr. A. T. Croxon for their help with the high pressure technique. One of us (J. W.) would like to thank Imperial Chemical Industries for a Research Fellowship ; one of us (F. J. W.) acknowledges the award of a maintenance grant from the Department of Scientific and Industrial Research.

References

Berman, R., 1951, *Proc. Roy. Soc.* A, **208,** 90.
Berman, R., Simon, F. E., and Wilks, J., 1951, *Nature, Lond.*, **168,** 277.
Buchmann, E., 1933, *Z. physik. Chem.* A, **163,** 461.
Casimir, H. B. G., 1938, *Physica*, **5,** 495.
Dugdale, J. S., and Simon, F. E., 1953, to be published.
Keesom, W. H., and Keesom, A. P., 1936, *Physica*, **3,** 105.
Peierls, R. E., 1929, *Ann. Phys., Lpz.*, **3,** 1055 ; 1935, *Ann. Inst. Poincaré*, **5,** 177.
Webb, F. J., Wilkinson, K. R., and Wilks, J., 1952, *Proc. Roy. Soc.* A, **214,** 546.

LXXI. *Notices of New Books and Periodicals received*

Symmetry. By H. Weyl. [Pp. 168.] (Princeton University Press ; London : Geoffrey Cumberlege.) Price 24*s.*

A delightful series of lectures, with 72 illustrations or figures, on what in mathematical language would be called 'some aspects of group theory': Professor Weyl shows that it is possible to enjoy the beauty of the fundamental ideas, and to understand some spectacular results, of this branch of mathematics without going through the elaborate formalism of the theory. In fact, the small amount of mathematics in this book can be understood with very little previous knowledge, though it requires a great deal of precise and careful thinking.

With the aid of many examples taken from art and architecture, Professor Weyl shows that the beauty and order of symmetry has been appreciated already for thousands of years, while a great deal of thought was spent on its philosophical aspects.

The character of the book is best indicated by mentioning that the illustrations vary from the Baptisterium in Pisa to drawings in *Kunstformen der Natur* by Haeckel, and from the filling of space by tetrakaidekahedrons. Also pictures from *Vogue* 1951. Where the author has to be superficial he never fails to excite wonder and where he has to be formal, the reader is always shown why it pays to state a simple situation in a seemingly unnecessarily involved way. Professor Weyl's book contains general science in the best sense of the word. D. P.

The Theory of Homogeneous Turbulence. By G. K. Batchelor. (Cambridge University Press.) [Pp. 197.] Price 25*s.*

Dr. Batchelor's book, based on one of the successful essays for the 1949–50 Adams Prize makes an eminently satisfying start to the new series of Cambridge Monographs on Mechanics and Applied Mathematics.

Homogeneous turbulence is defined as "a random motion whose average properties are independent of position in the fluid" and the mathematical tools required for attacking it are collected together in a most useful early chapter. The subject is then developed through its kinematical to its dynamical aspects. Once the dynamical aspect is reached the complexity of the problem limits the exact deductions and rapidly forces the introduction of intuitive hypotheses of which the most far reaching is Kolmogoroff's theory of local similarity (now termed the universal equilibrium theory).

The author then goes on to consider in detail the decay of turbulence behind a grid (a subject which requires considerable interplay between theory and experiment—and nowhere has this interplay been more successful than in the Cavendish) and the information it yields about homogeneous turbulence generally, and the energy spectrum, the joint-probability distribution of the velocities at a number of points and pressure correlations in particular. These considerations serve as the basis for further tentative hypotheses which it is reasonable to hope will ultimately lead to the formulation of a general theory.

Whilst no one would claim that finality has yet been reached in this subject it is quite evident that considerable progress has been made and that the time was ripe for such an account as Dr. Batchelor gives. This raises one's hopes that in the not too distant future a similar account may be given of turbulence in shear flow. L. H.

Heat Transfer Phenomena : the flow of heat in physical systems. By R. C. L. Bosworth. (Sydney : Associated General Publications Pty. Ltd. ; New York : John Wiley & Sons, Inc. ; distributed in the United Kingdom by Pergammon Press Ltd.) [Pp. 211+xii, with numerous illustrations.] Price 42*s*. net.

Dr. Bosworth has attempted in this book to review fundamental knowledge of heat transfer, including the most recent developments. His book is therefore, a monograph on the essential physics of heat transfer phenomena, rather than a mathematical or physical text-book concerned with the solution or elucidation of particular heat transfer problems. As such, it succeeds admirably and fills a gap in the modern literature of Physics. The subject of heat transfer has always tended to be the Cinderella of Physics, but Dr. Bosworth's book, if not perhaps decking it in a gown of gold, does, at least, present it properly at the ball.

The unifying theme throughout is that heat transfer by any mechanism is one of a more general class of transport phenomena, including, for example, the diffusion of matter, momentum, or electric charge. The first chapter introduces the general concept of transport processes by means of ' carriers ' ; succeeding chapters then deal first with thermal conduction and thermal radiation, those phases of heat transfer in which the theory is, in general, well-developed, and allows the use of the methods of classical mathematical physics. Then follow chapters on natural and forced convection and the simultaneous transport of heat and mass, in which the empirical approach must be introduced, since, mostly, the mathematical systems are intractable. The power of the general approach to heat transfer, as one of a class of transport phenomena, is brought out in two illuminating final chapters on the use of the equivalent electric circuit in experimental studies of heat transfer phenomena, and on thermodynamic similarity as applied to the representation of any particular transport process by a more convenient physical model.

Particular mention should be made of the excellent and exhaustive bibliographies, conveniently appended to each chapter, in addition to a comprehensive list of symbols, and subject and author indexes. On the debit side, it may be considered a pity that Dr. Bosworth has not made more use of specific problems by way of illustration.

The book is, in general, very well produced, but the price is unusually high, and the numerous illustrations are neither drawn nor reproduced so well as a book of this quality merits. These are, however, minor points ; more important is that the book can be highly commended to anyone who is interested in or concerned with heat transfer phenomena, and is a veritable *vade mecum* as regards the formulation of heat transfer problems. C. K. T.

Table of the Reciprocal of the Gamma Function for Complex Argument. By J. P. Stanley and M. V. Wilkes. (Computation Centre, University of Toronto, 1950.) Price 36*s*.

This table gives values, to seven figures, of the reciprocal of the gamma function of a complex argument. The values were obtained in the electronic digital computer EDSAC at the Mathematical Laboratory, Cambridge. The tables will be of use in several branches of mathematical physics, for instance in the computation of solutions of the Schrödinger equation for a Coulomb field and positive energy. N. F. M.

[*The Editors do not hold themselves responsible for the views expressed by their correspondents.*]